Enhancing the Thermal Stability of Plasticized Polyvinyl Chloride Films Using Sustainable and High Dispersity Surface-Functionalized Layered Double Hydroxides

BY

HOSSEIN IPAKCHI

THESIS

Submitted in partial fulfilment of the requirements

for the degree of Master of Applied Science in Chemical Engineering

in the School of Graduate Studies of

McMaster University, 2024

Hamilton, Ontario, Canada

Master's Committee:

Associate Professor Li Xi, Adviser

Professor, Michael Thompson

Associate Professor, Charles de Lannoy

Master Of Applied Science, Chemical Engineering

McMaster University, Hamilton, Ontario, Canada

TITLE: Enhancing the Thermal Stability of Plasticized Polyvinyl Chloride Films Using Sustainable and High Dispersity Surface-Functionalized Layered Double Hydroxides

AUTHOR: Hossein Ipakchi

SUPERVISOR: Dr. Li Xi, (McMaster University)

Abstract

Polyvinyl chloride (PVC) is a long-standing thermoplastic with excellent performance in chemical resistance, healthcare, construction, and packaging. However, this versatile thermoplastic has low thermal resistance during processing and service life. In this project, Layered Double Hydroxide (LDH) is used as an environmentally friendly thermal stabilizer in two stages: before surface modification and after surface treatment. The successful synthesis of MgAlZn-LDH structures with a constant molar ratio of Mg+Zn/Al=2 and three different molar ratios of Mg/Zn=0.5, 1, and 2 is confirmed by powder X-ray analysis. The plasticized PVC compounds show improved thermal stability for all PVC-LDH samples compared to the reference sample, with C-R2 (Mg/Zn=2) exhibiting the best thermal stability. However, EDS results reveal that LDHs have a nonuniform distribution in PVC with weak dispersity, indicating a tendency for LDHs as inorganic additives to agglomerate in PVC. To enhance the distribution of LDHs in PVC, the surface of LDH-2R is organo-treated with Oleic Acid (OA) as a surfactant derived from renewable resources. Different molar ratios of OA/LDH (3, 6, 9, 12 mmol) are used for the surface modification. Powder X-ray analysis shows that the modification process not only preserves the integrity of LDHs but also increases the crystal size with fewer defects. Additionally, XPS analysis confirms that the surface chemistry of LDHs changes after modification, leading to a decrease in surface energy and more stable structures. EDS maps demonstrate the uniform distribution and strong dispersity of the finest surface-modified LDH in PVC, indicating excellent compatibility between LDH and PVC in compounds. Furthermore, the MC-9OA PVC compound exhibits excellent static thermal stability compared to the reference compound. Discoloration tests reveal significant color stability in the modified compounds, with uniform color change indicating the uniform distribution of LDHs in PVC. Raman spectroscopy analysis illustrates the thermal stabilization of LDH in PVC degradation through the formation of metal chloride during the thermal decomposition of

PVC. Modified compounds exhibit lower rates of metal chloride formation, demonstrating the significant impact of OA on the efficiency of LDHs in absorbing and neutralizing the HCl released during PVC thermal degradation.

Acknowledgements

I would like to express my deepest gratitude to my supervisor, Dr. Li Xi, for his unwavering support and invaluable guidance throughout this challenging journey.

I am also grateful to Oligomaster Company for their financial support, which made this work possible. Additionally, I extend my heartfelt thanks to Dr. Mekonnen for his generosity in granting me access to his laboratory facilities at the University of Waterloo.

I am thankful to all my friends in the Xi research group for their camaraderie and encouragement. I am incredibly fortunate to have the most supportive and caring parents, as well as wonderful sisters who have always been there for me.

Above all, I want to express my profound appreciation to my wife, Mitra, for her unwavering support and patience during this difficult time. Your acceptance of who I am and where I am in life has been a tremendous source of comfort, and knowing that I am deeply loved means the world to me.

Table of Contents

List of Figures

List of Tables

Chapter 1

Introduction

1.1 General Background

Polyvinyl chloride (PVC) is extensively used as a thermoplastic in a variety of applications, ranging from construction materials to medical uses. However, despite its commendable performance and cost-effectiveness, this polymer is limited in outdoor and high-temperature applications due to its low thermal and ultraviolet (UV) radiation resistance. To overcome this limitation, a wide range of additives, particularly thermal stabilizers, are employed to enhance the thermal stability of PVC in compound formulations, especially for plasticized products. Thermal stabilizers, which have been in use for a long time, prevent the thermal degradation of PVC by absorbing and neutralizing the hydrochloric acid (HCl) released during the degradation process. Among these additives, lead-based thermal stabilizers are widely used due to their effectiveness and low cost in improving color stability and long-term heating stability. However, the high toxicity and environmental concerns associated with lead-based stabilizers have led to their ban in Europe and North America.

Metal soaps, specifically calcium/zinc (Ca/Zn) stabilizers, have emerged as a viable al-

ternative to traditional thermal stabilizers, offering good efficiency and non-toxicity. While metal soaps provide safe and efficient performance, they still have certain limitations compared to lead-based stabilizers, particularly in terms of color stability. To address the demand for environmentally friendly and highly effective thermal stabilizers, Layered Double Hydroxide (LDH) shows great promise for PVC commercial products. LDH is a class of materials consisting of metal cations and hydroxide anions arranged in brucite-like structures, which possess the ability to absorb and neutralize HCl during PVC degradation. Despite extensive research and industrial utilization of LDH in commercial products, further research is needed to select and optimize metal cations, anion interlayers, synthesizing methods, and ensure uniform distribution of LDH in PVC.

1.2 Thesis Objectives

The primary objective of this thesis is to synthesize and modify the surface of MgAlZn-Layered Double Hydroxides (LDHs) through the pH constant co-precipitation method, hypotheses at developing advanced thermal stabilizers for plasticized polyvinyl chloride (PVC) compounds. By incorporating these LDHs, the goal is to enhance the thermal stability of PVC, which is critical in various industrial applications. The unique aspect of this study lies in the surface modification of LDHs using oleic acid, an environmentally friendly fatty acid, to improve compatibility and performance within PVC matrices.

This research specifically contributes to the following areas:

- Synthesis and Characterization of MgAlZn-CO-LDHs : The LDHs will be synthesized with varying metal cation compositions (Mg^{2}, Al^{3}, Zn^{2}), and their physicochemical properties will be characterized. A detailed analysis of the structure, morphology, and thermal properties will be conducted to establish the influence of cation composition on LDH performance in PVC stabilization.

- Application of LDHs as Thermal Stabilizers in PVC: The synthesized LDHs will be incorporated into plasticized PVC compounds to evaluate their performance as thermal stabilizers. The impact of these LDHs on the static thermal stability, color retention, and dehydrochlorination rate of PVC will be systematically examined.

- Optimization of Surface Treatment for Enhanced Compatibility: A key focus of the research is selecting the optimal LDH composition and surface treatment, with oleic acid being employed as a surface modifier. Oleic acid is selected due to its unique properties as a long-chain unsaturated fatty acid that is liquid at room temperature, offering ease of handling and potential for effective surface modification. The organo-modification is expected to improve the dispersibility of LDHs within the PVC matrix, thus enhancing the overall thermal stability and color performance of the material.

- Investigation of the Impact of Surface Modification on LDH Dispersibility and Performance: The study will assess how surface modification with oleic acid affects the dispersion of LDHs in the PVC matrix. Enhanced dispersibility is hypothesized to lead to improved interaction between the LDH and PVC, resulting in superior thermal and color stability. The mechanism of thermal stabilization introduced by the modified LDHs will also be explored using advanced analytical techniques such as Raman spectroscopy.

- Justification for the Use of Oleic Acid: Oleic acid was chosen as the surface modifier due to several factors. First, it is an organic molecule recognized for its sustainability and environmental friendliness, aligning with the current trend toward greener chemical processes. Additionally, its long aliphatic chain and unsaturated bond structure make it a promising candidate for integration into plasticized polymers, offering compatibility and enhanced interfacial adhesion between the LDH and PVC. The use of oleic acid as a surface modifier is supported by its liquid state at room temperature,

making it easier to work with compared to solid fatty acids like stearic acid, which have been similarly explored in the literature for their efficacy in polymer stabilization. Furthermore, oleic acid's unsaturated bond introduces the potential for further interactions within the PVC matrix, which may enhance the overall stabilization mechanism, a hypothesis that will be explored in this work.

In summary, the novel contribution of this thesis lies in the development of MgAlZn-LDH-based thermal stabilizers for PVC, with a particular focus on optimizing the performance of these materials through surface modification using oleic acid. This research will advance the understanding of how surface treatment can enhance the properties of LDHs, thereby contributing to more sustainable and effective thermal stabilizers for PVC applications.

1.3 Thesis Outline

This thesis focuses on the use of LDH material as a thermal stabilizer in PVC compounds and investigates the effects of surface treatment of LDH on the uniform distribution of LDHs in PVC and the improved thermal stability of PVC compounds. To achieve this, Chapter 2 provides a literature review on the structural defects in PVC and the reasons for the low thermal resistance of this polymer. It also explains the different types of stabilizers and their mechanisms for thermal stabilization in PVC compounds. Chapter 2 also provides background information on LDHs as thermal stabilizers and explains the key parameters of LDHs that contribute to the improvement of PVC thermal stability. Chapter 3 includes the selection of materials, methodologies such as synthesis methods, LDH characterization, preparation of compounds, and evaluation of the thermal stability of PVC compounds using TGA, Raman Spectroscopy, discoloration, Congo red, and dehydrochlorination methods. Furthermore, this chapter discusses the results of the project and provides a conclusion in the form of a paper. Chapter 4 highlights the significance of this study and presents

suggestions for future research.

Chapter 2

Literature Review

Polyvinyl chloride, also referred to as PVC, is one of the world's most frequently used and adaptable synthetic polymers [27]. Its chemical structure's main components are vinyl chloride monomers, which are then polymerized to produce a thermoplastic resin [28] as shown in **Figure. 2.1**. PVC's excellent durability, chemical resistance, and affordability are the reasons for its versatility. Numerous industries use this material extensively, including the building [29], healthcare [30], electronics [31], and automotive [32] sectors. Because they are easy to install and corrosion-resistant, PVC pipes and fittings are widely used in construction for drainage and water supply systems [33]. Furthermore, PVC is essential for producing electrical cables [34], apparel [35], and packaging materials [36], highlighting its vital role in modern manufacturing.

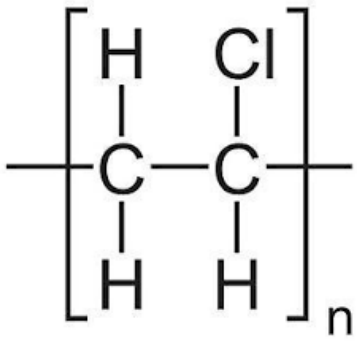

Figure 2.1: Molecular structure of PVC.

Despite its widespread popularity in industrial contexts, PVC faces a notable challenge in terms of its thermal stability due to structural defects [37]. This issue is of such significance that it has taken over 60 years to identify and address [27]. Researchers have directed their attention to mitigating this concern. Fortunately, incorporating additives, such as thermal stabilizers, has addressed this issue. However, it remains an undeniable challenge, constraining the use of PVC in specific processes like mechanical recycling [27]. Subsequent sections will delve further into an examination of this challenge.

2.1 History of PVC

During their scientific investigation in 1795, Dutch chemists synthesized dichlorethane, a substance believed to be the precursor of PVC. This development triggered a scholarly discourse on whether the compound constituted a simple amalgamation of chlorine and ethane or a more intricate combination [38]. Subsequently, in 1835, foundational steps for PVC production were undertaken within academic studies using vinyl chloride gas [39]. A pivotal advancement occurred in 1909 when it was discovered that chlorine could be effectively utilized in the liquid phase, signifying an important milestone in PVC manufacturing. The official acknowledgment of PVC as a novel and practical material occurred in 1912 [40]. During the First World War, various plasticizers were introduced in its formulation, and PVC underwent chlorination, enhancing its processability [38].

2.2 Commercial PVC

The advent of commercial PVC production commenced in 1930 when B.F. Goodrich, a rubber manufacturer in the United States, introduced plasticizers to PVC to enhance the elastic properties. This innovation placed PVC as a feasible replacement for rubber,

marking a pivotal milestone in its industrial production [40]. By the close of the 1930s, significant quantities of PVC were utilized in the electrical cable industry, and its applications expanded to include floor coverings, pipes for conveying various liquids, wall panels, building materials, tank linings, and pipe systems [41, 42]. The period between the 1930s and 1960s detected a substantial increase in commercially available plasticizers, introducing numerous novel emollients. This period saw the establishment of the plasticization of polymers as a distinct subfield within polymer science [43]. Nowadays, reports indicate the production of over 100 grades of PVC resin in the United States, underscoring its pivotal role in industry and academia [44].

Classifying PVC grades proves challenging due to their diverse range. However, a broad categorization based on general applications classifies them into plasticized and Unplasticized (UPVC or rigid PVC) [45, 46]. The degree of plasticization is typically determined by the quantity of plasticizer incorporated into the formulation, tailored to the product's specific applications [47]. In the context of rigid PVC, commonly employed for pipelines and windows, classification is contingent upon structural modifications within the PVC [48]. For instance, various grades suitable for piping applications include chlorinated PVC (C-PVC)**Figure. 2.2**, which is recognized for its high corrosion resistance, durability, and exceptional impact resistance. Another noteworthy variant is molecularly oriented PVC (PVC-O), honored for its corrosion resistance, water quality preservation, cost-effectiveness, recyclability, and an unmatched equilibrium between strength, stiffness, and flexibility. High-impact PVC (PVC-HI) stands for its high resistance to impact and strength [49].

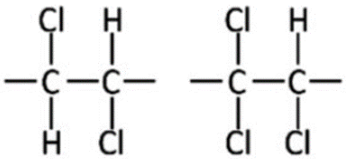

Figure 2.2: Molecular structure of C-PVC.

2.3 PVC Applications and Market

Within the thermoplastic polymers, PVC distinguishes itself due to its multifaceted applications in diverse sectors, including food packaging [50], military uses [51], the coating industry [52], optical applications [53], and construction elements like window frames and shutters [54]. While PVC stands as the world's third most employed polymer [27], its broad functionality presents difficulties in preparing customized formulations for particular purposes. Achieving a convenient recipe requires the informed selection of an appropriate PVC grade (considering molecular weight and synthesis method) and the incorporation of well-suited additives like plasticizers, thermal stabilizers, UV stabilizers, etc, to meet customized specifications [55]. The effective integration of additives relies on their compatibility with PVC and homogeneous distribution within the matrix, achievable through various blending structures at the nano, micro, and macro scales [56]. Moreover, considering the high sensitivity of PVC to thermal degradation and excellent processability, the appropriate processing approach becomes a crucial factor, allowing its application in various techniques, including injection molding, rotational molding, extrusion, blow extrusion, and thermoforming [57].

Injection-molded plastics with comparable properties in military applications have supplanted conventional metal devices [58]. This utilization spans from employing injection-molded PVC nanocomposites on military vehicles to augment visual detectability to constructing components to extrude reinforced detection apparatus on military ships and aircraft [59]. In the aerospace industry, the integration of PVC nanocomposites with polymers like polycarbonate (PC), poly methyl methacrylate (PMMA), and polyether ether ketone (PEEK) has proven effective in reducing structural weight by up to 50% while simultaneously enhancing flame retardant properties and promoting cost-effectiveness [51]. PVC micro-composites have gained notable attention, particularly in the optical industry, where their combination with polystyrene (PS) facilitates the design of optical films [60].

In the construction sector, a growing demand for building materials incorporating PVC microparticles is driven by economic considerations and the need to reduce structural weight [61]. Additionally, in the commercial packaging domain, PVC macro blends have emerged as successful packaging materials due to their recognized strength, lightness, stability, impermeability, and ease of sterilization [62]. Notably, using PVC in food packaging proves advantageous as it does not influence the taste and quality of the packaged food, preserving its natural flavors and protecting against external contaminants [63]. Mixing PVC with other thermoplastics, such as polyester, creates innovative materials characterized by promoted physico-mechanical properties, including enhanced wear resistance and tensile strength. Combining PVC with polyester or PVC/ polyolefin rubber enhances thermal stability and chemical resistance and raises the temperature threshold for practical use. Various packaging applications benefit from the versatility of PVC blends, including bottles, clear or blister packs, perforations, cap seals, and rigid thermal foils [51].

According to the above statements, it is reasonable to anticipate a growing demand for PVC within industrial sectors. Statistical evidence reveals that, by 2022, roughly 47% of the collective market share for PVC in North America is expected to be allocated to rigid PVC, with the United States leading with a predominant share of 45%. The market's valuation reached USD 2.37 billion in 2022, with a projected Compound Annual Growth Rate (CAGR) of 4.5% from 2023 to 2030 [64]. In addition, a discernible transition is noted in the demand for PVC resin in packaging, specifically gravitating towards food packaging products. This paradigm shift is attributed to an escalated demand for convenience food and online food services, stemming from evolving consumer perspectives after COVID-19. Notably, stockpiling and pandemic-induced purchasing of food, groceries, and essential household items is expected to exacerbate this trend in the world [65, 66]. Additionally, an upswing in demand for PVC resin is anticipated in the context of premium goods and packaging. This surge is envisaged particularly pronounced for non-food items as

supermarkets and convenience stores resume routine operations.

2.4 PVC and Future

Although PVC is widely recognized for its versatility and popularity as a third-ranked plastic worldwide [27], it is imperative to exercise rigorous monitoring and control in the production process to address the accumulation of waste from both PVC and its additives [67]. A comprehensive case study in China in 2020 reported [68] the annual production of PVC from 1980 to 2050 using a dynamic model. The results indicate a projected PVC material usage of 45.3 million metric tons in 2050, reflecting a substantial 182.8% increase compared to 2015 levels. Additionally, the anticipated PVC in-use stock in 2050 is expected to reach 761.9 million metric tons, a 7.1-fold increase from 2015. In this context, the estimated accumulation of PVC waste from 2016 to 2050 is approximately 495.7 million metric tons, representing a 7.5-fold increase compared to the waste accumulated from 1980 to 2015 (66.30 million metric tons). Moreover, it is shown that 1479 million metric tons of plastics were produced in the United States from 1950 to 2018, with PVC accounting for 15.9% of this total [69]. These unsettling statistics highlight the escalating demand for PVC-related products in the global industrial landscape.

In recent years, substantial attention has been dedicated to PVC products, primarily focusing on three key areas. Firstly, efforts have been concentrated on refining synthesis methods and overseeing the improvement of structural defects to enhance the thermal stability of this material [70]. Secondly, there is a noteworthy emphasis on incorporating bio-based and environmentally friendly additives, particularly within plasticizers and thermal stabilizers [71]. Phthalate plasticizers, identified as the primary pollutants among PVC additives, not only contaminate the environment and risk the well-being of living organisms but also pose health threats to humans by disrupting hormonal balance and

compromising the immune system [72]. Consequently, eliminating such substances from additives has markedly contributed to environmental amelioration and the regulation of toxin release [73]. Furthermore, attention has been directed towards using heavy metals, such as cadmium and lead [74]. Lead exposure, in particular, can result in severe health complications, significantly impacting the central nervous system and kidneys, with children exhibiting heightened vulnerability to disruptions in cognitive development [75]. Despite the prohibition of lead-based heat stabilizers in America and Europe, their persistence in certain Asian and African countries remains a concern. Thirdly, there has been a notable surge in the development and expansion of mechanical, chemical, electrochemical, and thermal recycling methods for products associated with PVC, signifying substantial progress in recycling technologies [76].

Accordingly, thorough scrutiny and proactive measures become essential for addressing the environmental challenges linked to the anticipated course of PVC production. Projections anticipate a noteworthy escalation in both the production of PVC and the accumulation of waste by 2050, underscoring the critical need for conscientious management. Thus, ongoing endeavors and global collaboration offer prospects for a future characterized by diminished environmental impacts.

2.5 Thermal Degradation of PVC

2.5.1 Foundational Concept of Structural Defects and Thermal Degradation

Current knowledge indicates that various mechanisms are involved in generating structural defects during PVC synthesis [77, 78]. As an illustration, these defects arise spontaneously through secondary reactions in radical polymerization processes, as detailed in

Figure.2.3 [1]. It necessitates careful investigation to address the challenges of thermal degradation in PVC. The chlorine atoms within these irregular structures are prone to easy removal, making them initiation points in the degradation process. Suppression of side reactions through modifications in the polymerization process holds promise for yielding PVC with heightened thermal stability [79]. In addition, as illustrated in **Figure.2.4- a**, one such mechanism elucidates that the uncommon head-to-head arrangement of monomers results in significant chemical consequences, leading to the formation of structures such as ethyl branches (EB), methyl branches (MB), and chloroalic end groups (A1 and A2), which exhibit relative resistance to heat [79, 80]. This process involves rapidly converting radicals from type 1 to type 2**Figure.2.4- a**, encompassing chlorine transfer reactions from radicals 2 and 3 to monomers, facilitating chain extension without requiring single-molecule β cleavage [2]. The progression and amplification of these processes are further explained by introducing the mechanism outlined in **Figure.2.4- b**, presenting a novel perspective on the genesis and transformation of unstable internal chlorophyll (IA) groups. This mechanism delineates the formation of type 4 radicals through intramolecular hydrogen abstraction (absence of 1,6) and β-chlorine elimination, suggesting an alternative or supplementary pathway for chain transfer to PVC [81]. In this context, unstable chlorinated moieties undergo dechlorination under reduction with Bu_3SnH, resulting in the formation of diverse terminal cyclopentane (MCP) branches, signifying disorder within the PVC structure [82].

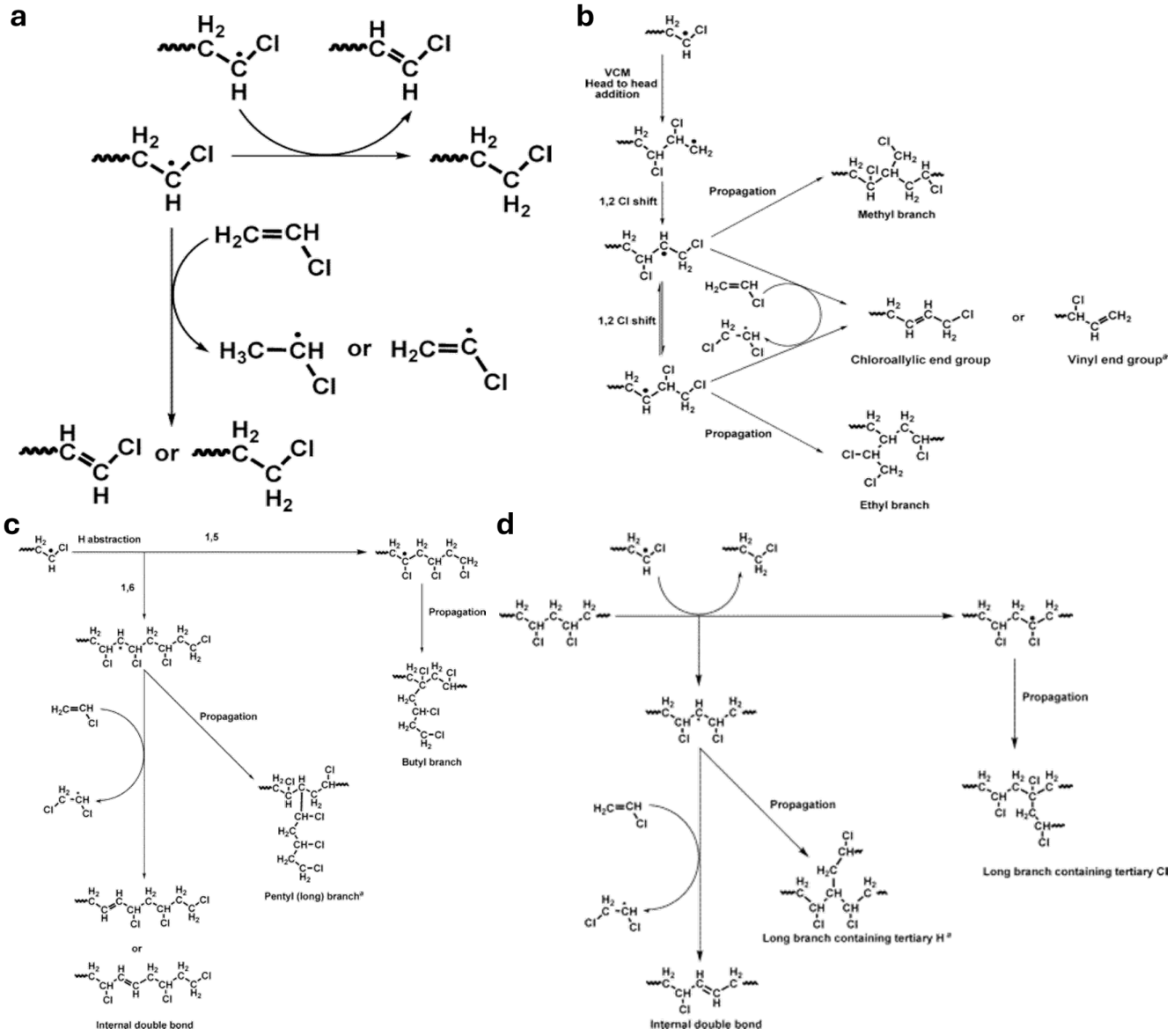

Figure 2.3: a) Termination by either disproportionation or transfer to monomer results in the generation of end groups, b) The emergence of defect structures ensues after head-to-head addition, c) In the course of radical VC polymerization, intramolecular hydrogen transfer reactions occur during propagation, d) Interactions involving intermolecular hydrogen transfer take place in the course of radical VC polymerization [1].

The reactions stemming from the mentioned processes culminate in the creation of structural defects, thereby contributing to a decline in PVC thermal stability [83]. Notably, the formation of internal allylic functional groups and the presence of tertiary chlorine signify defects capable of initiating the degradation process. Consequently, achieving PVC

with heightened thermal stability mandates the restraint of side reactions and meaningful alterations to the polymerization process [1]. Subsequent investigations in this domain will underscore the impact of structural irregularities on the ultimate properties of PVC, including the intrinsic sensitivity of specific functional groups formed during hydrogen transfer reactions [1, 79]. As depicted in **Figure.2.3- c,d**, these groups, formed both intermolecularly and intramolecularly, are identified through spectroscopy. While disorders such as methyl, ethyl branches, and chloroalic end groups may not overtly affect thermal stability, they play a pivotal role in comprehending polymerization's processes and reaction kinetics (**Figure.2.4- b**) [81]. The primary challenge lies in suppressing side reactions leading to the production of these defects and, consequently, the premature degradation of PVC. Hence, researchers strive to expand solutions for enhancing the polymerization process, leveraging insights from defect identification and analysis.

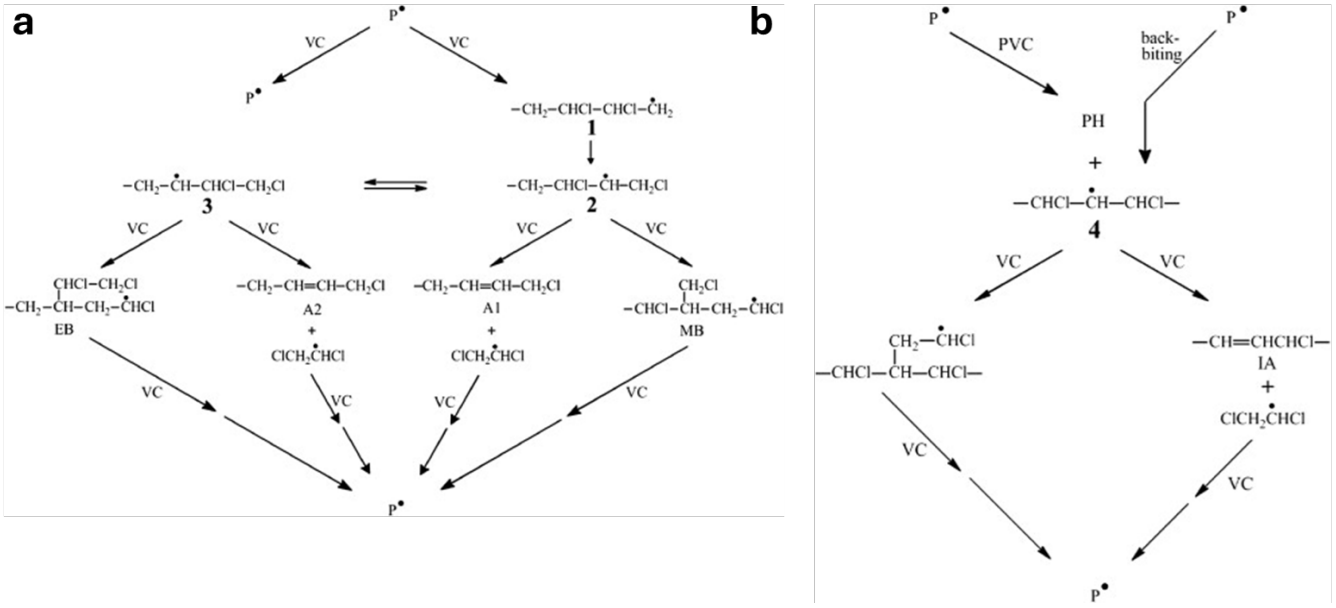

Figure 2.4: a) The chemical processes arise from the head-to-head positioning of VC during its polymerization, wherein P• signifies the head-to-tail macroradical,b) An additional mechanism for transferring chains to the monomer is observed during VC polymerization, where P• represents the head-to-tail macroradical [2].

2.5.2 Thermal Degradation Mechanisms

The pyrolysis process of PVC generally consists of two main stages of weight loss. According to the report by Gonzales et al [84], the first stage occurs between 200-350°C and involves the dehydrochlorination of PVC and the formation of polyene. The second stage occurs between 350-450°C for pure PVC and is characterized by the cracking and decomposition of polyene, leading to the formation of graphite structures. The report also mentions that the difference between the start and end of these stages, as well as the amount of weight loss, is directly related to the presence of atactic bonds. Due to the complexity of PVC thermal degradation, various models have been proposed in the literature.

Marcilla et al [85]suggested a three-stage process of thermal degradation of PVC, which includes the formation of HCl and intermediate complexes in the first stage, followed by the production of polyene from these complex structures. In the third stage, the polyene converts into carbon structures such as toluene or other aromatic materials. Jordan et al [86], on the other hand, divide the PVC thermal degradation into four stages. They propose that the first step corresponds to the final stage of dehydrochlorination, followed by random chain scission, subsequent recombination, cyclization/aromatization, and finally degradation leading to coke formation.

There are also different opinions regarding the dehydrochlorination stage. Gonzales et al [84] presented a two-step model, where the first step involves the degradation initiated by unstable Cl atoms at lower temperatures, resulting in a high weight loss rate of over 20%wt of PVC. In the second step, more stable Cl atoms are involved in the degradation process at higher temperatures, resulting in a lower weight loss rate. These more stable Cl atoms often have a higher level of syndiotactic sequences. Other studies emphasize that in the first step, two different reactions occur simultaneously, both of which are related to different configurations in the PVC structure with different thermal stabilities (head-to-head and

head-to-tail configurations). The second step includes two different competitive reactions, where the intermediates undergo rearrangement after their generation is complete [87,88].

Furthermore, various mechanisms have been proposed for the first step. Fisch et al [89] suggest that in primary degradation, the dehydrochlorination process occurs at the surface molecules, as these molecules have greater mobility compared to the inner molecules. As shown in **Figure.2.5- a**, in the early stages of degradation, the formation of C=C bonds is random and slow. As the degradation progresses, the dehydrochlorination process involves the inner molecules through complex mechanisms. In cases of high-level dehydrochlorination, HCl is released through a four-center quasi-ionic mechanism **Figure.2.5- b** [77], which occurs due to the charge separation of the C-Cl bond in a four-center transition state. With further elimination of HCl, a six-center concerted mechanism occurs **Figure.2.5- c** [77]. As the concentration of HCl increases in the system, HCl acts as a catalyst and removes the Cl atom from the backbone through a free radical mechanism**Figure.2.5- d** [77]. This process is referred to as the auto-catalytic zip degradation of PVC.

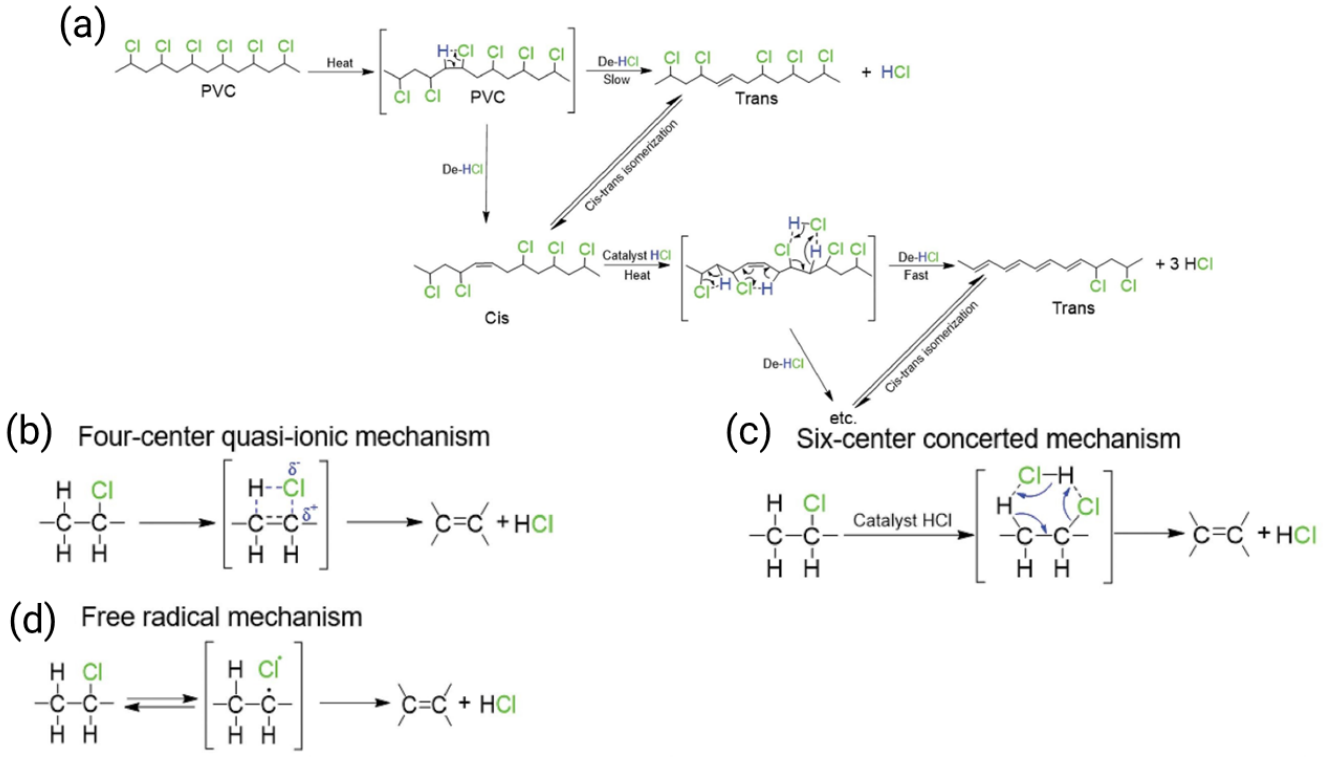

Figure 2.5: a) Dehydrochlorination mechanism in surface molecules at Primary degradation. b) Four-center transition state. c) Six-center transition state. d) Free radical mechanism [3].

2.6 Thermal Stabilizers

Thermal stabilizers or heating stabilizers represent a significant category of additives used not only for PVC but also for various polymers, including polyolefins. The primary classes of stabilizers encompass metal soaps, lead salts, and organotin compounds. While lead salts offer excellent long-term thermal stability, concerns regarding their toxicity have arisen. Consequently, policymakers and researchers are actively pursuing environmentally friendly alternatives to ensure the production of safer products. Here a brief report provides the different types of thermal stabilizers and their stabilization mechanisms.

2.6.1 Types of Thermal Stabilizers

Categories of lead salts, including tribasic lead sulfate, dibasic lead phosphite, and dibasic lead stearate, are highly regarded as effective thermal stabilizers in PVC applications [90]. Michell [91] introduced a stabilization model known as "True Stabilization," which is based on the free-radical mechanism. In this mechanism, lead-stearic salt not only delays thermal dehydrochlorination but also effectively prevents the formation of HCl. The interaction between the reacted stearic groups and lead compounds enhances their mobility and compatibility with PVC through the formation of carboxylates. When lead salts react with the released HCl during PVC degradation, lead chloride and aliphatic carboxylate free radicals are formed, which subsequently trap Cl^- ions and prevent the autocatalytic effect [91]. Lead compound thermal stabilizers offer several advantages, such as low cost, excellent color stability, long-term thermal stability, and outstanding electrical insulation. However, it is important to note that the main drawback of these compounds is their high toxicity [4]. The most severe effects of lead exposure are observed in the central and peripheral nervous systems, the hematopoietic system, the cardiovascular system, as well as in organs like the liver and kidneys [92]. According to reports from the World Health Organization (WHO), lead significantly affects the central nervous system and the development of children. Additionally, lead can interfere with learning ability, impair memory, lower IQ, and hinder growth and development [93]. While researchers have attempted to develop biobased composites such as Pb-LDH thermal stabilizers to reduce lead toxicity, these efforts have not been successful. Consequently, the European Union banned the use of lead-based thermal stabilizers in 2015 [5].

Organotin stabilizers typically consist of fatty acid salts, such as dimethyl tin, di-n-butyl tin, di-n-octyl tin, maleate, maleate monoester, mercaptan, and mercaptan-based fatty acid salts [94]. Generally, tin stabilizers have three different types of bonds, namely Sn-C, Sn-O, and Sn-S. Of these, the stability of the Sn-C bond is particularly crucial [95].

Research indicates that thioglycolate exhibits greater reactivity than other structures, and maleate exhibits greater reactivity than laureate [96]. Tin-based stabilizers are commonly used in packaging due to their high transparency, thermal stability, and compatibility [95]. However, organotin compounds have been found to exhibit signs of toxicity, including neurotoxic effects in humans and, in extreme cases of high exposure, even leading to death. Consequently, the use of organotin compounds as thermal stabilizers has been prohibited in Europe, while they are still employed in North America [5]. Despite the limitations associated with using organotin compounds, researchers continue to develop new types of these stabilizers. In order to enhance thermal stability effects, pentaerythritol stearate, a multifunctional group, was utilized in the synthesis of pentaerythritol stearate ester-based tin (II) metal alkoxides (PSE-Sn) thermal stabilizer, as depicted in **Figure.2.6- a** [4]. This multifunctional tin-based stabilizer not only enhances the thermal and color stability of PVC compounds (as shown in the **Figure.2.6- b**), but also provides plasticizing effects and lubrication action on PVC.

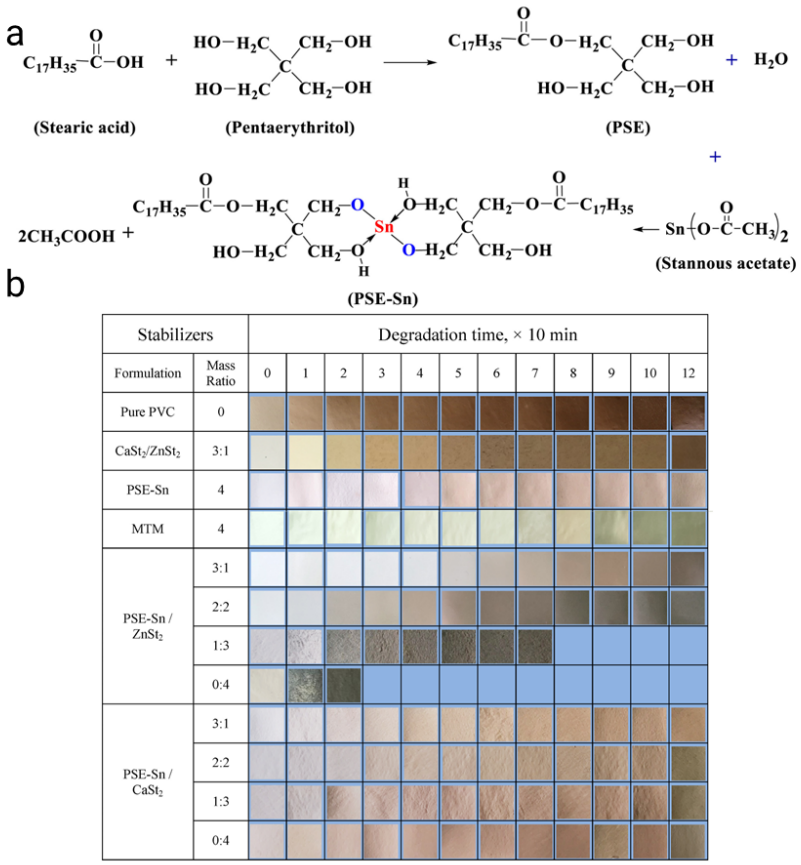

Figure 2.6: a)Chemical structure of PSE-Sn. b) Color change profile in thermal aging test. [4].

The metal soap thermal stabilizer, unlike the organotin group, only has a single M-O bond [95]. Additionally, it not only reacts with HCl but also replaces the unstable Cl^- group with the PVC backbone. Lead stearate, Barium stearate, and Cadmium stearate are the oldest types of metal soap thermal stabilizers [97]. However, due to concerns about human health and the environment, these types of metal soaps are now limited or banned. The newest member of this group is Zinc stearate ($Znst_2$), which exhibits better thermal color and stability. However, the main issue with this stabilizer is its reaction with HCl and the formation of $ZnCl_2$. $ZnCl_2$ is an active compound that acts as a catalyst for auto-catalytic degradation in PVC [98]. The reaction between HCl and $Znst_2$, as well as the role of $ZnCl_2$ in PVC degradation, can be observed in **Figure.2.7- a**. To address this problem,

researchers have utilized Calcium stearate ($Cast_2$) as a neutralizing compound for $ZnCl_2$. The use of $Cast_2$ not only absorbs the Cl element from $ZnCl_2$ compounds and prevents the catalytic effect of $ZnCl_2$, but also provides a synergistic effect with $Znst_2$ to enhance the long-term thermal stability of PVC, as depicted in **Figure.2.7- b**. Nowadays, Ca/Zn heating stabilizers are widely used in the PVC industry, and researchers have conducted numerous studies on these compounds.

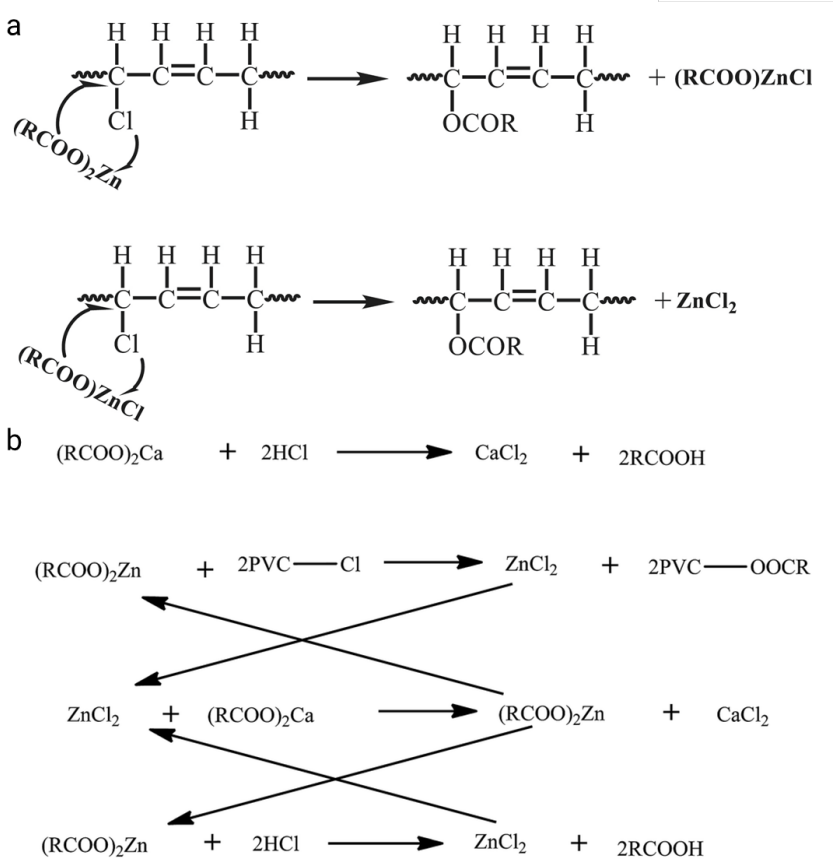

Figure 2.7: a)Mechanism of $ZnCl_2$ on the PVC degradation [5]b) Ca/Zn stabilizing mechanism of PVC [6].

Wu et al. [99] conducted a synthesis of zinc dehydroacetate (ZnL_2), a novel type of thermal stabilizer for zinc soap. This involved the combination of zinc acetate and dehydroacetic acid (DA). The results of the Congo red test did not demonstrate any specific effects when comparing $Znst_2/Cast_2$ with ZnL_2. However, the static thermal stability

of PVC increased by more than 1.5 times when using the compound $Cast_2/ZnL_2$. Furthermore, it was observed that $Cast_2$ provided better color stability than the $Cast_2/ZnL_2$ thermal stabilizer. To enhance the properties of $CaSt_2$ and $ZnSt_2$, aromatic amide groups were introduced separately as N-(2-amino ethyl) tung maleamic acid (LAETMA) and N-(2-amino phenyl) tung maleamic acid (LAPTMA) [7]. The incorporation of a double amide group into the para-position of phenyl rings significantly raised the initial thermal degradation to higher temperatures (see **Figure.2.8- a**) and improved the color stability of PVC compounds (see **Figure.2.8- b**) [7]. The introduction of humic acid as a modifying agent for the Ca/Zn thermal stabilizer (**Figure.2.8- c**), with varying ratios of Ca/Zn, resulted in a new biobased thermal stabilizer [8]. It was found that the optimal thermal stability was achieved when the Ca/Zn ratio was 4, causing the initial thermal degradation to shift to higher temperatures (see **Figure.2.8- d**). Additionally, the detrimental zinc-burning effect was significantly reduced [8].

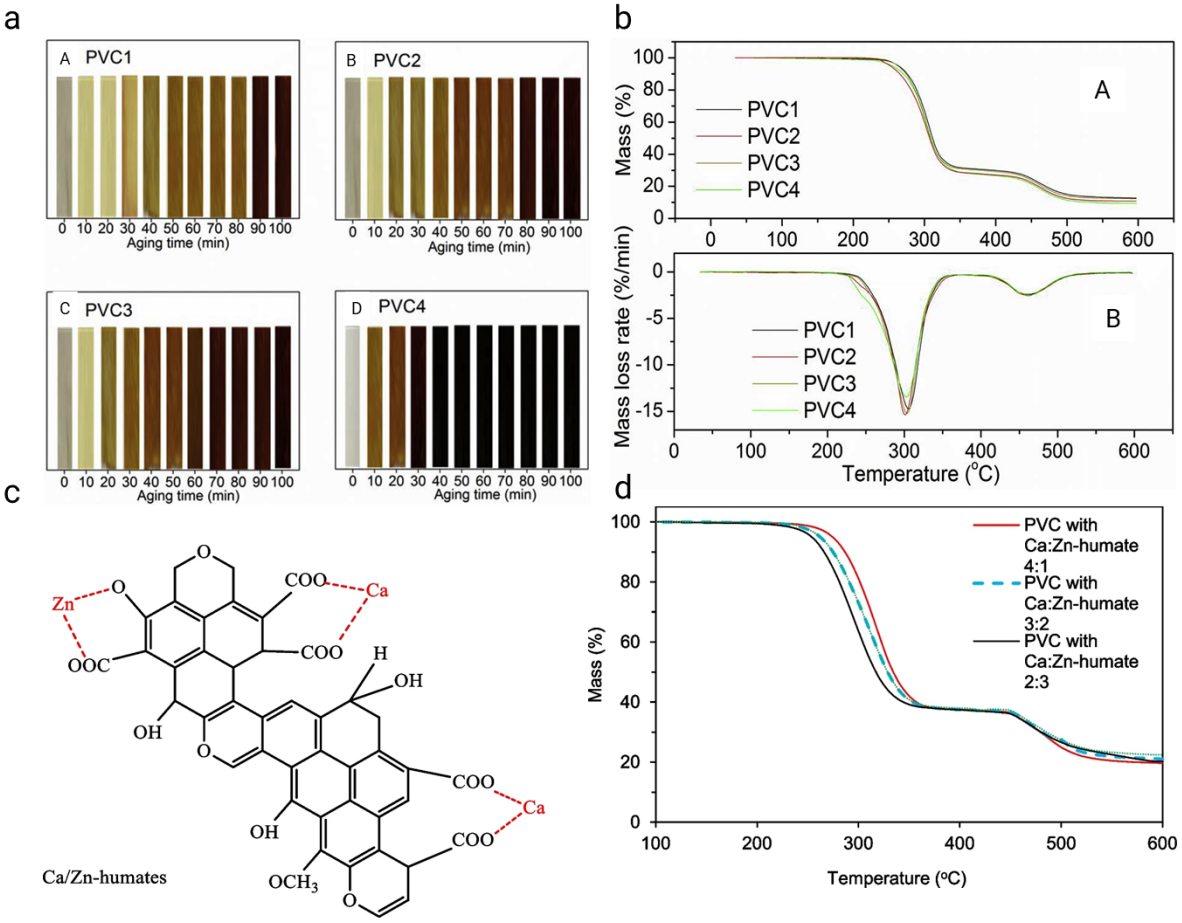

Figure 2.8: a) Color change profile of PVC compounds at 180 °C (in sample A(LAPTMA-Ca/LAPTMA-Zn=4.8:1.2), sample B(LAETMA-Ca/LAETMA-Zn=4.8:1.2), sample C (LABTMA-Ca/LABTMA-Zn=4.8:1.2) and sample D (CaSt2/$ZnSt_2$=2.4:1.6)). b) TGA (A) and DTG (B) curves of the PVC compounds [7]. C) The general structure of Ca/ZN/humic acid thermal stabilizer, and d) Effect of Ca/Zn-humates thermal stabilizer on PVC compounds [8].

The new types of thermal stabilizers can be classified into organic thermal stabilizers, metal alkoxides, and functional materials [5]. Among the organic type, the Polyphosphates group has received significant attention in the past five years. The findings confirm that polyphosphates have the ability to enhance the initial color stability of PVC compounds, while also reducing the rate of polyene formation in the presence of polyphosphates. Additionally, tris(hydroxymethyl)aminomethane (THAM) and its derivative (DHD 2-([1,3-dihydroxypropan-2-ylidene]amino)-2- (hydroxymethyl)propane-1,3-diol) have been intro-

duced as novel organic thermal stabilizers [100]. When THAM is incorporated, it reacts with the chlorine detached from the PVC backbone nitrogen atom, leading to the formation of C-N bonds by attacking the carbocation. Moreover, the released HCl in the system is scavenged by another THAM molecule to form a salt. The results indicate that THAM improves the whiteness and long-term thermal stability of flexible PVC compounds.

2.6.2 Thermal Stabilization Mechanism

Based on different stabilization mechanisms, there are three types of thermal stabilizers: preventive, suppressive, and curative thermal stabilizers [101]. Although researchers have provided the thermal stabilization mechanisms for synthesized heating stabilizers in a wide range of studies, it is difficult to determine the precise performance of these stabilization mechanisms.

Figure.2.9 presents a thermal stabilization mechanism for the PSE-Sn heating stabilizer [4]. In **Figure.2.9-a**, the OH group of PSE-Sn chelates with free $SnCl_2$ and $ZnCl_2$, preventing the degradation of PVC. This complexation is crucial for the superior long-term thermal stability observed with PSE-Sn stabilizers. In **Figure.2.9-b**, PSE-Sn replaces the labile chlorine atoms, inhibiting the formation of polyene and improving the thermal stability of PVC compounds.

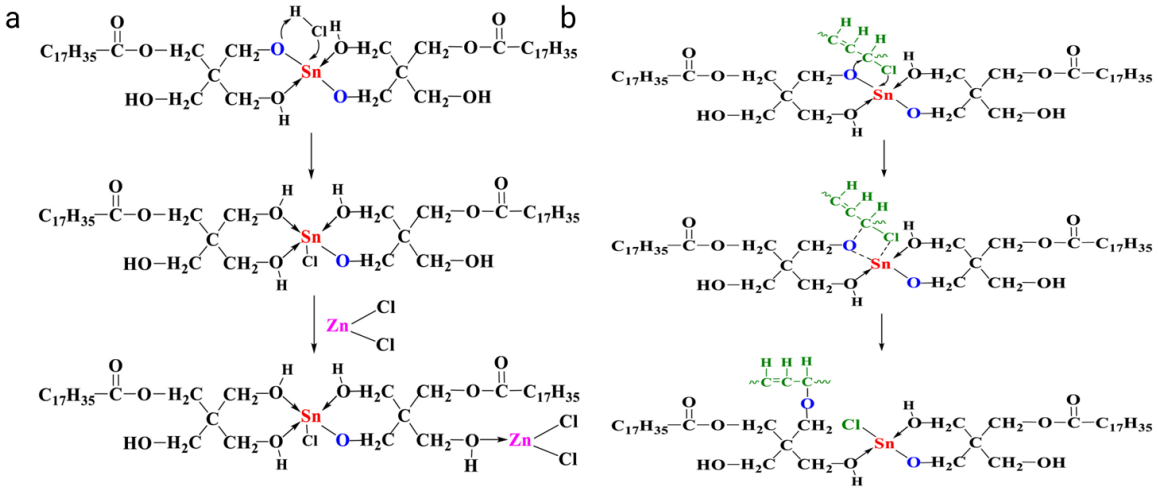

Figure 2.9: a)Suggestion mechanism for PSE-Sn neutralizing HCl and chelating $ZnCl_2$, b)Suggestion mechanism for PSE-Sn replacing the labile chlorine atoms of PVC [4].

The Ca/Zn synthesized from Tris[di(hydroxymethyl)amino]-1,3,5-triazine (HHTT) and tung-maleic anhydride (TMA) and converted to zinc soap (Zn-HTMA-1 and Zn-HTMA-2) or calcium soap (Ca-HTMA-1 and Ca-HTMA-2) contain hydroxyl and nitrogen-rich groups [9]. The suggested thermal stabilization mechanism for PVC/$CaSt_2$/Zn-HTMA-2/HTMA-2 compound shows the replacement of labile chlorine atoms by hydroxyl groups, forming stable crosslinked compounds and reducing the formation of polyenes, as shown in **Figure.2.10-a**. Zhang et al. [10] synthesized a multifunctional antibacterial agent, thermal stabilizer, plasticizer, and lubricant with pentaerythritol p-hydroxybenzoate ester-based zinc metal alkoxides (PHE-Zn). The results showed that with an increase in PHE/Zinc acetate, the thermal and color stability improved, and the rate of HCl release and polyene formation decreased. As shown in the suggested mechanism in **Figure.2.10-b**, in the first step, the alkyl oxygen in metal alkoxides attacks the labile chlorine, replacing it. Also, in the second step, the released HCl is neutralized by PHE-Zn-3 with HCl absorption, and in the last step, the production of $ZnCl_2$ is complexed by hydroxyl groups, decreasing the autocatalytic "zinc burning" phenomenon.

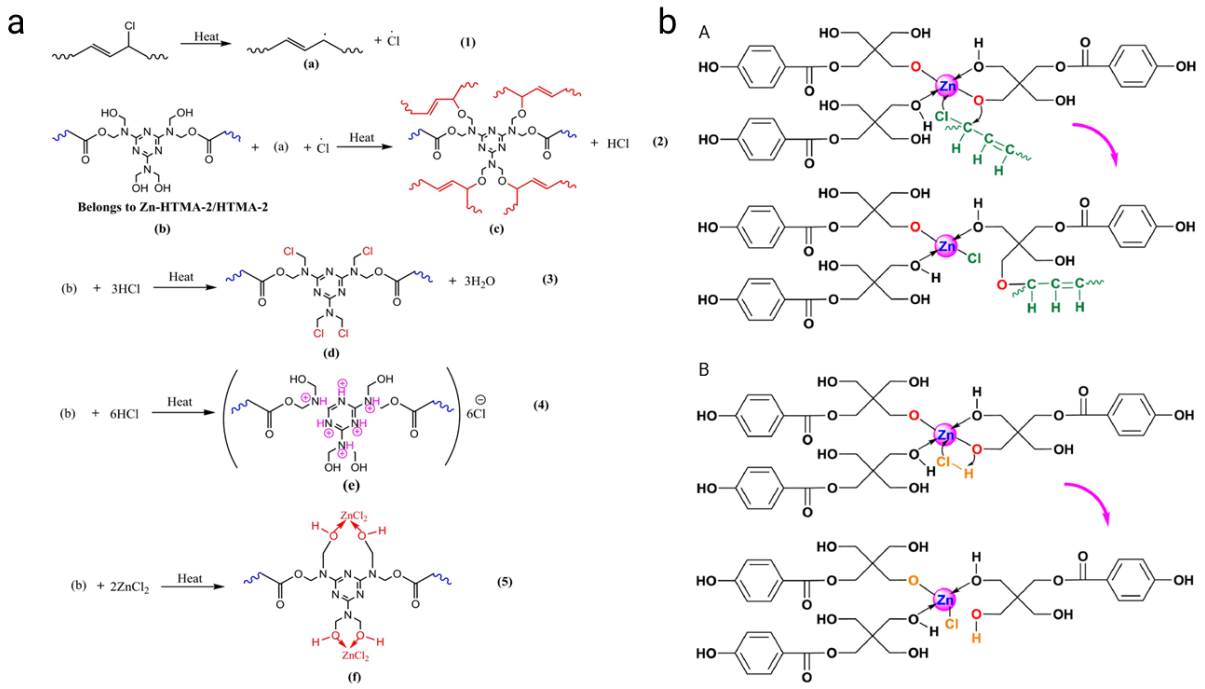

Figure 2.10: a)Thermal stabilizing mechanism of PVC/$CaSt_2$/Zn-HTMA-2/HTMA-2 [9], b)A) Suggested thermal stability mechanism of PHE-Zn-3 on PVC and B) A possible way for PHE-Zn-3 to neutralize HCl. [10].

2.6.3 Thermal Stability Characterization Methods

There are various testing methods available for assessing the thermal stability of PVC compounds and the subsequent release of HCl during the process of thermal degradation.

The Congo red test, as described in ISO 182-1 (1990), is a widely utilized method for evaluating the thermal stability of PVC. This test involves subjecting a PVC sample to a temperature of 180°C, while simultaneously observing the release of HCl, which serves as an indication of degradation. Adjacent to the PVC sample, Congo red paper, a pH-sensitive indicator, is positioned. Upon exposure to heat, the PVC sample undergoes degradation, emitting HCl and causing a decrease in the pH level near the paper. Consequently, the Congo red paper undergoes a color change from red to blue, signifying the initiation of degradation. The duration required for this alteration in color is documented as the ther-

mal static time, providing a direct measure of the PVC's thermal stability. Notably, a lengthier thermal static time corresponds to greater stability of the PVC material. Another method is the dynamic thermal stability test, which evaluates the thermal stability of PVC compounds under shear and temperature conditions. In this test, a compound is kept at a constant temperature and speed in a batch mixer, and the point at which the torque sharply decreases is recorded as the dynamic thermal stability of the PVC compounds. The thermal aging test is used to study the whiteness or color stability of PVC compounds. Based on ISO 305-4, 1990, this test involves keeping samples at 180°C in a heating oven and measuring the color change of the samples using a color meter every 10 minutes until the samples turn black and undergo complete degradation. To measure the rate of HCl released during degradation, the dehydrochlorination test, based on ISO 182-2: 1990-12, is employed. In this method, samples are kept at 180°C in an oil bath and the test tube is sealed. The released HCl is carried by nitrogen to 100 cc of deionized water, increasing the water's electroconductivity. The change in the electroconductivity of the water indicates the rate of PVC degradation.

Furthermore, several other methods are commonly used to study the thermal stability of PVC compounds. For example, Thermo-Gravimetric Analysis (TGA) is an important characterization technique in this field, as it provides information about the weight loss of compounds with increasing temperature. Advanced versions of this method, such as TG-FTIR and TG-Mass, are also helpful in assessing thermal stability. In addition, TGA results can be used to measure the activation energy and thermodynamic parameters, which in turn determine the degree of degradation reaction.

2.7 Layer Double Hydroxide (LDH)

Layered Double Hydroxide (LDH) emerges as a promising candidate for this purpose. LDHs conform to the general chemical formula:

$$[M^{2+}_{1-x}M^{3+}_{x}(OH)_2]^{x+}[A_{x/n}]^{n-} \cdot m\mathrm{H_2O}$$

general formula. These compounds consist of brucite-like layers, where the basic layers are composed of metal cations and the anions reside in the interlayer region. The basic layers consist of divalent For divalent metals M^{2+} : $\mathrm{Mg}^{2+}, \mathrm{Fe}^{2+}, \mathrm{Co}^{2+}, \mathrm{Cu}^{2+}, \mathrm{Ni}^{2+}$, and Zn^{2+} and for trivalent metals M^{3+} : $\mathrm{Al}^{3+}, \mathrm{Cr}^{3+}, \mathrm{Ga}^{3+}, \mathrm{In}^{3+}, \mathrm{Mn}^{3+}$, and Fe^{3+} metal cations, while the anions in the interlayer gallery $\mathrm{NO}_3^-, \mathrm{Cl}^-, \mathrm{CO}_3^{2-}, \mathrm{SO}_4^{2-}$, and RCO_2^- are connected to the metal cations through electrostatic attraction, hydrogen bonding, and ionic bonding [12,102]. This arrangement achieves intercalation assembly while maintaining electrical neutrality. The molar ratio of $M^{2+}/M^{2+} + M^{3+}$, denoted as x, typically ranges between 0.25 and 0.33, indicating a molar ratio of M^{2+} to M^{3+} in the range of 2-4. During LDH synthesis, water molecules are associated with the anions in the interlayer and are represented by the variable n in the general formula [103]. **Figure.2.11-a** illustrates the structure of LDH material. The chemical and physical properties of LDHs are directly influenced by the cations in the host layer, the anions in the interlayer, and the size of the crystals. These parameters allow for the synthesis of tailor-made LDHs for a wide range of applications [103].

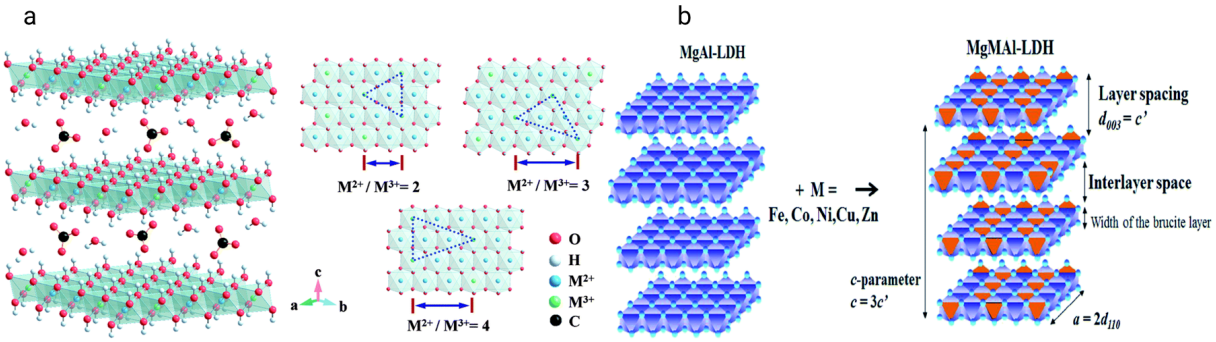

Figure 2.11: a)Schematic structure of LDH with different ratio of M^{2+}/M^{3+} [11], b)Schematic of preparation MgAl and MgMAl LDHs (M:Fe, Co, Ni, Cu, Zn) LDHs [12].

For example, in the host layer, when the molar ratio of divalent cations to trivalent cations is in the range of 2-4, DLH structures are formed. As a result, a wide range of various compositions can be designed. Furthermore, by using metal cations of the same valence state and similar radius, it is possible to design ternary or even quaternary LDH structures. These structures can simultaneously incorporate different cations, as shown in **Figure.2.11-b**. Additionally, the anions in the interlayer can be exchanged with other anions, such as polymer, organic, and inorganic, due to weak van der Waals and hydrogen bonding interactions with the host layer. The use of customized anions in the interlayer allows for the tuning of properties such as conductivity, catalytic efficiency, selective adsorption, and absorption capacity. Moreover, by adjusting synthesis parameters such as temperature, pH, and time, it is possible to control the size of crystals, the distribution of crystal size, and the degree of crystallinity during synthesis [11, 103]. All of these tunable parameters and customized LDH properties make them a unique structure with a wide range of applications. These applications include their use as additives in polymers, adsorption materials, precursors for functional materials, as well as in pharmaceutics, photochemistry, and electrochemistry [104].

In recent years, LDH has played a crucial role in the field of adsorption and environmental purification. This is due to its ability to tailor the pore size, pore distribution, and absorption capacity of materials [105]. For instance, LDH-based materials with mesopores

have effectively adsorbed biomolecules such as bovine serum albumin, which measures 5 $\times$ 7 $\times$ 7 nm^3 [106]. Sun et al. [107] synthesized a NiCoAl-LDH/Kao hybrid nanocomposite to enhance the degradation of antibiotics. They observed that the introduction of Al doping in the NiCoAl-LDH/Kao nanosheets increased the exposure of active sites, surface area, and unsaturated defect vacancies through partial dissolution of Al^{3+} species. This resulted in remarkable catalytic performance in degrading various pollutants, confirming the universal applicability of this hybrid nanocomposite. In another study, a CO_3O_4/LDH composite catalyst was developed using a combined strategy of morphology regulation and LDH assistance to enhance the generation of hydroxyl radicals for photocatalytic toluene oxidation [108]. The optimized spi-CO_3O_4/LDH catalyst demonstrated superior toluene degradation and mineralization rates of 473.28 and 466.67 $ppm.g^{-1}.h^{-1}$, respectively, outperforming recently reported catalysts.

In the field of biomedicine, LDH, both in its free form and when incorporated into composite hydrogels containing Boswellia serrata extracts (BSE) and Gellan gum (GG), has demonstrated significant potential for cartilage tissue regeneration [109]. The composite hydrogels, specifically GGHL/LDH-BSE, exhibit a promising BSE delivery system with a unique combination of mechanical and biological properties that are well-suited for applications in cartilage repair. Moreover, LDH-based nanovaccines have shown promise in enhancing both cellular and humoral immunity by optimizing their nanoscale size and surface charge, which facilitates efficient internalization by antigen-presenting cells (APCs) [110]. By combining LDH adjuvants with programmed CpG/Aptamer DNA strands, bone marrow-derived dendritic cells (BMDCs) can be significantly activated and in vivo immune responses can be improved. Thus, LDH adjuvants serve as a potent supplement to traditional alum adjuvants. LDH-based hydrogels, particularly those with the composition of hydroxyapatite (HAP)/hyaluronic acid methacrylate (HAMA) -LDH, are designed to mimic the hierarchical anisotropic structure of natural bone [111]. As a result,

these hydrogels offer enhanced mechanical strength and a highly organized arrangement that is beneficial for regenerating bone defects. The LDH components present in the scaffold play a critical role in promoting osteogenic differentiation and vascularization, thereby demonstrating significant potential for stimulating new bone formation and modulating the osteoimmune environment in clinical applications.

2.7.1 Thermal Stabilizer Application of PVC

In 1981, the Kyowa Chemical Industries of Japan introduced a patent that highlighted the considerable influence of LDH materials on the thermal stability of PVC compounds [13]. This sparked widespread interest in LDH as a cost-effective and environmentally friendly solution, leading to its large-scale production. Over time, LDH has found extensive application in polymer compounding, specifically in areas such as UV stabilization [112], electromagnetic shielding [113], improvement of mechanical properties [114], flame retardancy [115], and absorption [116] in the PVC, polyolefin, and bio-membrane industries.

Several studies have been conducted to investigate the impact of size, host metal compositions, and type of anion in the interlayer of LDH on the enhanced thermal stability of PVC. Wen et al. [117] conducted a study on the influence of processing and crystallization time on the particle size of CaAl-LDHs and the thermal stability of flexible PVC compounds. Their findings showed that increasing both processing and crystallization time to four hours resulted in the synthesis of smaller particles (0.5-2 μm). Moreover, when 4phr of the synthesized LDH was used in the PVC compound, the color of the sample tended to yellow after 80 minutes and turned black after 110 minutes, while the pure compound turned black after 20 minutes at 195°C. In a recent study [118], the effect of Mg_2Al-CO_3-LDH particle sizes on the thermal stability of PVC compounds was investigated. The results revealed that the dynamic and static thermal stability of PVC compounds is significantly influenced by particle size. It was also observed that smaller particles are not suitable

for improving thermal stability. The researchers reported that MgAl-CO_3-LDH particles with an average size of 220 nm provided the best thermal stability in PVC compounds within the range of 202 to 334 nm, as shown in **Figure.2.12-a**. They also mentioned that very small particles had a high tendency to agglomerate, while larger particles were less compatible with PVC [101].

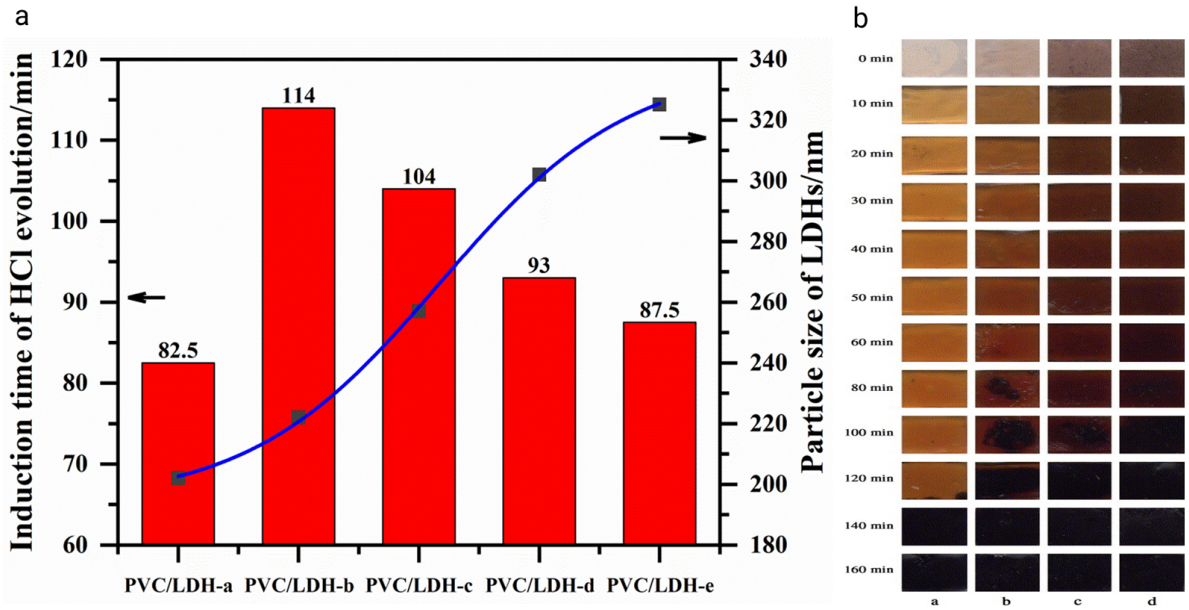

Figure 2.12: a) Effect of LDH particles size on the induction time of HCl [13], b)Effect of the molar ratio of Mg/Al on the color stability of PVC compounds (a=2,b=2.5,c=3 and d=3.5) [14].

Metal host compositions have a direct impact on crystal parameters, such as basal space, crystal size, and electrostatic charge balance in LDH. Previous studies have demonstrated that in different compositions of Mg/Al, the optimal ratio is 2 [14]. This is because as the Mg/Al ratio increases, the charge density decreases, leading to a weaker electrostatic attraction between the metal cation in the host layer and the anions in the interlayer. Consequently, the driving force for the entry of Cl^- into the interlayer galleries is reduced. **Figure.2.12-b** illustrates the effect of different compositions on the color stability of PVC compounds. As the charge density decreases, the samples turn black within a shorter period of time. Furthermore, research has shown that in ternary LDHs, the composition of

M^{2+} metal cations is a key factor in the thermal stabilization efficiency of LDH. In ternary MgAlZn-LDHs with a constant M^{2+}/M^{3+} ratio of 2, the incorporation of Zn results in changes to the average bond length and area of the layers. This leads to an enhancement of HCl absorption and thermal stability [119].

There are several reports available regarding the impact of different metal cations on the thermal stabilizing efficiency of LDHs. It has been demonstrated that among the ternary LDHs, namely MgAlZn, MgAlFe, and MgAlCu, the MgAlZn-LDH exhibits the highest initial weight reduction rate in TGA. This indicates the influence of $ZnCl_2$ on the autocatalytic effect in PVC degradation [15]. Additionally, as depicted in**Figure.2.13-a** MgAlCu-LDH demonstrates superior thermal stability compared to MgAlFe-LDH. Moreover, the MgAlFe-LDHs decrease the peak heat release rate (pHRR) from 623±8 kWm^{-2} to 253±5 kW m^{-2}, but increase the total heat release from 68±2 $MJmm^{-2}$ to72±3 MJm^{-2}. In separate studies focusing on LDHs such as $[Mg_4Al_2(OH)_{12}] \cdot CO_3{\cdot}4H_2O$, $[Mg_3ZnAl_2(OH)_{12}] \cdot CO_3{\cdot}$ $4H_2O$, $[Mg_3CuAl_2(OH)_{123}{\cdot}4H2O$, $[Mg_4AlFe(OH)_{12}]_3{\cdot}4H_2O$, and $[Ca_4Al_2(OH)_{12}] \cdot CO_3{\cdot}$ $5H_2O$, it was found that $[Mg_4A_l2(OH)_{12}] \cdot CO_3 \cdot 4H_2O$ exhibits the most favorable dynamic thermal stability.On the other hand, $[Mg_3ZnAl_2(OH)_{12}] \cdot CO_3 \cdot 4H_2O$ demonstrates the best color stability during thermal aging, as shown in **Figure.2.13-b** [16] . Furthermore, the $[Mg_3CuAl_2(OH)_{12}] \cdot CO_3{\cdot}4H_2O$ LDH exhibits a significant impact on the results of static thermal stability, indicating that it absorbs more HCl and delays the PVC degradation process.

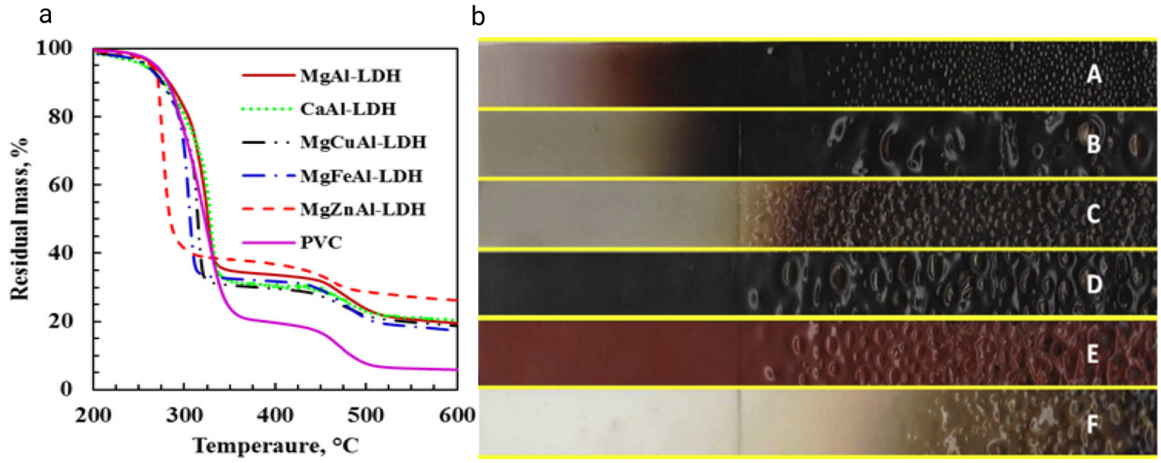

Figure 2.13: Effect of LDH compositions on a) the thermal stability of PVC compounds [15]and, b) color stability ((A) Neat PVC; (B) MgAl-LDH; (C) CaAl-LDH; (D) MgCuAl-LDH; (E) MgFeAL-LDH, and (F) MgZnAl-LDH) [16]

In recent years, there has been a growing interest in incorporating rare earth (RE) elements due to their potential as non-toxic, high-efficiency additives that exhibit a good synergetic effect with other stabilizers [13]. Jia et al. [120] utilized Lanthanum (La) as a RE in the ZnAlLa-LDH and ZnLa-LDH thermal stabilizers. The results showed that both ZnLa-LDH and ZnLaAl-LDH greatly enhanced the thermal stability of PVC compounds. Specifically, the static thermal stabilizer exhibited a receptivity of 63 minutes and 45 minutes, respectively, highlighting the potential of RE as a thermal stabilizer. In another study, researchers demonstrated that the addition of 2.5 phr of Zn/Al/La with a molar ratio of 20/8/2 increased the thermal stability of PVC compounds from 138 minutes to 186 minutes [121]. They attributed the improved PVC heating stability to the coordination of allylic chlorine atoms by ZnAlLa-LDHs, which effectively suppressed the degradation of PVC resin. To further investigate the effect of RE/Al molar ratio, a range of MgAlCe-CO_3-LDHs was synthesized with varying ratios of RE/Al (0.025, 0.05, 0.075, and 0.1) [122]. Among the synthesized LDHs, the sample with a RE/Al molar ratio of 0.075 exhibited the finest characteristics. Additionally, it was observed that the color of this sample tended to

become black after 190 minutes.

2.7.1.1 Modification of Interlayer Anions in LDH

The presence of guests within the interlayers plays a pivotal role in augmenting the thermal stability of PVC resin, thereby demonstrating a considerable impact on the efficacy of LDH. Specifically, these anions dictate the ability of LDH to absorb HCl during the degradation of PVC. Currently, carbonate intercalated is the most commonly utilized guest in commercial production. Nevertheless, owing to its singular functionality, the performance of this anion is inherently restricted. Consequently, the incorporation of multifunctional anions within the LDH interlayer presents a formidable challenge, as bridging this gap is crucial for fostering LDH efficiency in this specific field [13].

To investigate the impact of guests on the stabilization effect, CO_3^{2-}, NO_3^-, and Cl^- were considered as guests for MgAl-LDHs [13]. The discoloration test results revealed that the compound without LDH turned black after 60 minutes (**Figure.2.14-a**). However, the inclusion of LDHs enhanced the thermal stability of PVC compounds. This effect was particularly significant for $MgAl - CO_3 - LDHs$, which exhibited long-term stability for 180 minutes. As PVC degradation commenced, $MgAl - CO_3$-LDHs reacted with HCl in two stages: first, with the host layer, and then with the anions. This indicated a higher capacity for HCl absorption, with a capacity of 28.7 mmol HCl/g LDH. Conversely, MgAl-Cl-LDH (24.09 mmol HCl/g LDH) and MgAl-NO_3-LDH (21.77 mmol HCl/g LDH) only reacted with HCl through the host layer, providing a lower capacity to absorb the released HCl. Comparing the effects of Cl_O4^- and CO_3^{2-} as guests in MgAl-LDH thermal stabilizer, ClO_4^-exhibited better color and long-term stability (**Figure.2.14-b**) [17]. The intercalation of antimony trisulfide (Sb_2S^{3-}) in MgAl-LDH had a significant impact on the thermal stability of PVC compounds [18]. Sb-LDH hindered the growth of polyene-conjugated structures. However, Sb-LDHs have the po-

tential to be a PVC stabilizer for deep-colored PVC industrial polymer, as this filler is gray (**Figure.2.14-c**). In general, the capacity of guest anions in LDHs is reported as follows [123]: $NO_3^- < Br^- < Cl^- < F^- < OH^- < SO_4^{2-} < CO_3^{2-}$

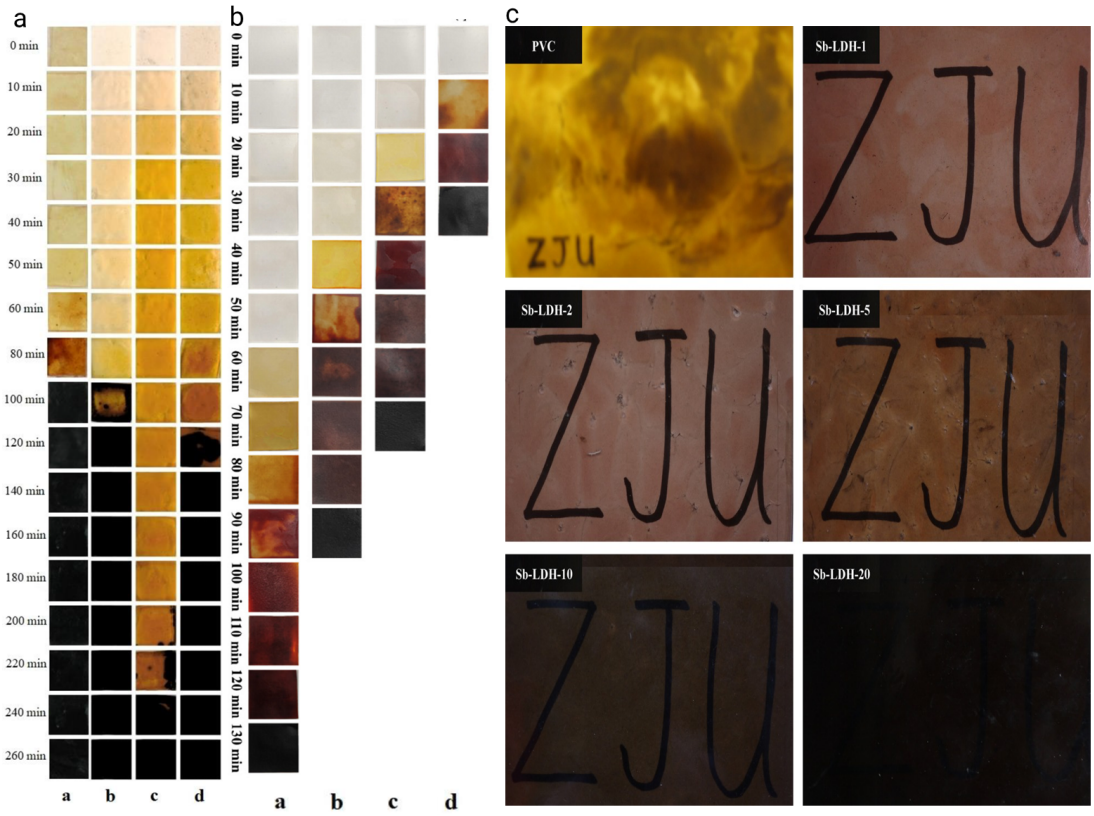

Figure 2.14: a)Thermal stabilizing effect of (a) $Ca(st)_2$+ $Zn(st)_2$, (b) $Ca(st)_2$+ $Zn(st)_2$+ $MgAl-NO_3-LDHs$, (c) $Ca(st)_2$+ $Zn(st)_2$+$MgAl-CO_3-LDHs$, and (d) $Ca(st)_2$+ $Zn(st)_2$+ MgAl-Cl-LDHs on PVC [13], b) Effect of MgAl-LDH on the thermal stability of PVC compounds (a)PVC, b) PVC+Ca/Zn, c)PVC+Ca/Zn+CO_3^{2-}-LDH and d) PVC+Ca/Zn+PVC+Ca/Zn+ClO_4^--LDH [17], and c) Transparency effect of MgAl-Sb-LDHs (1%wt, 2%wt, 5%wt, 10%wt and 20%wt) [18].

To investigate the impact of large anion groups on the effectiveness of layered double hydroxides (LDHs) in stabilization, Zhang et al. [124] employed 2-hydroxy-4-methoxybenzophenone-5-sulfonic acid (BP) as an interlayer guest in MgAl-LDH. The authors demonstrated that by incorporating an optimal percentage of BP, the interlayer spacing increased from 0.76 nm in the unmodified sample to 2.33 nm in the modified sample, thereby enhancing the capacity of the LDH. The addition of 3 phr of MgAl-BP-LDHs to PVC compounds resulted

in a significant improvement in the static thermal stability, increasing from 97 minutes for the pure compounds to 160 minutes. This improvement can be attributed to the strong supramolecular interactions between the LDH layers and the BP anions with HCl. It is worth noting that the dynamic thermal stability exhibited a similar trend to the static thermal stability, although PVC degradation occurred more rapidly due to shear force. Moreover, metaphosphoric acid (HPO_3) was employed as an anion in CaAl-LDH to enhance the heat stability of PVC compounds [19]. Comparatively, both CaAl-CO_3-LDH and CaAl-HPO_3-LDH exhibited notable improvements in the thermal stability of PVC compounds(**Figure.2.15-a**). As shown in (**Figure.2.15-b**), the optimum percentage of CaAl-HPO_3-LDH was found to be 4 phr. The interaction between HCl and the modified LDH occurred in two stages: initially, the guest anions tended to react with HCl, followed by the reaction between the carboxylic groups in the host layer and HCl. Consequently, the LDH structures were destroyed, and metal chloride was formed, as depicted in (**Figure.2.15-c**). Furthermore, the incorporation of MgAl-LDH-dipentaerythritol (Dpe) into the PVC compound significantly enhanced its static thermal stability [20]. (**Figure.2.15-d**) illustrates that even after 60 minutes, the PVC/MgAl-Dpe-LDH sample remained yellow, and after 90 minutes, it transformed into a light brown color, indicating excellent resistance to thermal degradation of the PVC sheets. It was reported that Dpe not only increased the HCl absorption capacity of LDH but also served as a heat-resistant plasticizer.

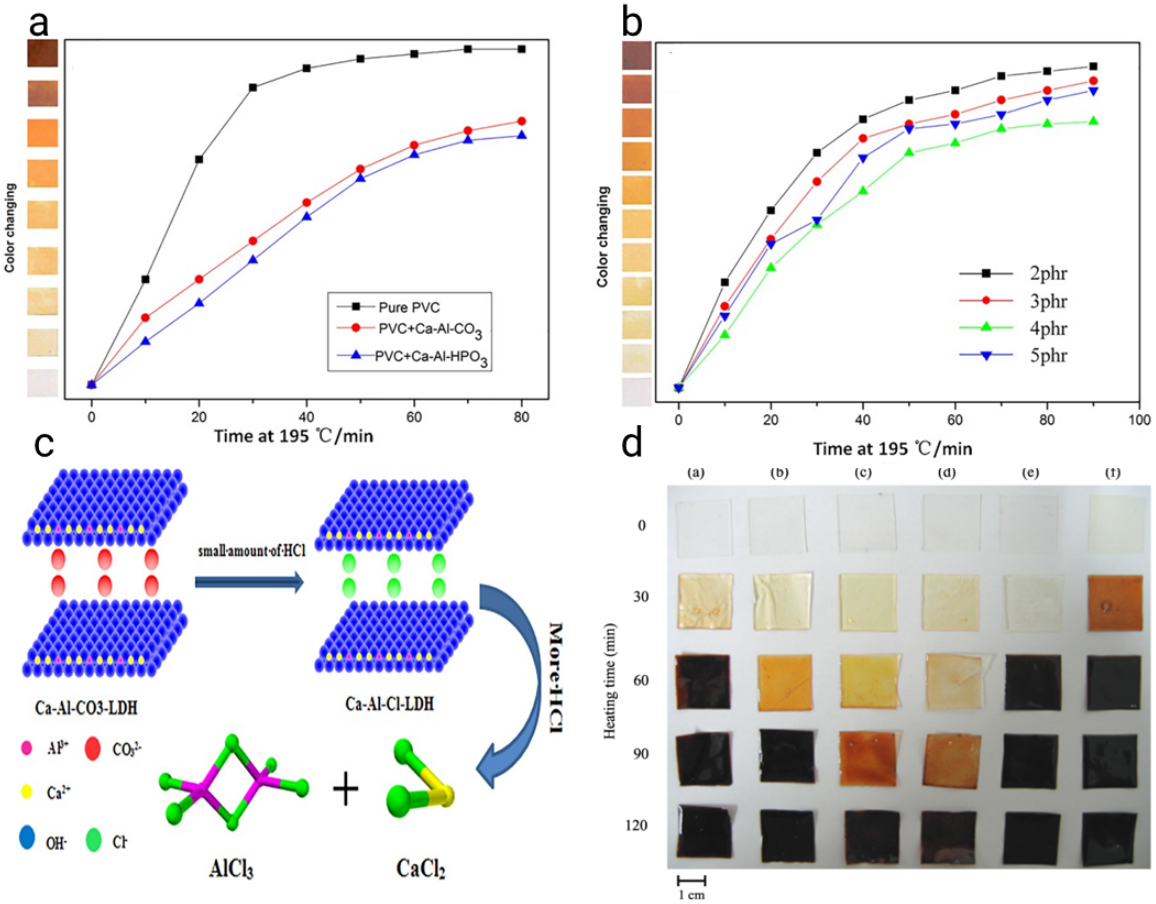

Figure 2.15: a)Comparison of CaAl-CO_3-LDH and CaAl-HPO_3-LDH on the thermal aging of PVC compounds, b) Influence of different amount of CaAl- HPO_3-LDH on the thermal stability of PVC sheets, c) Schematic diagram of the hydrocalumite reaction of CaAl-CO_3-LDH with HCl [19],and d)Effect of MgAl-Dpe-LDH on PVC compounds ((a) PVC, (b) PVC/MgAl-CO_3-LDH, (c) PVC/[Mg–Al-CO_3-LDH+Dpe], (d) PVC/MgAl-LDH-Dpe, (e) PVC/LiAl-LDH-Dpe, and (f) PVC/C18M) [20].

2.7.1.2 Surface Modification of LDH

One of the primary issues in polymer composites is the significant propensity of inorganic additives to agglomerate within the matrix. Modifying the surface properties of inorganic additives and adjusting the balance between hydrophilicity and hydrophobicity on the surface of these materials through chemical alterations is a commonly used and effective approach in this context. Surface modification not only enhances the compatibility and dispersibility of inorganic additives in polymer matrices, but also promotes increased in-

terfacial interactions between the additive and the polymer chains. This recommendation extends to LDHs as well, as chemical surface modification is widely suggested to enhance the performance of polymer-LDH composites in various studies [125, 126]. There are two methods of LDH surface modification: 1- surface treatment using organic surfactants, typically referred to as "organo-modified". These surfactants possess a hydrophilic head that reacts with LDH hydroxyl groups, and a hydrophobic tail that enhances compatibility and dispersibility within the polymer. Hence, organo-modified processes reduce the tendency of additives to agglomerate, resulting in improved composite performance. Products obtained using this method are usually employed in melt processing using extruders, batch-mixers, or two-roll mill machines. Alternatively, 2- a solution mixing process involves simultaneous modification of LDHs and mixing with the polymer. In this method, LDH surface modification occurs using organic solvents rather than organic anions, leading to enhanced interaction between LDH and the polymer [101].

In a recent study, Tong et al. [21] presented a novel method for in-situ surface treatment of MgAl-CO_3-LDHs to enhance the dispersity of LDHs in flexible PVC compounds. This method involved the use of a silane coupling agent (ML) and polyacrylic acid (PAA) in an in-situ polymerization process with PVC, as depicted in (**Figure.2.16-a**). Microscopy images confirmed the uniform dispersion of organo-modified LDHs in PVC. Statistical analysis revealed a narrow size distribution with relatively small particle sizes, as shown in (**Figure.2.16-b**). Moreover, the surface of CoAl-LDH and CoFe-LDHs was treated with Potassium monolauryl phosphate ($C1_2H_25OPO_3K_2$: LDH = 3:1, mole ratio), which served as a thermal stabilizer and flame-retardant agent in plasticized PVC [25]. The researchers reported that both organo-modified LDHs improved the thermal stability of PVC and reduced heat release and smoke release. Under a nitrogen atmosphere, the treated CoAl-LDHs exhibited superior thermal stability and generated less heat during degradation. In addition, EDS and Py-GC/MS analysis demonstrated that LDHs enhanced

the autocatalytic degradation of PVC during the oxidation process and decreased the release of HCl in a nitrogen atmosphere [22]. Furthermore, the introduction of sodium stearate (SS) to CaAl-LDH significantly enhanced the static thermal stability of PVC compounds, increasing this parameter more than fivefold compared to the pure sample. (**Figure.2.17-a**) illustrates that SS improved the compatibility and dispersity of LDHs in PVC, resulting in improved thermal stability of the polymer composite.

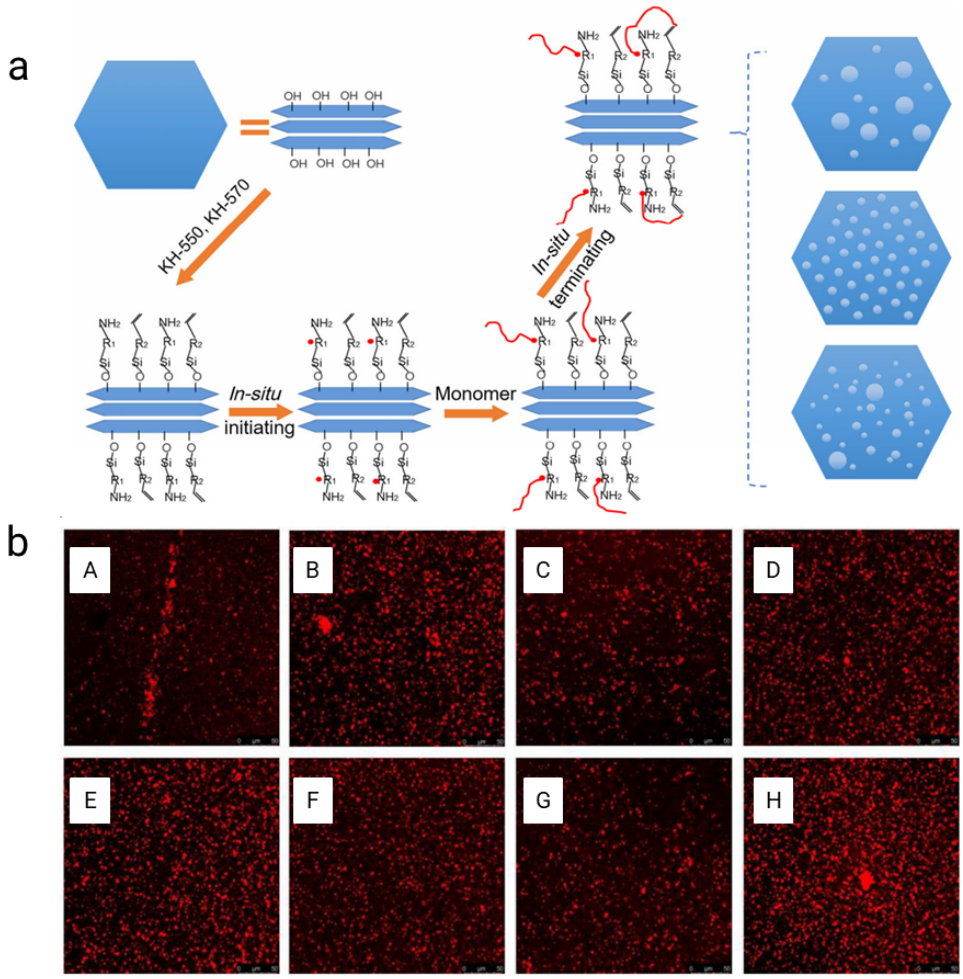

Figure 2.16: a)Schematic of the grafting the PAA on the surface of MgAl-LDHs , and b)Fluorescence microscopy images of A) MgAl-LDH, B) MLDH-5, C) 10%wtPAA@LDH, D) 20%wtPAA@LDH, E) 30%wtPAA@LDH, F) 40%wtPAA@LDH, G) 50%wtPAA@LDH and H) 60%wtPAA@LDH dispersed in PVC [21].

Furthermore, dodecyl sulfate anions (DS) were employed as a surfactant to treat MgAl-

LDH through both in-situ suspension polymerization and melt blending methods [127]. It has been reported that the LDH-DS nanoparticles not only reduce the average size of PVC resin particles, but also have minimal impact on the molecular weight and molecular weight distribution. Moreover, solution-based composites with LDH-DS exhibit better intercalation and exfoliation, whereas melt-blended composites show weaker distribution within the PVC matrix. The storage modulus below the glass transition region and the tensile strengths demonstrate superior performance for solution-made composites. In the same study, researchers compared the effects of DS and stearate ($C_{17}H_{37}COO^{-}$) as modifiers on the thermal stability of PVC compounds [23]. They observed a heterogeneous structure in the micrographs presented in (**Figure.2.17-b,A-B**), where nanoscale particles coexist with larger particles up to approximately 500 nm in thickness. This is likely due to the strong attraction force between the MgAl-LDH-NO3 layers and the difficulty for PVC macromolecular chains to intercalate and exfoliate. In contrast, (**Figure.2.17-b,C-F**) display TEM micrographs of PVC/LDH-DS (**Figure.2.17-b,C-D**) and PVC/LDH-stearate (**Figure.2.17-b,E-F**) nanocomposites, which exhibit no significant aggregates thicker than 100 nm, but instead prevalent particles with thicknesses ranging from 20 to 40 nm. As a result of the improved distribution and exfoliation of the modified samples, the static thermal stability increased by more than sixfold and fiftyfold compared to pure PVC for LDH-DS and LDH-stearate, respectively.

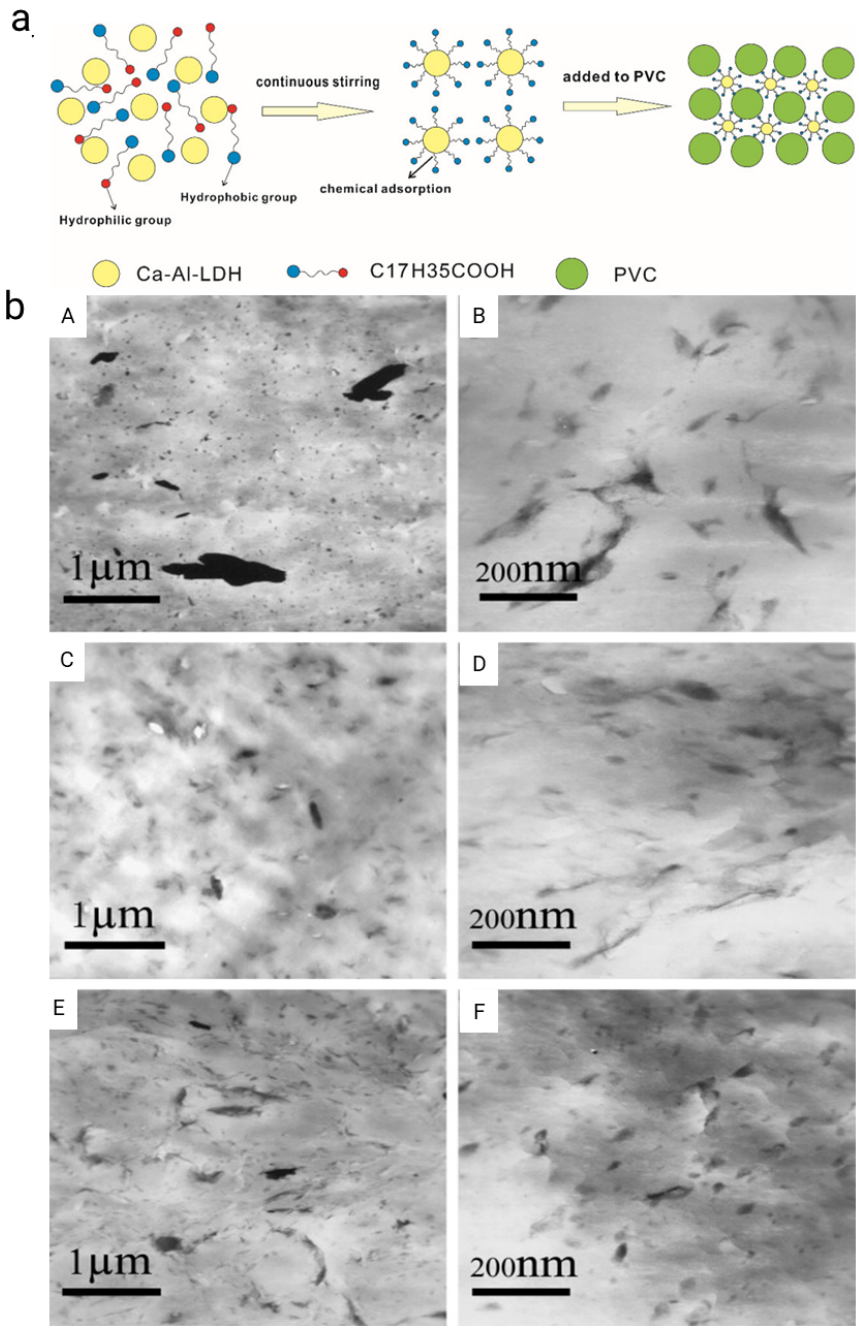

Figure 2.17: a)Schematic illustration for CaAl-LDH surface modification by sodium stearate [22] and b) TEM micrographs of (A,B) 5 wt% PVC/LDH-NO_3 composite, (C,D) 5 wt% PVC/LDH-DS nanocomposite and (E,F) 5 wt% PVC/LDH-stearate nanocomposite [23].

2.7.1.3 Thermal Stabilization Mechanism of LDH

LDHs belong to the group of suppressive thermal stabilizers that are capable of delaying PVC degradation by absorbing the released HCl or neutralizing it. Due to the complex nature of PVC degradation and the interactions between LDHs and PVC in enhancing thermal stability, various mechanisms have been suggested. However, two main mechanisms are explained here.

In the first model, HCl absorption occurs in two steps. Firstly, the anions in the interlayer gallery react with HCl, exchanging chloride ions with the interlayer and forming Cl^- intercalated LDHs. As PVC degradation progresses and more HCl is released into the system, the metal cations and hydroxyl groups react with HCl, forming metal chloride compounds. In this situation, the LDH structures are destroyed [101]. It should be noted that anions such as SO_4^{2-} and NO_3^- between LDH layers cannot be displaced by Cl^- ions in step (1) due to their similar acid strength to HCl. Wang and Zhang [128] proposed that the stabilization mechanism is attributed to the electrostatic interaction between the electron cloud of chlorine atoms in the PVC chain and the positive layer charge of LDHs. This interaction decreases the electron cloud density of chlorine atoms, weakening their activity and consequently restricting the initiation of dehydrochlorination. In the second model, researchers proposed a three-stage mechanism. In the first stage, the LDH layers initiate the stabilization process by reacting with HCl. In the second stage, the interlayer gallery reacts with HCl, exchanging chloride ions with the interlayer and forming Cl-intercalated LDHs. Finally, metal-Cl-LDH layers slowly react with HCl. Unlike the first model, this model is not applicable to all types of LDHs. For example, in Cl-intercalated LDHs, only the first step occurs [13]. In other words, the second model is based on the nature of available anions between the layers.

Jin et al. [24] proposed the mechanism depicted in **Figure.2.18-a** to explain the impact of the benzimidazole derivative (OBPB) as a surface modifier for ZnAl-LDH and

OBPB/ZLDH on the thermal performance of PVC. OBPB@ZLDH enhances the static thermal stability of PVC by absorbing and neutralizing HCl. This effect is further amplified by the synergistic interaction between OBPB and ZnAl-LDH, which are well-dispersed within the PVC matrix. However, caution is needed when using OBPB/ ZnAl-LDH, as the stabilization product ZnC_{l2} can unexpectedly lead to dehydrochlorination. The complex structure formed between OBPB and Zn suppresses PVC crosslinking, while also increasing dechlorination and oxidation of PVC . Despite these challenges, OBPB/ ZnAl-LDH holds promise for applications such as preparing hydrochars for alternative fuels at low temperatures. Fine-tuning the OBPB to ZnAl-LDH ratio is crucial for optimal performance. Additionally, the mechanism illustrated in **Figure.2.18-b** highlights the catalytic process of LDH [25]. In this process, HCl is absorbed, leading to the formation of Lewis acids (e.g., CoC_{l2}/FeC_{l3} or CoC_{l2}/AlC_{l3}) that promote PVC dehydrochlorination. The resulting increase in HCl concentration further accelerates dehydrochlorination. Ultimately, conjugated unsaturated structures and carbonium ions contribute to lattice formation through cross-linking and cyclization reactions, resulting in higher char residues at elevated temperatures—a desirable outcome for reducing heat and smoke release.

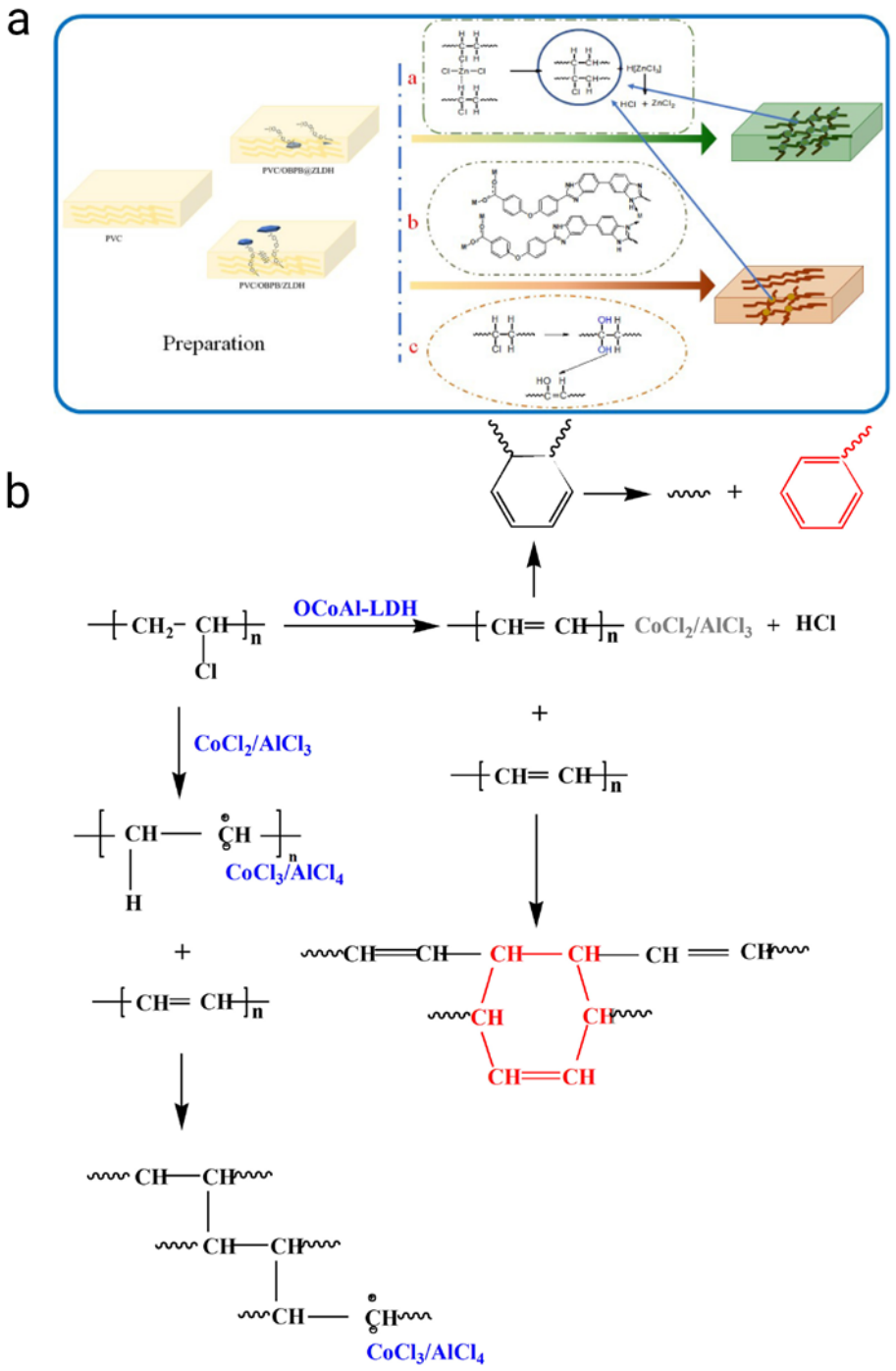

Figure 2.18: a)Schematic of OBPB@ZLDH and OBPB/ZLDH mechanisms on the thermal degradation of PVC compounds [24],and b)Mechanism of catalyze charring of the PVC-LDH composites [25].

Chapter 3

Materials and Methods

3.1 Materials

Zinc nitrate hexahydrate ($Zn(NO_3)_2{\cdot}6H_2O$), magnesium nitrate hexahydrate ($Mg(NO_3)_2{\cdot}6H_2O$), and aluminum nitrate nonahydrate ($Al(NO_3)_3 \cdot 9H_2O$) were obtained as analytical reagents (AR) with a purity greater than 99.0% from Sigma Aldrich. Sodium hydroxide (NaOH, AR, >96.0%) and sodium carbonate (Na_2CO_3, AR, >99.5%) were also purchased from Sigma Aldrich. Additionally, OA, ($CH_3(CH_2)_7CH = CH(CH_2)_7COOH$) was sourced from the same supplier (**Figure.3.1-a**). ShinTech Inc supplied the PVC resin suspension (grade K=70), while diisononyl phthalate (DINP, $C_{26}H_{42}O_4$)(**Figure.3.1-b**) and the calcium/zinc thermal stabilizer came from Evonik Oxeno LLC and AM Stabilizers, respectively.

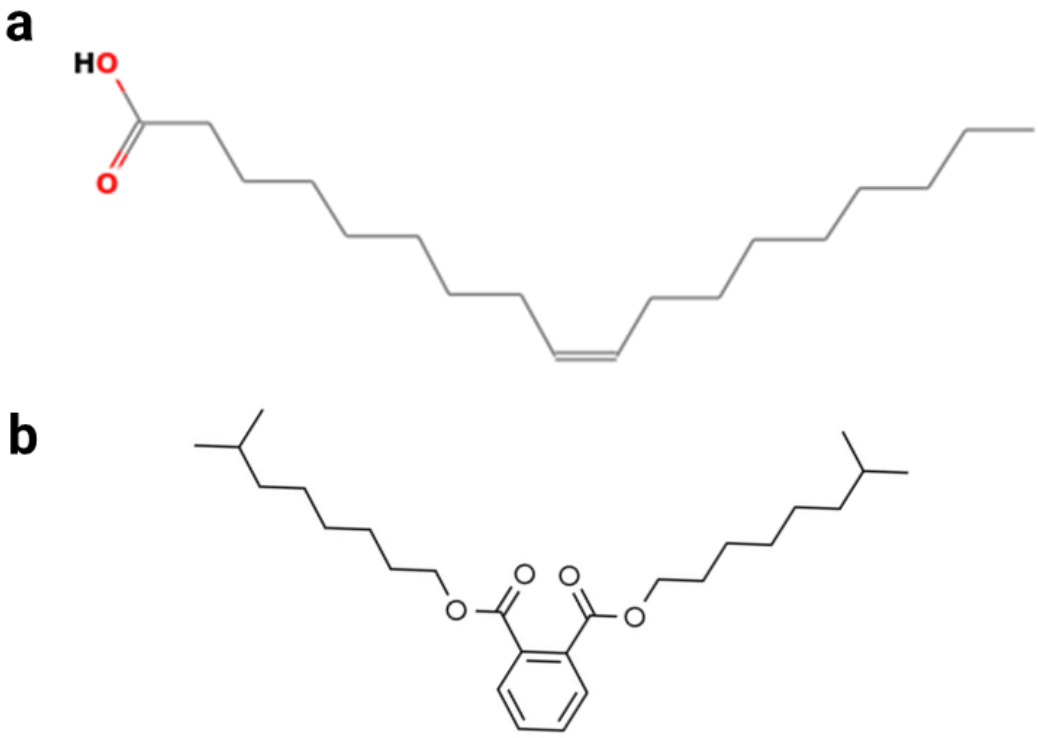

Figure 3.1: Chemical structures of a) Oleic Acid and b) DINP.

3.2 Methods

3.2.1 Synthesis of LDH-derivatives

To synthesize LDHs, three different metal compositions were considered. The Mg/Zn ratio, denoted as 'R,' varied at 0.5, 1, and 2 (detailed in **Table.3.1**). Initially, the metal hexahydrates were dissolved in 500 mL of deionized water (referred to as solution A). The precipitant solution (solution B) consisted of 1 mol/L NaOH and 0.1 mol/L Na_2CO_3 blended in 100 mL of deionized water. Next, 100 mL of deionized water was added to a three-necked flask, followed by the addition of solution A, which was vigorously stirred. Solution B was then gradually added dropwise at 80°C, maintaining the solution pH at 11±0.1 throughout the reaction. The resulting precipitate was incubated at 80°C for

24 hours under a nitrogen atmosphere and subsequently centrifuged three times using a mixture of deionized water and ethanol (1:1). Finally, the thick slurry solution was vacuum-dried for 18 hours at 60°C until a white powder was obtained. A schematic of the procedure is shown in (**Figure.3.2-a**).

Table 3.1: Formulation of synthesized LDHs.

Sample Code	Mg (mmol)	Al (mmol)	Zn (mmol)	R (Mg/Zn)	Mg+Zn/Al
LDG-0.5R	0.65	1	1.3	0.5	2
LDH-R	1	1	1	1	2
LDH-2R	1.3	1	0.65	2	2

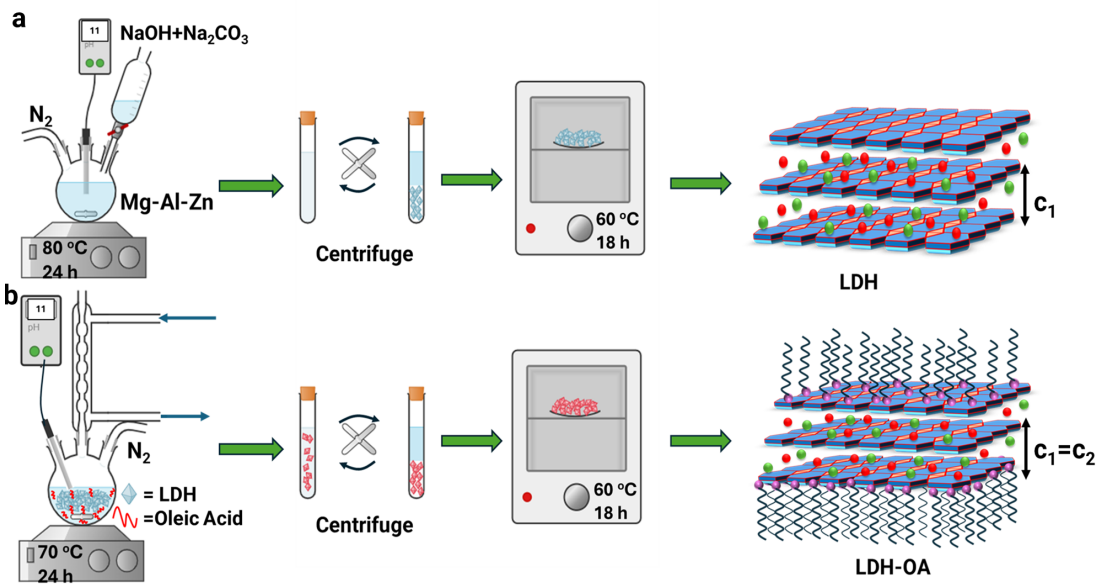

Figure 3.2: Schematic of LDH a) synthesis and b) surface modification.

3.2.2 LDH surface modification

In their study, Obata et al. [129] investigated sodium oleate (SOA)/Mg–Al–SO_4–LDH systems for drug delivery applications. When the SOA/LDH concentration was $\geq$ 5 mM, the SOA group modified the LDH surface without ion exchange. However, for SOA/LDH

concentrations $\leq$ 10 mM, SOA penetrated between the layers, leading to ion exchange. Interestingly, there is no available information for SOA/LDH concentrations between 5 and 10 mM. To address this gap, we explored OA/LDH ratios of 3, 6, 9, and 12 mM (detailed in **Table.3.2**). The surface-modified LDHs were prepared as follows: Methanol and OA were mixed under stirring, and MgZnAl-CO_3 LDHs were added. The temperature was maintained at 70°C for 24 hours, followed by centrifugation and drying, similar to the previous steps as shown in (**Figure.3.2-b**).

Table 3.2: Formulation of surface-modified LDHs.

Sample Code	Mg (mmol)	Al (mmol)	Zn (mmol)	R (Mg/Zn)	Mg+Zn/Al	OA/LDH mmol
LDH-2R-3OA	1.3	1	0.65	2	2	3
LDH-2R-6OA	1.3	1	0.65	2	2	6
LDH-2R-9OA	1.3	1	0.65	2	2	9
LDH-2R-12OA	1.3	1	0.65	2	2	12

3.2.3 Preparation of PVC-compounds

To prepare the plasticized PVC compounds, first, the dry blends were created based on the formulation reported in **Table.3.3**. Subsequently, all the dry blends underwent melt mixing under identical conditions: a temperature of 150°C and a torque of 50 rpm for 7 minutes using a batch mixer. After compounding, the plasticized PVC sheets were prepared via compression molding. The process involved maintaining the compounded mixture at 150°C for 5 minutes as a preheating step, followed by applying a pressure of 10 MPa for an additional 5 minutes. The plasticized PVC sheets are presented in **Figure A.1** in the Appendix A.

Table 3.3: Formulation of plasticized PVC compounds.

Sample Code	PVC	Plasticizer	Thermal stabilizer	LDH	LDH code	Sample ID
Control	100	45	2.5	0	-	CS
Compound1	100	45	2.5	2.5	0.5R	C-R0.5
Compound2	100	45	2.5	2.5	R	C-R
Compound3	100	45	2.5	2.5	2R	C-R2

*The unit for all components is phr (per hundred resin).

3.3 Material characterization

3.3.1 LDH characterization

3.3.1.1 Structural Analysis

The crystallinity of the synthesized LDH was determined through powder X-ray diffraction (PXRD) analysis conducted at the McMaster Analytical X-Ray Diffraction Facility (MAX). $CuK\alpha$ radiation ($\lambda = 0.154nm$) was employed within a 2θ range from 5° to 80°. Additionally, the infrared spectra were acquired using a Thermo Scientific Nicolet 6700 FT-IR Spectrophotometer, covering the wavenumber range of 4000–400 cm^{-1}. The powder sample was mixed with KBr and pressed into pellets. The FTIR spectra were collected with 64 scans and a resolution of 1 cm^{-1}.

3.3.1.2 Textural and Morphological Analysis

The specific surface area (SSA) and pore size distribution measurements were conducted using a Quantachrome ASiQwin instrument. Nitrogen gas (N_2) served as the adsorbate at 77 K. The Brunauer-Emmett-Teller (BET) method was employed to determine the surface area through a multipoint approach, while the Barrett-Joyner-Halenda (BJH) desorption

method was utilized to calculate the pore size distribution. Before analysis, samples were degassed at 120 °C for 12 hours to remove any adsorbed species. Additionally, the surface morphology of the LDH was investigated using scanning electron microscopy (SEM) with an FEI Magellan 400 instrument, operating at an accelerating voltage of 1-2 kV. LDH suspensions in water were deposited onto a holder, affixed to a platinum-coated grid, and imaged after natural drying at room temperature.

3.3.1.3 Surface and Compositional Analysis

X-ray photoelectron spectroscopy (XPS) analyses were conducted using a PHI Quantera II scanning XPS microprobe (Physical Electronics, USA). High-resolution scans were performed for the C 1s, O 1s, Zn 2P ($2P_{\frac{3}{2}}$ and $2P_{\frac{1}{2}}$), Al 2P, and Mg 1S regions. Peak fitting for the C 1s, O 1s, Zn 2P ($2P_{\frac{3}{2}}$ and $2P_{\frac{1}{2}}$), Al 2P, and Mg 1S peaks involved Gaussian functions after background subtraction. Additionally, inductively coupled plasmaatomic emission spectroscopy (ICP-AES) was employed to determine the metal elemental composition.

3.3.1.4 Thermal Analysis

The thermal gravimetric analysis (TGA) thermograms were obtained during the heating process using a Thermo Gravimetric Analyzer (TA Q50) under a nitrogen gas atmosphere. The heating rate was set at 10 °C/min, ranging from room temperature to 700°C.

3.3.2 PVC compounds characterization

3.3.2.1 Structural and Morphological Analysis

Raman spectroscopic measurements were conducted using a Renishaw InVia spectrometer equipped with an Ar ion laser (532 nm and 785 nm, power 50 mW), a Leica DMLM confocal microscope, and a CCD detector. The Raman spectra were recorded using 5%

of the laser power, covering the spectral range of 200–4000 cm^{-1} with a resolution of 3 cm^{-1}. Three data points were collected for each investigated sample. Additionally, FT-IR was employed to study PVC sheets, covering the wavenumber range of 4000–400 cm^{-1}. Furthermore, to investigate the morphology and compatibility of LDHs with PVC, SEM and energy-dispersive spectroscopy (EDS) analysis of SEM micrographs were performed.

3.3.2.2 Thermal stability of PVC compounds

To determine the thermal properties of PVC compounds, we employed Congo Red (ISO 182-1, 1990), Dehydrochlorination (ISO 182-2: 1990-12), Discoloration (ISO 305-4, 1990), and TGA methods. In the Congo Red test, a PVC sample was placed in a closed test tube, and a strip of Congo Red paper was positioned at the top of the tube. The color change was observed when the test tube was immersed in an oil bath at 180°C. For the discoloration test, PVC films (cut to 10×10 mm with a 1 mm thickness) were heated in an oven at 180°C, and the color change was monitored every 10 minutes. Color measurements were obtained using a VEYKOLOR Pro color meter by Equation (3.1):

$$\Delta E^2 = \sqrt{\Delta L^2 + \Delta A^2 + \Delta B^2} \tag{3.1}$$

Where ΔL^2, ΔA^2, and ΔB^2 values represent white (+) and black (-), red (+) and green (-), and yellow (+) and blue (-), respectively. The ΔL^2 and ΔB^2 value is chosen to describe the discoloration of PVC sheets which measures the difference between the sample before thermal aging as a reference and the sample after thermal aging. A low ΔE^2 value corresponds to minimal color difference. In the dehydrochlorination test, 2 grams of PVC compounds were placed in a test tube within an oil bath at 180°C (**Figure A.2** in the Appendix A). The released HCl gas in the test tube was carried by N_2 gas to 100 ml of deionized water at room temperature. The conductivity of the water was measured

using a Metrohm 913 pH meter with a resolution of 0.01. Before conducting the tests, the negligible conductivity value provided by the conductometer was assumed to be zero. Additionally, we performed TGA characterization on PVC compounds, heating them from room temperature to 700°C in an N_2 atmosphere.

Chapter 4

Impact of LDH on PVC

4.1 Structural analysis of LDH

The powder X-ray reflection pattern of LDHs comprises two main groups: strong (003) reflections at low angles, indicating the basal spacing of LDHs. It represents the thickness of a brucite-like layer along with an interlayer [130]. The basal spacing depends on factors such as the water content between the layers, the composition of anions in the interlayer gallery, and the average charge of the metal cations [131]. This parameter is denoted as c and can be determined using the procedure in [132]:

$$c = \frac{1}{3}(3d_{003} + 6d_{006} + 9d_{009}) \tag{4.1}$$

The (110) position at an angle of $2\theta = 60$ corresponds to the lattice parameter $a_0(a_0 = 2d_{110})$, which represents the distance between metal-metal cations [16,133] . As depicted in **Figure.4.1-a**, the reflection patterns observed at specific crystallographic planes, namely (003),(006),(009), and (110), exhibit narrow widths. This observation suggests the presence of well-organized crystal lattices devoid of any impurities or accompanying by-products. The corresponding indices align with the diffraction angles illustrated in the **Figure.4.1-**

a, confirming that each plane reflects X-rays at distinctive angles. This finding serves as concrete evidence of the sample's high purity and crystalline nature [132]. Additionally, the intensity of the peaks observed at the mentioned planes confirms the presence of a rhombohedral crystal lattice, which is typically expected in brucite-based structures [134].

As depicted in **Table.4.1**, the values of c and a_0 decrease with the increase of the $\frac{Mg}{Zn}$ ratio. This is consistent with previous studies, which have shown that as the $\frac{Mg}{Zn}$ ratio in $M^{II}Al$ LDHs increases, the smaller ionic radius of $Mg^{2+}(0.72\mathring{A})$ compared to $Zn^{2+}(0.74\mathring{A})$ leads to a reduction in cation-cation distances, thereby decreasing the value of a_0 under similar conditions [12, 130]. Specifically, the equation $a_0 = \sqrt{2d(M-O)}$, d(M-O) that M-O is the metal-oxygen band length, demonstrates the direct relationship between the radius of metal cations and a_0 [130]. Molecular dynamics simulations performed by Riahi et al. [135] have shown that Zn(II) ions exhibit distinctive solubility structures and hydration energies compared to Mg(II) ions. Consequently, the reduction in lattice parameter c with a higher $\frac{Mg}{Zn}$ ratio can be attributed to the variations in hydration and ionic radii of Zn(II) and Mg(II) ions. The Zn(II) ions not only have a slightly larger ionic radius but also more favorable hydration energy, resulting in enhanced solubility and expanded interlayer spacing.

Table 4.1: Lattice parameters of unmodified LDHs.

Sample Code	$2\theta(003)$	$2\theta(006)$	$2\theta(009)$	$2\theta(010)$	d_{003}	c	a_0	D
LDH-0.5R	11.526	25.226	38.726	64.546	0.767	2.169	0.306	24.017
LDH-R	11.563	25.233	37.783	60.443	0.764	2.165	0.288	23.156
LDH-2R	11.588	25.308	38.698	60.828	0.763	2.163	0.269	23.11

*The unit of θ is degree and the unit of crystal parameters are nm.

The stronger interaction between Zn(II) ions and water molecules, along with the larger hydration shell surrounding Zn(II) ions, causes the layers to move further apart, thereby increasing the lattice parameter c. The average crystal size in (003) direction is reported

in **Table.4.1** and calculated by Scherrer's equation [14]:

$$D = \frac{0.9\lambda}{\beta \cos\theta} \tag{4.2}$$

λ is the wavelength of the X-ray used in nm, β is the full width at half maximum (FWHM-in radian) of peak (003), and θ is the Bragg diffraction angle in degree.

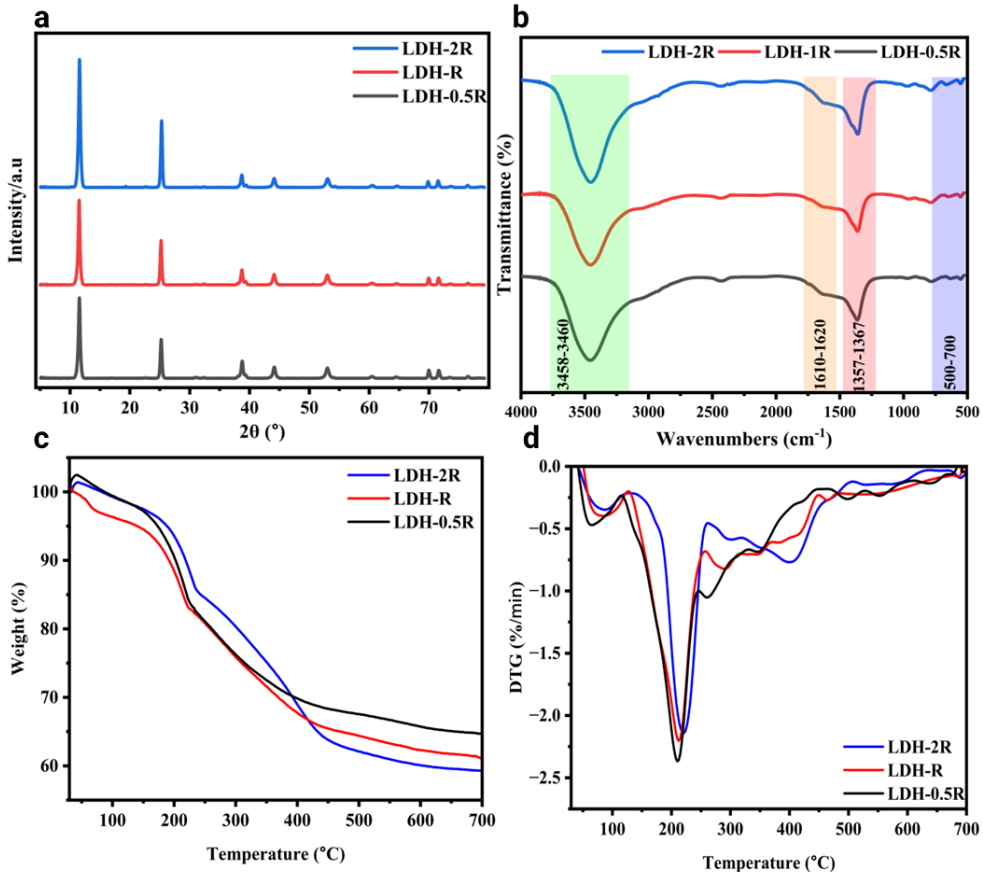

Figure 4.1: a) Powder X-ray diffraction patterns, b) FT-IR spectra, and c) TGA of LDH-0.5R, LDH-R, and LDH-R2.

The FTIR spectra of synthesized LDHs are shown in **Figure.4.1-b**. The broad peak observed between 3450-3460 cm^{-1} can be attributed to the stretching of OH groups bound to Al, Mg, and Zn ions in the layers and interlayer water molecules [132, 136]. The strong antisymmetric vibration of CO_3^{2-} is evident at 1357-1367 cm^{-1} [137]. The weaker peak

observed at around 1610-1620 cm^{-1} corresponds to the bending mode of water molecules [138,139]. Additionally, several absorption peaks below 800 cm^{-1} can be attributed to the stretching vibration patterns between the metal cation and oxygen atoms, such as Mg—O, Zn—O, and Al—O [137,139].

The results of the LDHs' thermal stability, measured by TGA, are presented in **Figure.4.1-c**. All samples exhibited a weight loss of up to 58% across four degradation stages. The TGA results indicate a step-by-step decomposition process, consisting of four stages. The first stage occurs between 50 °C and 150 °C, the second range between 150 °C and 255 °C, the third stage between 255 °C and 515 °C, and the fourth temperature range lies between 515 °C and 700 °C. In the first stage, water and absorbed gases are lost [16]. The weight loss during the second stage (150°C -255°C) is attributed to the loss of interlayer water molecules [140]. As mentioned earlier, the increase in the amount of Zn in LDHs formulations leads to a higher absorption of water between the layers due to the greater affinity of Zn towards water. Consequently, the weight loss values during this stage were observed to be 17.08%, 16.6%, and 15.8% for LDH-0.5R, LDH-R, and LDH-2R, respectively. In the third stage (255°C - 515°C), weight loss is associated with the decomposition of CO_3^{2-} anions, resulting in the release of CO_2 and water due to the dehydroxylation of OH groups [141]. As shown in **Figure.4.1-d**, with increased R ratios (which indicates a higher Mg content), the third stage shifts to a higher temperature, and the rate of mass loss increases. This shift to a higher temperature can be attributed to the greater thermal stability of the Mg-rich phases, which require more energy (higher temperature) to decompose. Consequently, the decomposition and subsequent weight loss are delayed. The observation that LDH-0.5R exhibits a lower weight change in stage 3 (16.86%) is due to a greater loss of interlayer water molecules in stage 2. Conversely, with the increase in Mg content, the weight loss for LDH-R (19.54%) and LDH-2R (24.57%) increases in stage 3. This is because the higher Mg content leads to the formation of more thermally stable

phases, resulting in greater weight loss at higher temperatures. The higher temperatures observed in the fourth stage (515 °- 700 °C) can be attributed to the formation of metal oxides [142]. This stage entails the final decomposition and creation of stable metal oxide structures, which further contribute to the overall decrease in weight. Regarding the residual weight, it should be noted that despite the increased R ratio resulting in greater mass loss in stage 3, LDH-2R ultimately ends with a lower final weight. This can be explained by the overall extensive decomposition and loss of CO_3^{2-} and OH groups in the third stage, which more than compensates for the lesser weight loss observed in stage 2.

Table.4.2 shows the BET surface areas (δ_{BET}), total pore volumes (ν_p), and pore radius (R_p) for synthesized LDHs. The BET surface areas were obtained for LDH-2R, LDH-R, and LDH-0.5R samples 7.825 m^2g^{-1}, 7.752 m^2g^{-1}, and 7.732 m^2g^{-1}, respectively. Furthermore, the radius and volume of the pores decrease as the Mg/Zn ratio increases. This is evident from the greater X-ray diffraction intensity (**Figure.4.1-a**) of the LDH-2R compared to LDH-0.5R in the 003 phase, indicating a more packed and denser arrangement of crystal lattice structures. Additionally, the ICP analysis reveals that the ratios of Mg/Zn and (Mg+Zn)/Al are consistent across all samples, albeit with some minor deviation. **Figure.4.2** displays the SEM images depicting the structure and morphology of the synthesized LDHs. The structure of LDH nanoparticles transforms from a lumpy structure to a hexagonal flake structure as the Mg/Zn molar ratio increases. The structural analysis confirms that the synthetic materials belong to the category of LDH materials, displaying various compositions within the metal host. In particular, the morphology of LDHs closely aligns with the MgAlZn-LDH synthesized by Labuschagn [15] for thermal stabilizer application. Furthermore, Zhou [143] demonstrated that the $d_0$03 basal spacing value for MgAlZn-CO_3 is 0.778 nm, which closely corresponds to our findings.

Table 4.2: Structural Parameters and ICP-MS results of unmodified LDHs.

Sample Code	δ_{BET} (m^2g^{-1})	ν_p (ccg^{-1})	R_p (Å)	Atomic ratio (R^1)		*ICP*
				Theoretical	Experimental	
LDH-0.5R	7.825	0.053	19.457	0.5	0.516	$[Mg_{1.20}Zn_{2.32}Al_{1.69}(OH)_{10.1}]\cdot(CO_3)_{5.07}$
LDH-R	7.752	0.053	19.232	1	1.006	$[Mg_{1.70}Zn_{1.69}Al_{1.66}(OH)_{10.1}]\cdot(CO_3)_{5.07}$
LDH-2R	7.732	0.051	19.194	2	2.041	$[Mg_{2.41}Zn_{1.18}Al_{1.67}(OH)_{10.1}]\cdot(CO_3)_{5.07}$

$1\cdot R = Mg/Zn$.

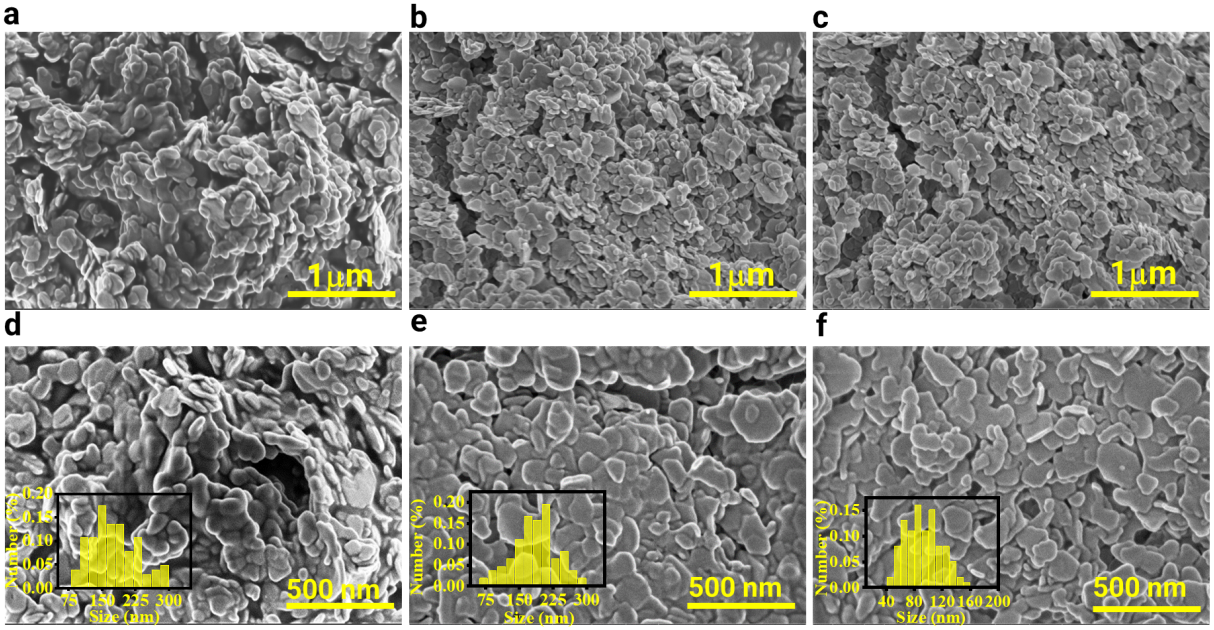

Figure 4.2: SEM images of a) LDH-0.5R, b) LDH-R, and c) LDH-2R ($1\mu m$, × 80 000). The bottom row shows the same materials at higher resolution: d) LDH-0.5R, e) LDH-R, and f) LDH-2R (500 nm, × 150 000).

4.2 Impact of LDH on Thermal Properties of PVC Compounds

The FTIR spectra of PVC compounds containing the LDH materials are shown in **Figure.4.3 -a**. In the CS samples, the peaks at 2957 cm^{-1} and 2925 cm^{-1} can be attributed to CH stretching in $CH-Cl$ and $C-H$ stretching in CH_2, respectively [144, 145]. The peak at

1720 cm^{-1} corresponds to the C=O bond of DINP, while the peak at 1122 cm^{-1} corresponds to the C−O bond of DINP. Additionally, the peak at 1427 cm^{-1} signifies CH_2 bending, while the peak at 1354 cm^{-1} represents C-H bending in CH−Cl [146]. Furthermore, the peak at 1074 cm^{-1} corresponds to the C−C stretching of the PVC backbone [145, 146], and the peak at 961 cm^{-1} signifies CH_2 bending. All the peaks at 830 cm^{-1}, 700 cm^{-1}, and 614 cm^{-1} can be assigned to C−Cl bonds [146]. The peaks at 1600 cm^{-1} and 1579 cm^{-1} are attributed to C=C bonds [144]. The peak at 1256 cm^{-1} represents the bending bond of C−H close to Cl [146, 147]. With the introduction of LDHs to PVC compounds, the broad peak around 3420-3450 cm^{-1} indicates the presence of OH groups and interlayer H_2O of LDHs in the compounds. Additionally, the peaks at 583 cm^{-1} (**Figure.4.3 -b**) and 611 cm^{-1} (**Figure.4.3 -c**) are assigned to the metal-O stretching of LDHs [13].

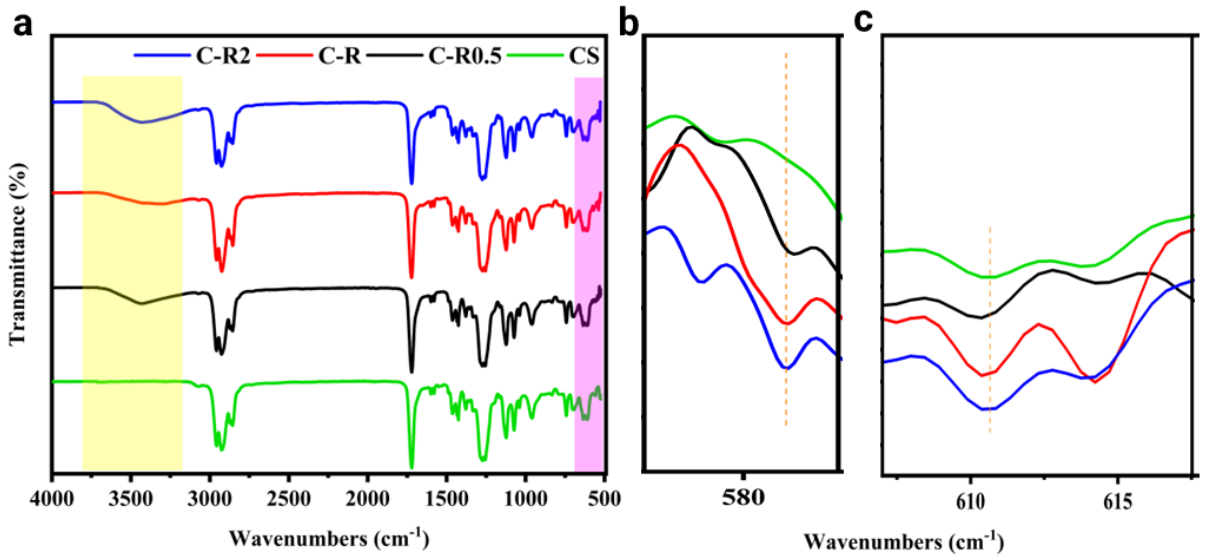

Figure 4.3: FT-IR spectra of a) unmodified PVC compounds and b-c) the enlarged view near metal-oxygen bands.

With the initiation of PVC degradation, HCl is released into the system. The starting time for this process can be determined using the Congo red test as a measure of static thermal stability (STS) [17] (**Figure.4.4 -a**). The indicator paper of the CS compound changed from orange to red after 55 minutes, indicating the autocatalytic degradation of

PVC and an increase in HCl concentration in the system. By incorporating LDHs into PVC compounds, the degradation time increased to 80, 87, and 96 minutes for the C-R0.5, C-R, and C-R2 samples, respectively. This corresponds to a 42% improvement in STS for the C-R2 sample compared to the CS, demonstrating the LDHs' ability to scavenge released HCl and inhibit PVC autocatalytic degradation. Labuschagne et al [16] reported with the incorporation of MgAlZn-LDH (Mg+Zn/Al=2) the STS increased from 25 to 98 minutes which is close to our results. In the dehydrochlorination test, PVC degradation was monitored using the water electroconductivity trend (**Figure.4.4 -b**). In this method, the released HCl is carried by N_2 gas to deionized water, and the increasing rate of H^+ concentration indicates the rate of PVC degradation. Guo et al. [118] defined the onset time of degradation as the induction time (t_1), and the minimum point of electroconductivity as the stability time (t_2). For the C-R2 sample, the electroconductivity after 160 minutes was 4.35 mS/cm, while the corresponding times for the CS, C-0.5R, and C-R samples were 116, 130, and 145 minutes, respectively. This demonstrates that LDHs, particularly at higher Mg/Zn ratios, possess the highest capacity to regulate the release of HCl. These results are consistent with the study by Wang et al. [119], which investigated the effect of metal compositions on HCl absorption in PVC compounds.

The color changes of the samples, maintained at 180 °C for 10 to 180 minutes, are depicted in **Figure.4.5 -a**. Over time, all samples transitioned from yellow to brownish-yellow and eventually to black. The CS compound turned yellow after 20 minutes, and black spots appeared on the CS sheets after 70 minutes. The CS sample became black within 80 minutes, earlier than the degradation of all LDH-treated compounds. This suggests that the zipper autocatalytic dehydrochlorination process was more rapid in the CS sample than in LDH-treated samples [148]. During the early stages of testing, the C-0.5R compound demonstrated better color stability compared to C-R and C-R2 compounds. However, after 30 minutes, the C-0.5R sample rapidly changed color to brown. As dis-

cussed in the previous section, the Zn cation has a larger radius, and its electronegativity (1.65) exceeds that of Mg (1.31). These parameters have distinct effects on the thermal stability of PVC compounds over short and long durations [130].

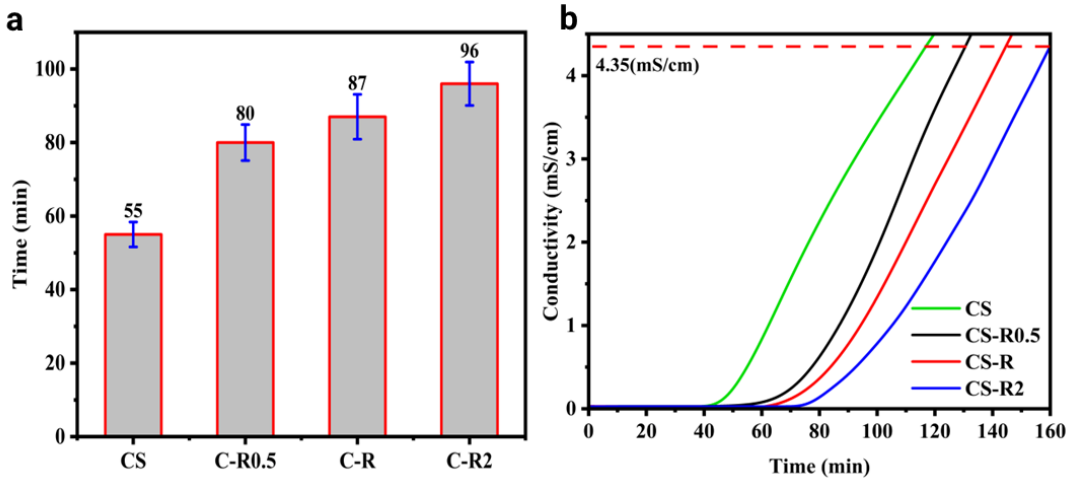

Figure 4.4: a) Static thermal stability (Congo red) at 180 °C, and b) HCl release curves for the PVC samples heated at 180 °C (Dehydrochlorination) of CS, C-0.5R, C-R, and C-R2 compounds.

In the short term, Zn's greater electronegativity influences the interactions between hydroxyl groups and host layers, while its larger radius weakens M-O bonds. These reactions facilitate HCl absorption by LDHs and prevent HCl migration within the system. However, in the long term, Zn can form $ZnCl_2$ groups during PVC degradation—a phenomenon known as zinc burn. This acts as a superior catalyst for the dehydrochlorination reaction, accelerating PVC degradation55. **Figure.4.5 -a,c** illustrates the changes in ΔB and ΔE (in 4.1) as functions of PVC degradation. The ΔB value for CS-0.5R is initially lower than that of the C-R2 compound within the first 30 minutes. However, after 40 minutes, ΔB sharply increases and then decreases with a high slope. In contrast, the ΔB of the C-R2 compound increases more gradually, remaining nearly constant between 100 and 140 minutes before decreasing. This behavior highlights Mg's ability to enhance the long-term thermal stability of PVC compounds. Similarly, ΔE follows a similar pattern. Initially, the C-0.5R sample exhibits better thermal stability than other LDH-treated samples. However,

with increasing time, the C-0.5R sample experiences sharp increases in ΔE. Meanwhile, ΔE increases more moderately with Mg incorporation, and the ΔE value decreases when additional Mg is incorporated into the compounds.

Generally, the color stability of PVC is primarily attributed to the formation of polyenes, which are conjugated double bonds that originate from dehydrochlorination and lead to discoloration. However, achieving color stability is not solely dependent on polyene formation. Specific stabilizers, such as Mg and Zn in the form of MgAlZn-LDH, have distinct roles in interacting with the degradation process. At a molecular level, the presence of Mg enhances thermal stability by scavenging chloride ions and inhibiting dehydrochlorination, thereby delaying the breakdown of the polymer. On the other hand, Zn has a more noticeable influence on color stability as it restricts polyene formation and interacts with UV light to minimize discoloration. The difference between thermal and color stability lies in their respective focuses: thermal stability impedes polymer breakdown, while color stability regulates visual degradation such as the occurrence of yellowing resulting from the emergence of conjugated structures.

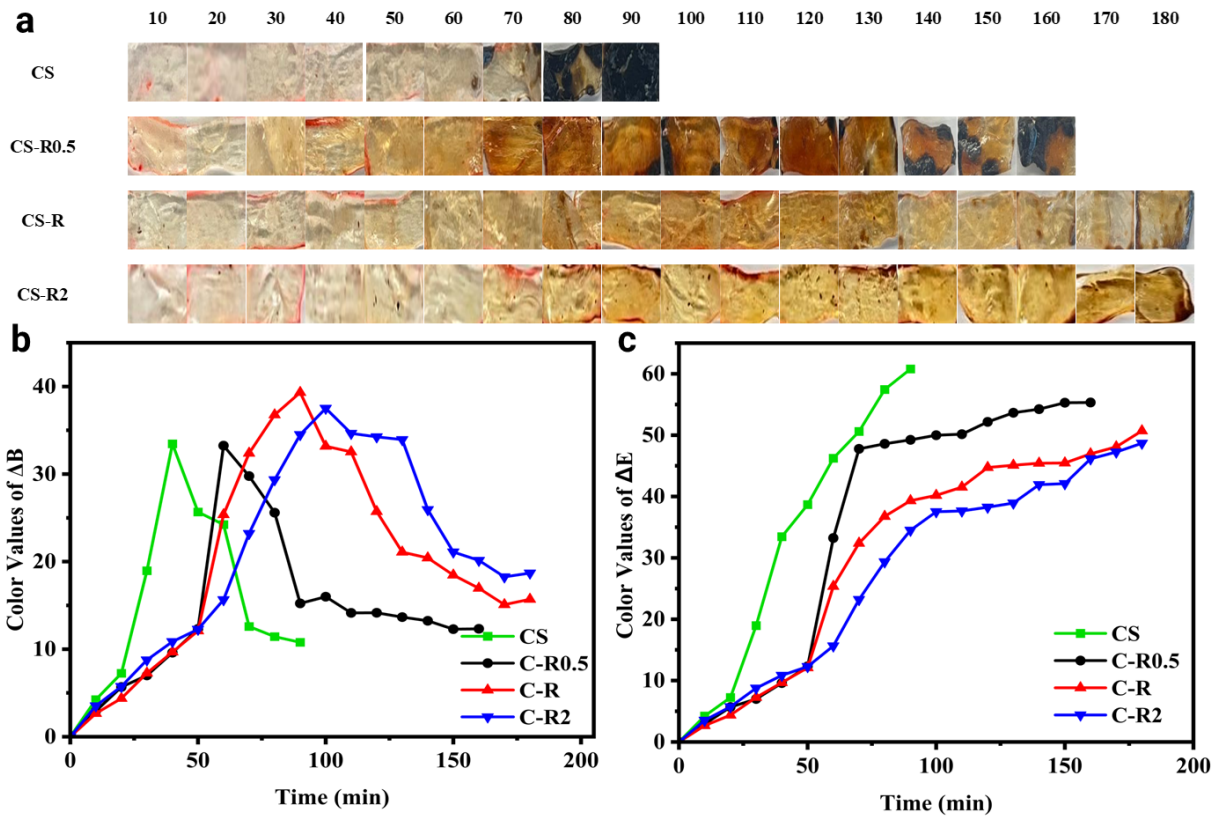

Figure 4.5: a) Changes in color profile of discoloration test for unmodified LDHs-PVC compounds at 180 °C from 10 to 180 minutes. Color change test results for a) δB and b) δE at 180 °C.

The thermal gravimetric analysis (TGA) and differential thermogravimetry (DTG) curves of PVC compounds in an N_2 atmosphere are presented in **Figure.4.6 -a** and **Figure.4.6 -b**, respectively. The curves reveal two distinct stages of thermal degradation in all the compounds. The first stage occurs within the temperature range of 250-400°C and is associated with dehydrochlorination. The second stage, which takes place between 400-550°C, is attributed to the degradation of polyene sequences and remaining polymer structures, as well as the formation of char [149]. In comparison to the LDH-doped samples, the CS sample exhibits these stages at lower temperatures. Detailed TGA data (in **Table A.1** in Appendix A) provide the assigned temperature for a 5% weight loss ($T_{5\%}$), which occurs after the T_{onset} (**Figure.4.6 -c**), indicating that the CS sample has a higher

or equivalent assigned temperature in comparison to the samples with LDHs. Furthermore, by incorporating LDHs with a higher Mg content, the T_{max} shifted to a higher temperature (**Figure.4.6 -d**), accompanied by a decrease in the intensity of weight loss. LDHs belong to the suppressive class of PVC thermal stabilizers, meaning that they absorb or neutralize the HCl produced during PVC degradation [150]. The reaction mechanism between LDHs and HCl occurs in two stages. In the first stage, the HCl gas reacts with the available anions in the interlayer gallery, resulting in the exchange of chloride ions (Cl^-) and the formation of intercalated Cl between the layers. As the rate of PVC degradation increases and more HCl gas is released, the hydroxyl groups (OH^-) in LDHs neutralize the acidic nature of HCl by absorbing hydrogen ions (H^+), leading to the formation of water (H_2O) and chloride ions (Cl^-). Subsequently, the metal cations (M^{2+} and M^{3+}) within the LDH structures react with Cl^- to form metal chloride compounds, thus inhibiting the migration of HCl throughout the matrix [19]. Hence, owing to the substantial absorption capacity of LDHs, they can markedly enhance the thermal stability of PVC.

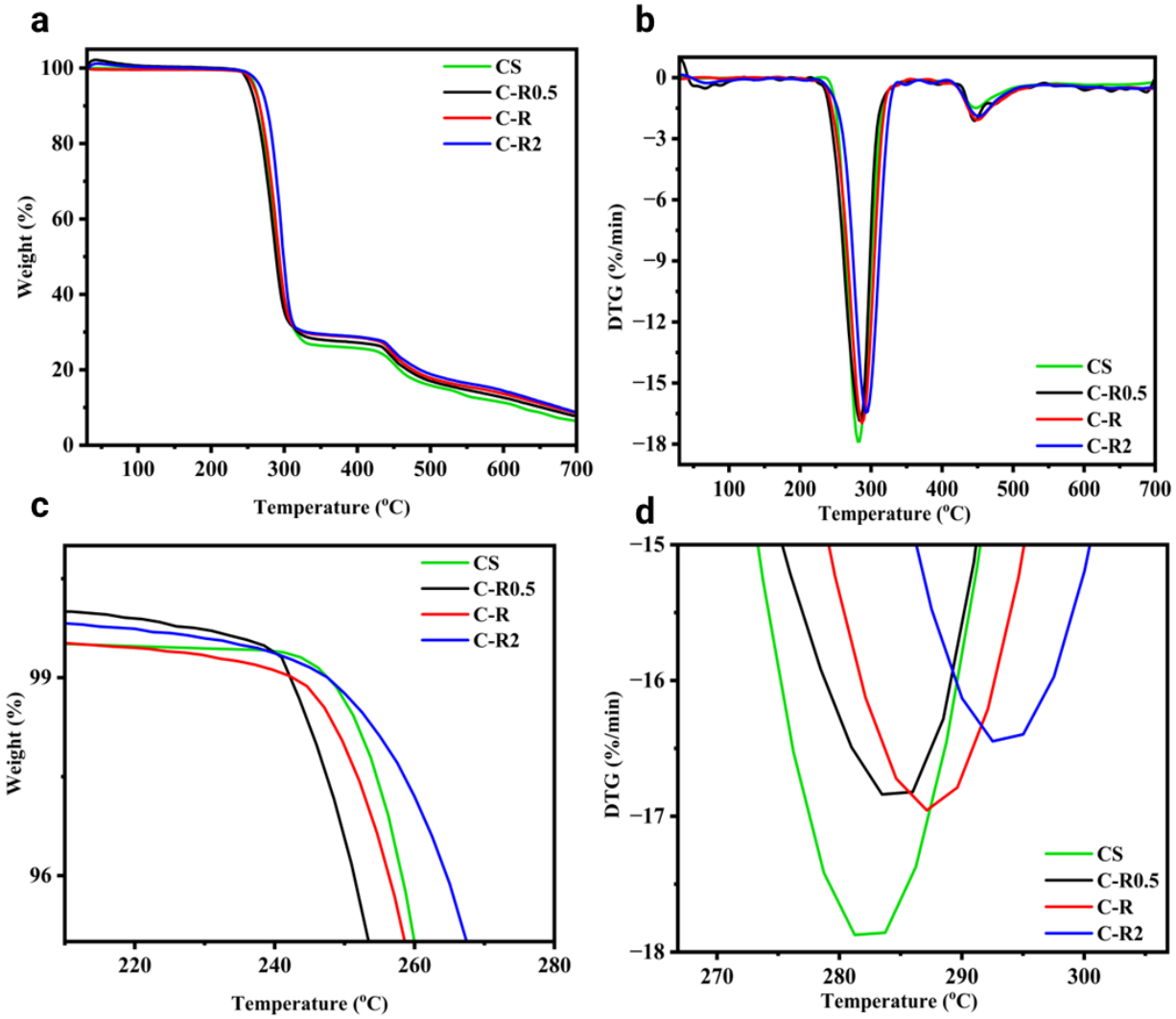

Figure 4.6: a) TGA, d) DTG, the enlarged view near c) T_{onset}, and d) DTG peak in stage I of CS, C-0.5R, C-R, and C-R2 compounds.

Chapter 5

Impact of LDH Surface Modification on PVC

5.1 Surface Modification of LDH with Oleic Acid

When OA is introduced to LDH structures, it interacts with LDH at two levels: either absorbed to the surface through its carboxylic acid head or placed between the layers [151]. These interactions directly impact the crystallinity of LDHs because of changes in the chemistry of the LDHs' surface and the interlayer distance [151, 152]. Powder X-ray patterns showed (**Figure.5.1-a**) distinct trends in the 2θ and FWHM values of LDHs modified with different amounts of OA.

The 2θ values for LDH-2R, LDH-2R-3OA, LDH-2R-6OA, and LDH-2R-9OA were relatively close, ranging from 11.58°to 11.61°. Additionally, the calculated basal space value (c) for these samples, as shown in **Table.5.1**, fell within the same range, indicating that OA groups are grafted onto the LDH surfaces, instead of being inserted between layers. As the amount of OA in the system increased, it gradually entered the interlayer spaces, as demonstrated by the LDH-2R-12OA sample with a decrease in 2θ to 11.45°degrees and

an increase in the c parameter to 2.180 nm.

Table 5.1: Lattice parameters of surface-modified LDHs compared with the unmodified case.

Sample Code	$2\theta(003)$	$2\theta(006)$	$2\theta(009)$	$2\theta(110)$	d_{003}	$Intensity_{003}$	$FWHM_{003}$	c	a_0	D
LDH-2R	11.588	25.308	38.698	60.828	0.763	22.32	0.407	2.163	0.269	23.110
LDH-2R-3OA	11.588	25.278	38.698	60.432	0.763	9.78	0.313	2.164	0.306	25.430
LDH-2R-6OA	11.618	25.328	38.688	60.408	0.761	13.54	0.291	2.161	0.306	27.330
LDH-2R-9OA	11.591	25.311	38.701	60.461	0.762	18.55	0.248	2.160	0.305	32.159
LDH-2R-12OA	11.440	25.150	38.54	60.42	0.772	15.580	0.315	2.180	0.306	25.288

*The unit of θ is degree and the unit of crystal parameters are nm.

The FWHM value provides information about the size and strain of crystal structures [153]. Among the samples that underwent surface modification, LDH-2R-9OA demonstrated the smallest FWHM value of 0.248, as reported in **Table.5.1**. This suggests that a moderate concentration of OA can enhance crystal size and reduce strain compared to higher (12OA) or lower OA (3OA and 6OA) concentrations (**Figure.5.1-b**). The narrower peak in the spectrum indicates larger and more ordered crystals. Several factors can contribute to this phenomenon, including the surfactant properties of OA and its interaction mechanisms with LDH [154]. Each OA molecule possesses a hydrophilic carboxylic acid group and a long hydrophobic tail, that facilitate their adsorption onto LDH surfaces. As a result, the surface energy decreases, preventing the formation of defects and promoting improved crystallinity in LDH-2R-9OA. This leads to favorable conditions for the growth of crystallites and the stabilization of LDH structures. In contrast, Xu et al. [155]demonstrated that the presence of OA in the surface modification of MgZnAl-LDHs increased the FWHM value compared to the unmodified sample and reduced crystal agglomeration.

Furthermore, the intensity of the 003 peak in LDH-2R-9OA is lower than that of the LDH-2R sample, indicating initial disruption of the LDH structure and changes in nucleation and growth dynamics due to the influence of OA on LDH crystallization [156]. When

OA is added to LDHs in lower concentrations, the intensity of the 003 peak decreases significantly, clearly demonstrating the effect of OA. However, with higher incorporation, the intensity increases, particularly in the case of LDH-2R-9OA. Therefore, at lower concentrations, OA leads to an unstable situation for crystal reorganization and alignment. However, as the concentration of OA increases, the surface energy of LDHs decreases due to the surface-active effect of OA. This reduction in surface energy facilitates the nucleation and attachment of precursor ions to the surface, promoting the formation of stable nuclei and facilitating the nucleation process.

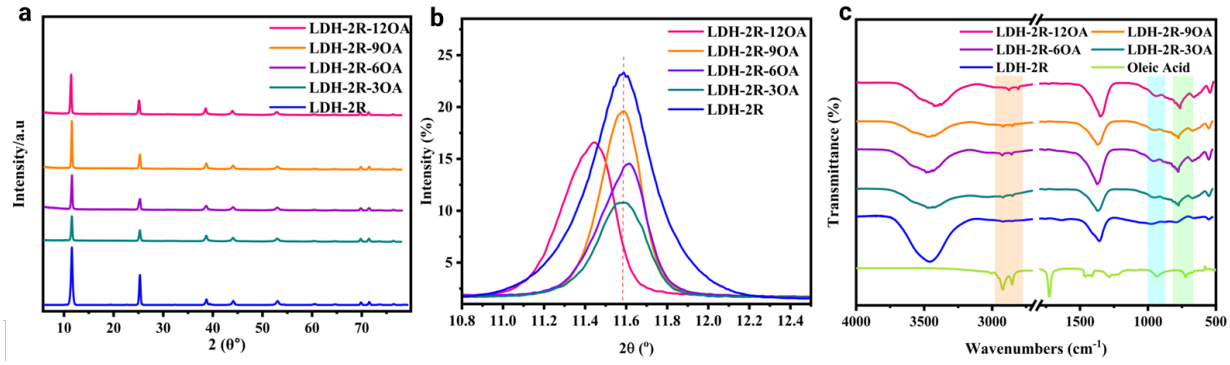

Figure 5.1: a) Powder X-ray diffraction patterns, b) Powder X-ray peaks of (003), and c) FT-IR spectra of LDH-2R (unmodified), LDH-2R surface modified with 3, 6, 9, and 12 OA.

The FTIR spectra of OA reveal several characteristic peaks as shown in **Figure.5.1-c**. The peak observed at 2860 cm^{-1} can be attributed to symmetric CH_2 stretching, while the peak at 2930 cm^{-1} corresponds to asymmetric CH_2 stretching modes [157, 158]. The peak at 3007 cm^{-1} is due to the C mode of the C bond adjacent to the C=C bond [159]. Furthermore, the peak at 1710 cm^{-1} indicates the presence of C=O, which arises from the O stretch67, [160]. The LDHs that underwent surface modification exhibited peaks that were closely like those shown in **Figure.4.1-b**. Lei et al. [161] showed in the modification of LDH by using fatty acid methyl esters the hydroxyl (−OH) group on the surface of LDH and the carboxyl (−COOH) group on the fatty acid were chemically bonded by dehydration condensation. The vibrational peaks confirm this bonding observed at 2922

and 2852 cm^{-1}, which originate from methylene asymmetric and symmetric stretches. In addition, the peak at 940 cm^{-1} is out of the plane mode of the carboxylic acid [162] , and the observed peak at 730 cm^{-1} is related to the out-of-plane bending vibrations of the C−H deformation bonds of the −CH=CH− group [163, 164]. These features indicate the presence of long alkyl chains that are branched on the surface of the LDH-2R-XOA LDHs. Taken together, these results point to the successful modification of OA on the surface of LDH-2R-XOA.

The oxidation state and chemical compositions of these LDHs were investigated using X-ray photoelectron spectroscopy (XPS). **Figure.5.1-a** presents the XPS full spectra of both modified LDHs and LDH-2R, confirming the presence of oxygen (O), carbon (C), aluminum (Al), zinc (Zn), and magnesium (Mg) elements in the binding energy range of 0-1600 eV.

The high-resolution O 1 s spectra in **Figure.5.2-b** reveals two peaks for LDH-2R samples and three peaks for surface-modified samples. The assigned binding energy for O 1 s in LDH-2R is 531.7 eV as reported in [165] before. However, after the surface modification process, the binding energy of the O 1 s peak in LDH-2R-3OA, LDH-2R-6OA, LDH-2R-9OA, and LDH-2R-12OA changes to 531.49 eV, 531.59 eV, 531.53 eV, and 531.74 eV, respectively. This indicates a significant effect of octadecyl chains on the LDHs' surface, where the C=O structures with a binding energy of 530.8 eV for LDH-2R-3OA, demonstrate the interaction between the carboxylic group of OA and the -OH group on the surface of LDHs [155, 166]. The peak area of H_2O in LDH-2R is 73.6%, while the H_2O peak area in LDH-2R-3OA, LDH-2R-6OA, LDH-2R-9OA, and LDH-2R-12OA is 41.81%, 32.69%, 34.43%, and 34.27%, respectively. These changes indicate alterations in the surface chemistry of the modified samples. Additionally, the lattice-oxide (M−O) group in LDH-2R is assigned a binding energy of 529.9 eV, which decreases by 0.49 eV after surface modification, resulting in a decrease in surface energy [165, 167]. This decrease in surface

energy contributes to the chemical stability of LDHs and improves their thermal decomposition at higher temperatures. The C 1 s XPS spectra as demonstrated in **Figure.5.2-c** show three peaks for modified and unmodified LDHs. The C bonds are observed around 284.45-284.5 eV, C bonds at 285.3-285.7 eV, and CO_3^{2-} groups at 289.4-289.5 eV. The intensity of C−C bonds increases from 3600 counts cp for LDH-2R to 4600 cp for LDH-2R-9OA, indicating the successful branching of octadecyl chains on the LDH surface, thus creating a hydrophobic environment around the LDH crystals [142,168]. Furthermore, with an increase in OA content, the CO_3^{2-} group decreases, especially in the LDH-2R-12OA sample, suggesting that the OA chains enter the LDH interlayer and increase the distance between layers. The spectra of high-resolution Mg 1 S (1303.5 eV), Al 2 p (74.4 eV), Zn $2\,p_{\frac{3}{2}}$ (1021.8 eV) and Zn $2\,p_{\frac{1}{2}}$ (1044.8 eV) which shown in **Figure A.3** in Appendix A, did not show significant changes in binding energy and peak intensity, indicating that the LDHs matrix remains unaffected by OA and that the metal sites are stable [169–172].

To quantify the amount of modification and the impact of surface modification on the thermal stability of LDHs, TGA was conducted. As depicted in **Figure.5.3-a**, the modified LDHs exhibit the same four stages of thermal decomposition as the unmodified samples. In the temperature range of 50-120°C, the changes in sample weight correspond to the desorption of physisorbed molecules [173]. However, when comparing the weight loss of unmodified LDHs with that of modified LDHs, the rate of mass loss decreases from 3.22% to 1.69% for LDH-2R and LDH-2R-12OA, respectively. This reduction in weight loss suggests that the modification reduces the release of water molecules, indicating that the modified samples are less hydrophilic and more hydrophobic. The incorporation of OA in LDH-2R-12OA likely enhances the hydrophobicity of the samples by making the surface less accessible to water, thereby reducing the amount of water retained and released during thermal decomposition. In addition, with the increase in the OA content, the second stage (120-225°C) shifted to higher temperatures (**Figure.5.3-b**), and the rate of weight loss

decreased as well. The cause of weight loss can be attributed to the presence of interlayer water molecules and the initial dehydroxylation of OH groups in the second stage.

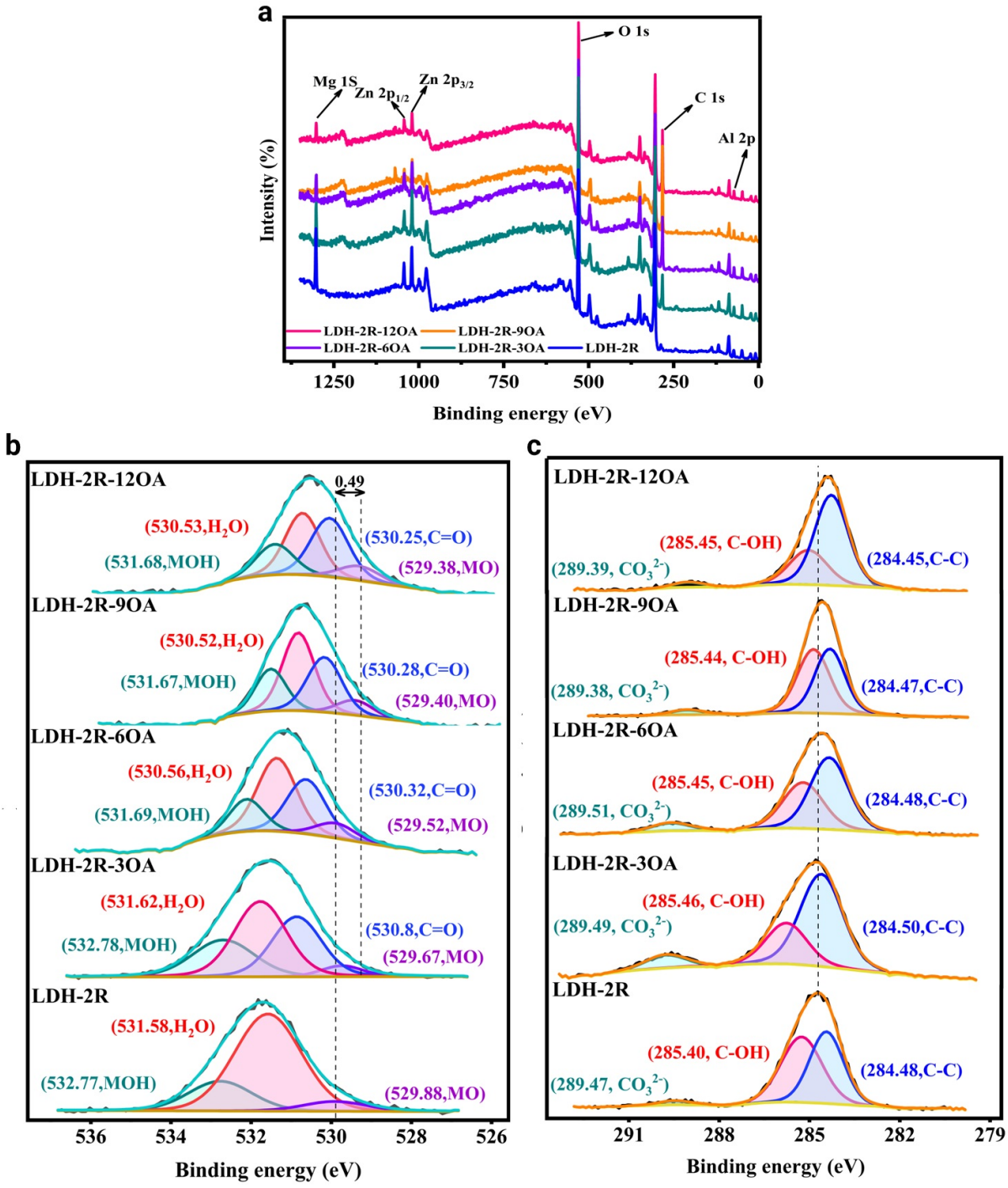

Figure 5.2: a)XPS spectra of the original and surface-modified LDHs XPS spectra for b) O 1 s, and c) C 1 s.

As shown in **Figure.5.3-c**, the weight losses at temperatures of 220°C, 232°C, 235°C, 237°C, and 240°C are 15.8% for LDH-2R, 14.5% for LDH-2R-3OA, 14.1% for LDH-2R-6OA, 13.8% for LDH-2R-9OA, and 13.3% for LDH-2R-12OA, respectively. The main event occurs in the third stage (255-504°C), involving the decomposition of interlayer anions and OA, as well as further dehydroxylation, which is more complex [174]. With an increase in OA content, the thermal degradation of this stage shifts to higher temperatures, indicating that OA improves the thermal stability of LDH samples. In a series of studies on LDHs modified with fatty acids, Xu et al. [174–176] demonstrated that in an inert environment, the degradation of organic content occurs through several processes, such as dehydrogenation, thermal cracking, and graphitization. They also suggested that the shift in decomposition to higher temperatures is due to the formation of more hydrocarbons instead of CO_2, thereby enhancing the thermal stability of OA-modified LDH samples. Furthermore, in this stage, the modified samples experience more weight loss, indicating the thermal decomposition of OA. These results are consistent with Zhang et al.'s [155] findings on LDHs modified by OA. Lastly, in the fourth stage (504-700°C), the weight loss varies, with samples containing higher OA content showing more significant weight losses due to the final decomposition of OA residues and the transformation into layered double oxide (LDO) [173].

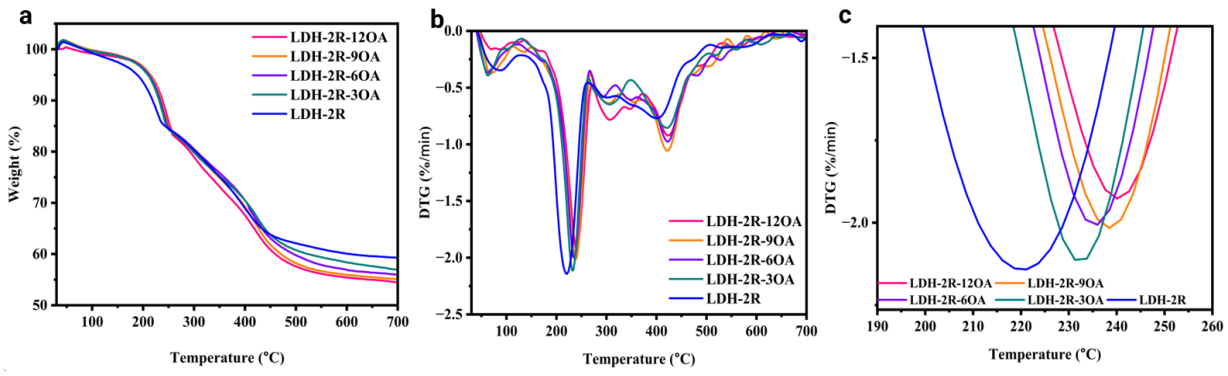

Figure 5.3: a) TGA, b) DTG, and c) DTG peaks (enlarged near stage II) of LDH-2R (unmodified), LDH-2R surface modified with 3, 6, 9, and 12 OA.

The textural parameters and the experimental atomic ratios obtained through ICP and TGA analysis are presented in **Table.5.2**. As the OA to LDH ratio increases from 3 to 12, the specific surface area exhibited a gradual increase from 8.025 to 8.852 m^2/g. Additionally, the pore size increased significantly from 15.3 to 19.2 with the increase in the amount of OA, which suggests that grafting oleic acid leads to the widening of existing pores or the formation of larger pore structures within the material.

The grafting amount in this study was determined by calculating the weight loss of the LDHs-OA samples based on the Tong method [21] for surface-grafted LDH. The grafting amount was determined using the TGA weight loss technique. After the thermogravimetric process, the remaining substances were identified as MgZnAl mixed metal oxides (MMO), with the formula $Mg_4Zn_2Al_3O_{10}$ based on the atomic molar ratio. These MMOs were decomposed from MgZnAl-CO_3-LDHs. By considering the molecular formula of LDHs, $Mg_4Zn_2Al_3(OH)_{21}CO_3$, the amounts of grafted polymers were calculated using the following equations:

$$\omega_{OA} = 1 - \omega_{MMO}(\frac{M_{LDHs}}{M_{MMO}}) \tag{5.1}$$

Where M_{LDHs} and M_{MMO} represent the relative molecular mass of MgZnAl-CO_3-LDH and the remaining MgZnAl-MMO after thermogravimetric tests respectively. The grafted polymers (ω_{OA}) were then quantified based on the residual weight ratio of MgZnAl-MMO (ω_{MMO}). The results showed that the amounts of OA grafted on the surface of LDH-2R-3OA, LDH-2R-6OA, LDH-2R-9OA, and LDH-2R-12OA were 49%, 51%, 59%, and 58% respectively. As evident from the data, samples 1 and 2 display comparable quantities of grafted OA. However, the presence of a greater amount of OA in sample 2 suggests its placement between the layers. The process of grafting OA onto LDHs induces a modification in their surface chemistry, resulting in a transition from hydrophilic to hydrophobic properties. Hydroxyl groups present between the layers act as a driving force, facilitating

the migration of OAs from the synthesis medium to the interlayer space. **Figure.5.4** depicts the reaction between OA and MgAl-LDH, as presented by Dao et al. [26], illustrating the interaction between OA and LDHs.

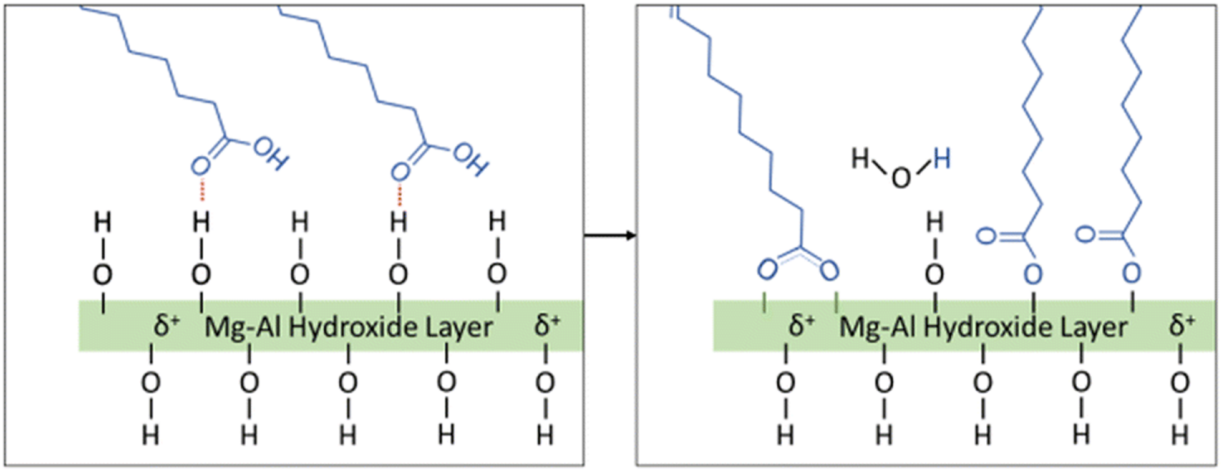

Figure 5.4: Interaction of OA with MgAl-LDHs [26].

The morphology of surface-modified LDHs is presented in **Figure.5.5** indicates that with an increase in OA, the surface of the LDHs becomes rougher.

Table 5.2: Structural Parameters and ICP-MS results of unmodified LDHs.

Sample Code	δ_{BET} (m^2g^{-1})	ν_p (ccg^{-1})	R_p (Å)	Atomic ratio (R[1])		*ICP*
				Theoretical	Experimental	
2R-3OA	8.025	0.039	15.326	2.037	2.140	$[Mg_{2.42}Zn_{1.19}Al_{1.69}(OH)_{10.1}](CO_3)_{5.07}(CH_3C_{16}H_{30}CO)_{3.3}$
2R-6OA	8.257	0.048	15.278	2.063	2.088	$[Mg_{2.38}Zn_{1.56}Al_{1.69}(OH)_{10.1}](CO_3)_{5.07}(CH_3C_{16}H_{30}CO)_{6.3}$
2R-9OA	8.556	0.035	19.250	2.028	1.990	$[Mg_{2.39}Zn_{1.18}Al_{1.79}(OH)_{10.1}](CO_3)_{5.07}(CH_3C_{16}H_{30}CO)_{9.01}$
2R-12OA	8.852	0.045	19.182	2.033	1.990	$[Mg_{2.39}Zn_{1.19}Al_{1.79}(OH)_{10.1}](CO_3)_{5.07}(CH_3C_{16}H_{30}CO)_{11.3}$

1·$R = Mg/Zn$.

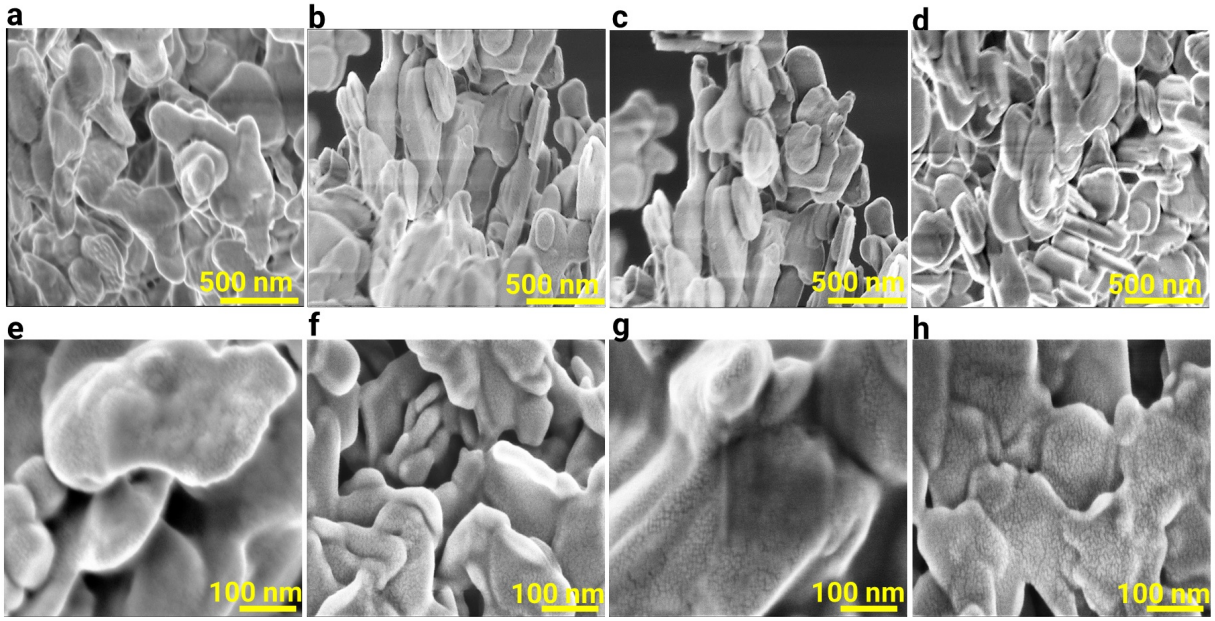

Figure 5.5: SEM images of a) LDH-2R-3OA, b) LDH-2R-6OA, c) LDH-2R-9OA, and d) LDH-2R-12OA (500 nm, $\times$150 000 000). The bottom row shows the same materials at higher resolution: e) LDH-2R-3OA, f) LDH-2R-6OA, g) LDH-2R-9OA, and h) LDH-2R-12OA (100 nm, $\times$500 000 000).

5.2 Thermal Stability Enhancement in LDH/OA-PVC Compounds

The modified LDH compounds were prepared using the same process as the unmodified compounds, and the detailed formulations are presented in **Table A.2** in Appendix A. As shown in **Figure A.4** in Appendix A, the surface-modified LDHs did not affect the transparency of PVC sheets.

The STS results for the modified compounds and C-R2 are presented in **Figure.5.6-a**. After the incorporation of OA, the STS duration increased from 96 minutes for C-R2 to 112, 121, 136, and 128 minutes for MC-3OA, MC-6OA, MC-9OA, and MC-12OA, respectively. It is worth noting that the STS duration for MC-9OA improved more than two times compared to the CS. These findings demonstrate the direct impact of the organo-modification

process of LDH nanoparticles on the thermal stability of PVC. Furthermore, the dehydrochlorination test (**Figure.5.6-b**) revealed that the compound with an OA/LDH ratio of 9 mmol exhibited a lower rate of HCl release. As the quantity of OA used as a surface modifier increased, the induction time also increased to 80 and 88 minutes for MC-9OA and MC-12OA, respectively. Moreover, at a conductivity of 2.97 mS/cm, the stability time for MC-9OA was 84 minutes, while for the C-R2 sample, it was 62 minutes.

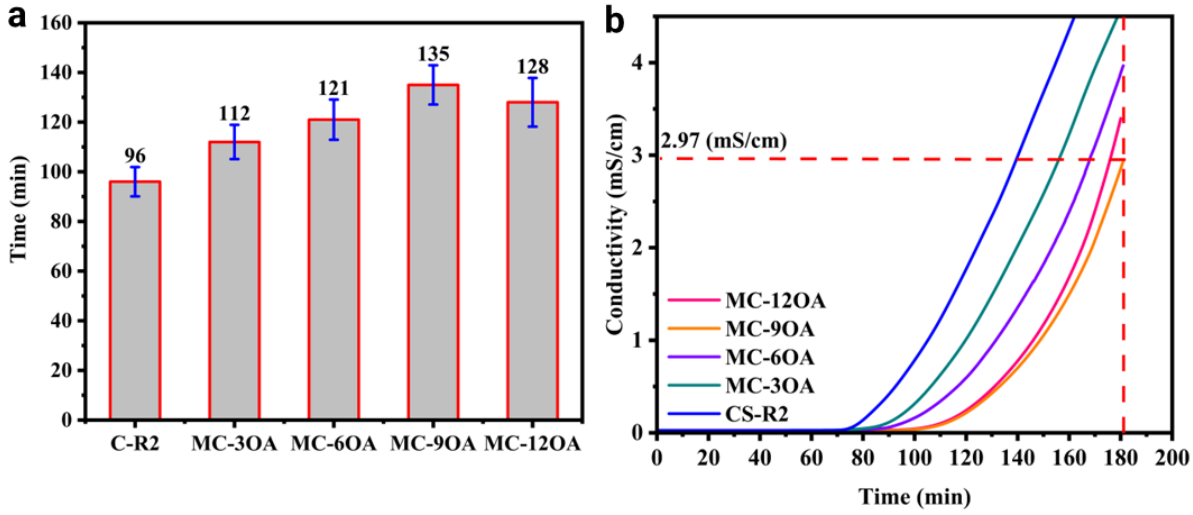

Figure 5.6: a) Static thermal stability (Congo red) at 180 °C, b) HCl release curves for the PVC samples heated at 180 °C (Dehydrochlorination).

The discoloration tests yielded significant findings regarding the color change behavior of the modified samples, as depicted in **Figure.5.6-a**. Initially, all the modified samples exhibited a consistent color for the first 50 minutes of the test at 180°C, except for MC-12OA. During the second stage of color change, the modified samples gradually transitioned to yellow for 100 minutes, after which a yellowish-orange shade emerged. As time progressed, the color shifted to a light orangish brown, and none of the modified samples displayed black areas on the surface of the sheets. In the presence of OA, the color profile of the compounds underwent two distinct changes. In the case of the unmodified samples (**Figure.4.5-a**), black spots appeared and expanded as time elapsed, whereas the modified samples did not exhibit these spots. This observation suggests that OA enhances the

interactions between the LDHs and PVC, resulting in homogeneous and stable compounds.

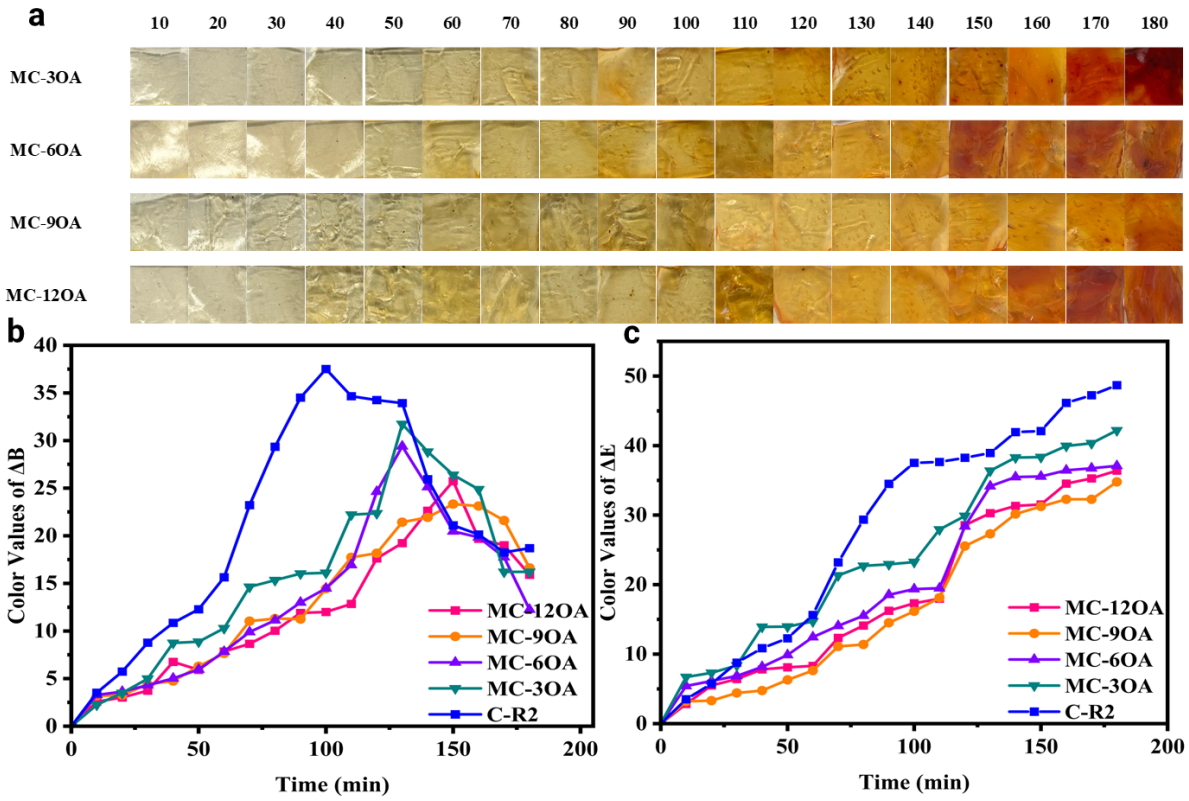

Figure 5.7: a) Static thermal stability (Congo red) at 180 ∘C, b) HCl release curves for the PVC samples heated at 180 ∘C (Dehydrochlorination).

The SEM images obtained from the cross-section of the samples confirm that the addition of OA improves the compatibility between PVC and LDHs. As depicted in **Figure.5.8-a**, there are noticeable gaps observed between the LDHs and PVC in the C-R2 samples. However, after the surface modification process, these gaps were eliminated (**Figure.5.8-b**) and enhanced interaction between LDHs and PVC was observed at the interface. In the unmodified case after thermal aging (**Figure.5.8-c**), the agglomerated LDHs were even segregated from the matrix. Conversely, the modified compounds exhibited a stable surface even after thermal aging, as shown in **Figure.5.8-d**. The SEM images of the modified compounds displayed consistent and unidirectional stripes. These findings align with prior research conducted by Li et al. [177, 178] on zinc-based thermal stabiliz-

ers modified by tung oil fatty acids [178] and dicarboxylic acids [177]. In their reports, they mentioned that the observed morphology was attributable to the fatty acids' compatibilizing effect, which improved the compatibility between the polymer and additives. Consequently, this compatibilization effect facilitated the formation of stable structures, even under thermal aging conditions. Additionally, another study [179] investigated the modification of Zinc Metal Alkoxide with Di-Mannitol Adipate as a thermal stabilizer, which resulted in a plasticizing effect on PVC. Nevertheless, our findings suggest that the fatty acids' compatibilizing effect holds greater significance, although we cannot disregard the plasticizing effect they have on the matrix.

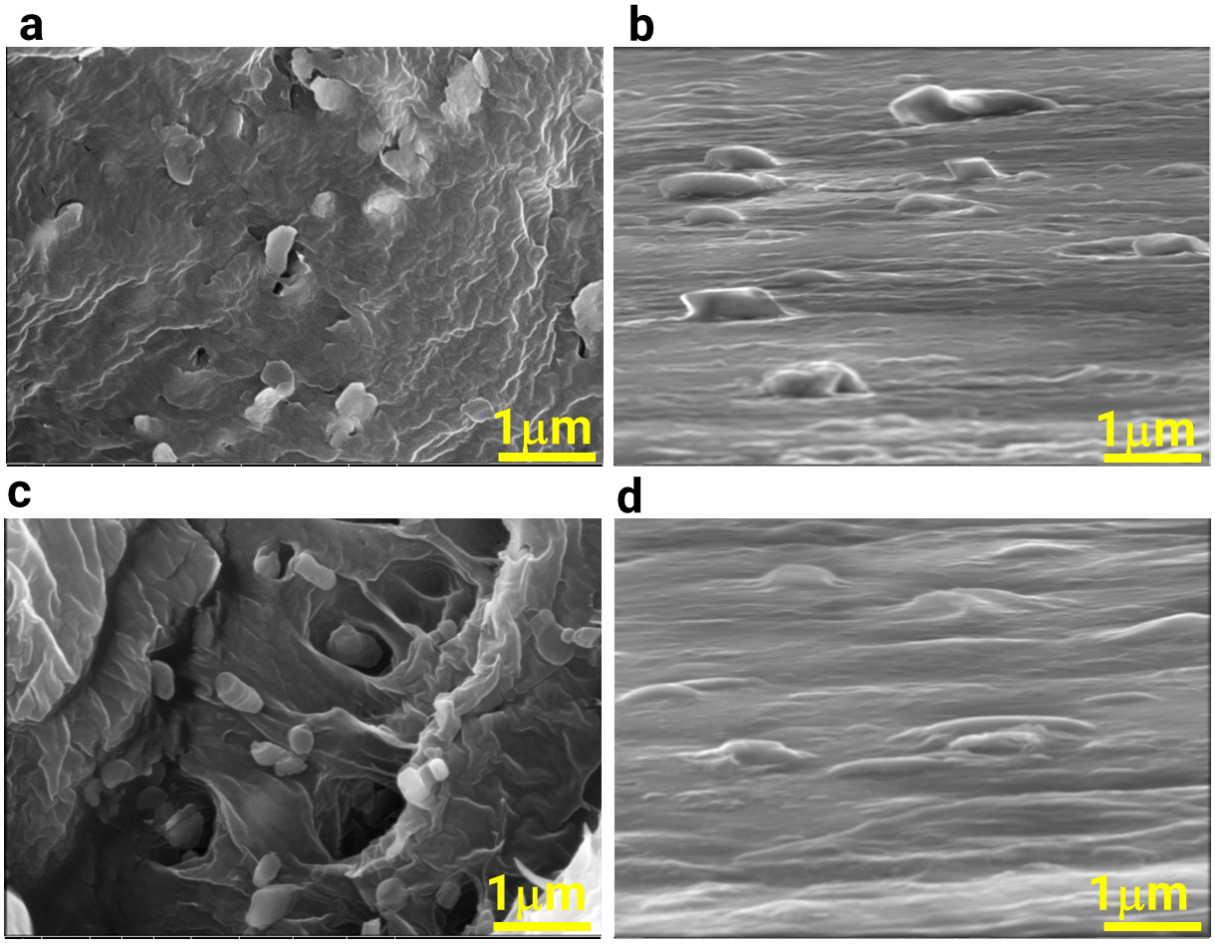

Figure 5.8: SEM image from cross-sections of a, c) C-R2 and b, d) MC-9OA. a, b) are before thermal aging, and c, d) after 180 minutes of thermal aging.

Additionally, in the unmodified samples, the color profile in **Figure.4.5-a** transitioned directly from yellow to brown, indicating a rapid progression of PVC degradation. In contrast, the modified compounds exhibited a color shift from yellow to orange and then to brown, suggesting a more gradual degradation process. This slower transition implies that OA effectively suppresses the auto-catalytic effect of PVC degradation, slowing down the overall degradation process. The changes in sheet color are represented by ΔB and ΔE (Equation.3.1) in **Figure.5.7-c,d**, respectively. The disparity in ΔB values between the modified and unmodified compounds is evident in **Figure.5.7-c**. The incorporation of OA leads to a decrease in ΔB_{Max} and a shift towards higher temperatures. Furthermore, the rate of ΔB exhibits a slight increase with a higher amount of surface modifier in the compounds. For instance, in MC-9OA, within the 130–170-minute range, ΔB demonstrates a gradual transition from orange to brown, as depicted in **Figure.5.7-a**. Moreover, the treated samples exhibit lower ΔE values, and these values moderately increase with time.

To investigate the thermal stability of the treated compounds, TGA and DTG curves were obtained for all samples, as illustrated in **Figure.5.9-a** and **Figure.5.9-b**, respectively. As shown in **Figure.5.9-a**, the modified compounds exhibited the same stages as the unmodified samples. In stage I, with the addition of LDH-OA to PVC compounds, the Tonset decreased with a slight difference compared to the C-R2 sample, as highlighted in **Figure.5.9-c**. The slight decrease in Tonset is attributed to the presence of small molecules and physically adsorbed OA molecules, rather than chemical bonding [125]. Consequently, the $T_{5\%}$ after Tonset is either lower or equal to that of the C-R2 compound, as reported in **Table5.3** As the temperature increases and the HCl absorption mechanism is activated by LDHs, $T_{25\%}$ increases from 287°C to 295°C for C-R2 and MC-9OA compounds, respectively. Moreover, with the incorporation of OA, T_{1Max} shifted to a higher temperature. The T_{1max} values for MC-6OA, MC-9OA, and MC-12OA are 296°C, 310°C, and 309°C, respectively. All these values exceed the T_{1max} of the C-R2 sample, except for MC-3OA.

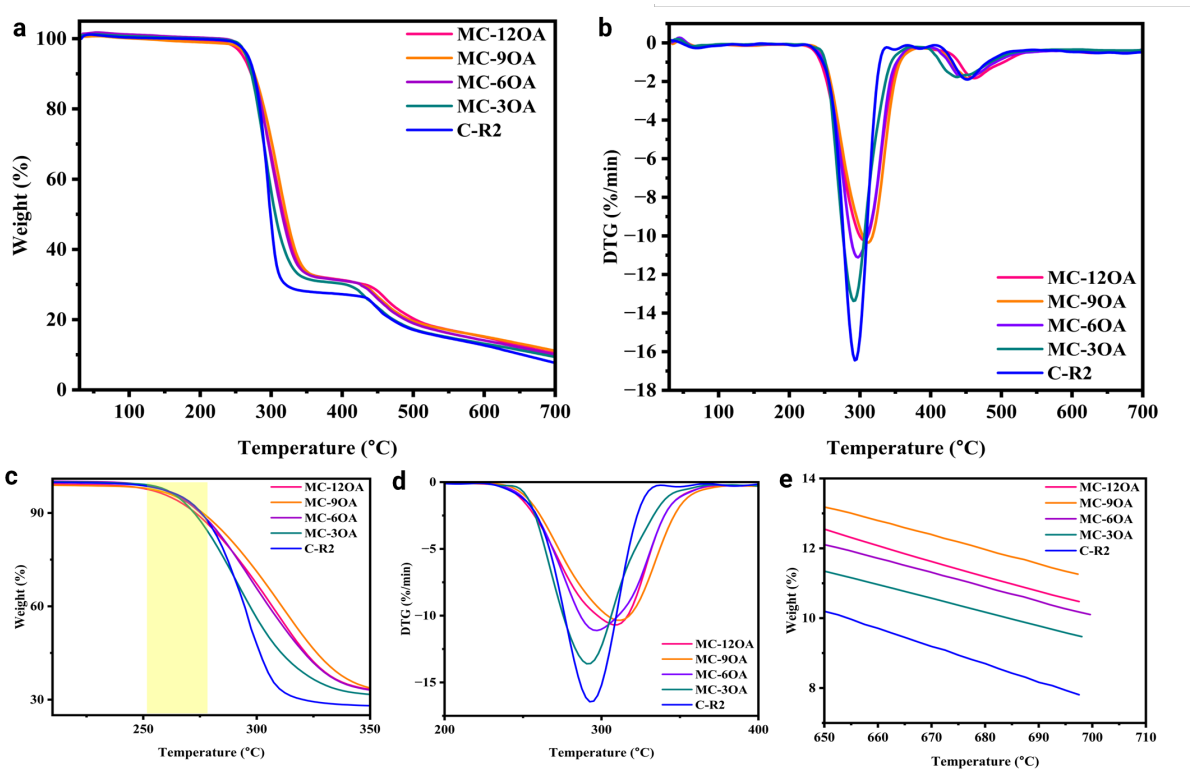

Figure 5.9: a) TGA, b) DTG, c) enlargement of TGA near stage I, d) enlargement of DTG near Tmax of Stage I, and e) residual weight (%) in TGA of MC-3OA, MC-6OA, MC-9OA, and MC-12OA modified compounds.

It is worth noting that the intensity of the DTG peak decreases as the OA content in the compounds increases, as shown in **Figure.5.9-b,d**. This phenomenon indicates the effect of the surface modification process on enhancing the thermal stability of PVC compounds. Several key factors contribute to the enhancement of PVC compounds by OA. As reported in SEM results, the introduction of surface-modified LDHs with fatty acid to PVC improves the compatibility between the nanoparticles and the matrix [23]. Furthermore, surface modification with OA improves the dispersion of hydrophobic LDHs in PVC and reduces the nanoparticles' agglomeration which could act as thermal degradation sites [23]. Additionally, in the presence of OA, LDHs exhibit a more uniform distribution, resulting in more consistent and stable compounds. The EDS results confirm this assumption, As shown in **Figure A.5** in Appendix A the EDS results showed a uniform distribution for

modified LDHs with high dispersity in the matrix while the unmodified samples show the LDH's agglomerations with weaker dispersity than the modified sample (**Figure A.6**in Appendix A).

Furthermore, the hydrophobic effect of OA acts as a barrier against destructive polar factors (such as $ZnCl_2, Cl^-$, and oxygen), thereby slowing down their migration to the matrix and resulting in reduced weight loss and color change rate. While the inclusion of OA between the layers increases the interlayer spacing and facilitates HCl absorption, the structure and concentration of OA must be optimized to achieve the desired balance, a field that is beyond the scope of this study.

The weight residue ($WR\%$) values from the TGA results indicate the amount of material remaining after the thermal degradation process, as shown in **Figure.5.9-e**. For the C-R2, the $WR\%$ is 8.65%, whereas the OA-modified samples exhibit higher $WR\%$ values, particularly MC-3OA (9.46%), MC-6OA (10.12%), and MC-9OA (11.25%), with a slight decrease in MC-12OA (10.48%). The increase in $WR\%$ with the addition of OA suggests that the modified LDHs enhance the formation of char during degradation, which can act as a protective barrier, thereby slowing down the decomposition of the remaining material. The slight decrease in $WR\%$ for MC-12OA compared to MC-9OA may indicate an optimal level of OA content for maximum thermal stability, beyond which the effectiveness slightly diminishes. Overall, the presence of OA in the LDH samples contributes to a higher residual weight, implying improved thermal resistance and char formation during the thermal degradation process.

Table 5.3: TGA results of surface-modified LDHs-PVC compounds.

Sample	$T_{5\%}$ (°C)	$T_{25\%}$ (°C)	$T_{50\%}$ (°C)	$T_{80\%}$ (°C)	T_{1Max} (°C)	T_{2Max} (°C)	WR (%)
C-R2	265	287	299	470	292	452	8.65
MC-3OA	266	286	305	472	292	438	9.46
MC-6OA	265	290	315	489	296	452	10.12
MC-9OA	265	295	320	495	310	452	11.25
MC-12OA	262	292	317	497	309	455	10.48

5.3 Discussions: Degradation Mechanisms and Kinetics

Thus far, we have investigated the effects of LDHs with varying compositions and studied the impact of organic surface treatment on both LDHs and PVC compounds. Based on our findings, we considered C-R2 as the finest unmodified compound, while MC-9OA was the best-modified compound for further in-depth study.

5.3.1 Polyene index and Polyene length

To investigate the correlation between the rate of thermal degradation and surface modification of LDHs following the discoloration test, three samples were selected for further analysis: one after 10 minutes, 90 minutes, and 180 minutes that showed in **Figure.5.7-a**. These samples were selected from the C-R2 and MC-9OA compounds. Raman spectroscopy was employed to examine metal chloride structures within the range of 130-330 cm^{-1}, which has been widely used by researchers to investigate diverse complex structures [180]. As depicted in **Figure.5.10-a**, the compounds before thermal treatment exhibited only background noise within the chosen range. However, after 10 minutes, two broad peaks at 220 cm^{-1} [181] and 250 cm^{-1} [182] emerged, both of which can be attributed to $ZnCl_2$. As previously mentioned, zinc possesses greater electronegativity, a larger atomic radius,

and a higher affinity for absorbing HCl than Mg. Furthermore, due to the utilization of a Ca/Zn thermal stabilizer in the compound formulation, zinc exhibits a higher level of incorporation into the system compared to other elements. Hence, the earliest appearance of the $ZnCl_2$ peak is not unexpected.

After 90 minutes, a new peak emerged at 265-267 cm^{-1} in both samples, signifying the presence of $MgCl_2$ [183] 91which overlapped with $ZnCl_2$. The FWHM of C-R2 was found to be lower than that of MC-9OA in both the 220 and 250 cm^{-1} peaks, while the intensity and area of MC-9OA were observed to be higher than those of the C-R2 compounds. This trend was also observed for $MgCl_2$ around 260 cm^{-1} (**Table A.3** in Appendix A). Two hypotheses have been proposed to explain these findings and the efficiency of LDHs in absorbing HCl, both in the presence and absence of OA. Firstly, the lower FWHM of unmodified compounds (C-R2) suggests better-organized structures and more interactions with PVC, indicating a superior HCl absorption efficiency of these compounds compared to modified LDH. According to this hypothesis, the unmodified LDH absorbed a greater amount of HCl in the system. Secondly, the higher intensity and area indicate a great capacity for HCl absorption by LDHs, as evidenced by the MC-9OA compound.

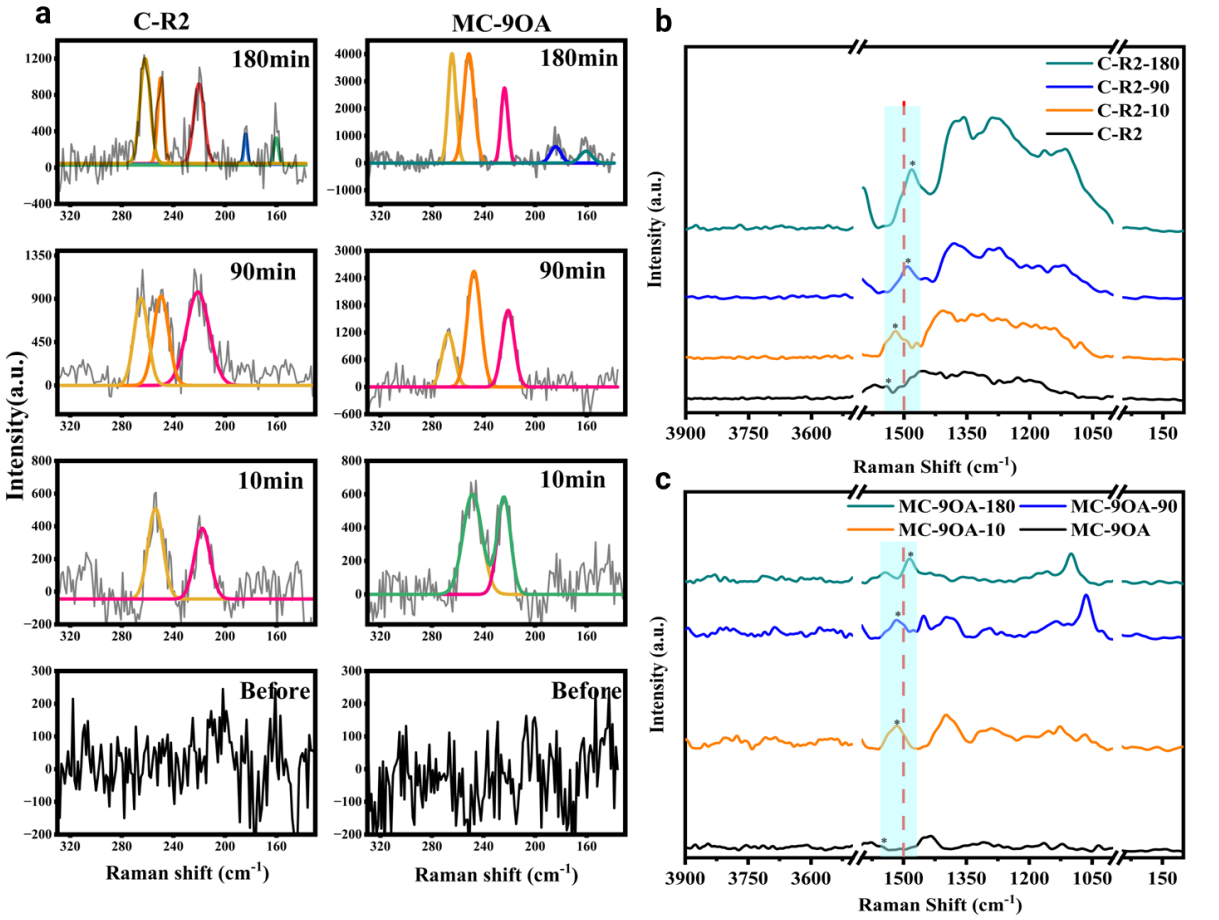

Figure 5.10: a) Multiple-peak fitting of Raman spectroscopy of C-R2 and MC-9OA compounds at 180 °C after 10, 90, and 180 min, Change of polyene length for b) C-R2, and c) MC-9OA compounds with time (10, 90, 180) at 180 °C

Based on the findings, these assumptions can be explained as follows. Although the unmodified sample exhibits higher efficiency in absorbing HCl, the quantity of HCl being released into the system needs to be taken into consideration. Consequently, the dehydrochlorination test (**Figure.5.6-b**) demonstrates that the rate of HCl released by the C-R2 sample surpasses that of MC-9OA under the same conditions, consequently leading to inferior thermal stability. Moreover, the presence of LDHs-2R-9OA enhances the interaction with PVC, diminishes the rate of HCl release, and serves as a barrier, which all amplify thermal stability. This discussion emphasizes the complex thermal degradation mechanisms of PVC and the crucial role of OA in influencing the dynamics of interaction

and thermal stabilization of LDH. As the duration extends to 180 minutes, new peaks arise at 184 cm^{-1} and 160 cm^{-1} in **Figure.5.10-a**, corresponding to the formation of $AlCl_3$ and $MgCl_2$, respectively, that reported in the references [184] for $AlCl_3$ and [183] for $MgCl_2$. These changes signify a more pronounced interaction between LDHs and HCl, as well as an increase in the polyene content within PVC structures. The findings of Raman spectroscopy in this research are aligned with the prior investigations on the effectiveness of MgCaAlZn-LDH [185]as a thermal stabilizer. They demonstrated that the cation can interact with HCl, which is produced during the degradation of PVC, to form $MgCl_2, ZnCl_2, CaCl_2,$ and $AlCl_3$.

To investigate the number of polyene sequences, equation 5.1 is employed [186]:

$$\nu^2 = (1461 + 151.2 \times exp(-0.7808n))\text{cm}^{-1} \tag{5.2}$$

In this equation, the wavenumbers of the C=C stretching vibrations around 1500 cm^{-1} (**Figure.5.10-b,c**) are designated asν_2, the length of polyenes is indicated as n, and the wavenumber of the C=C stretching vibration is a function of n [187]. The findings are presented in **Table.5.4**, which demonstrates that an elevation in temperature leads to an increase in the number of C=C bonds in PVC chains and an increase in polyene length as shown in **Figure 5.11**. Removing HCl from PVC effectively mitigates degradation by suppressing the autocatalytic dehydrochlorination mechanism. Eliminating HCl or Cl_2 prevents the formation of conjugated double bonds, disrupting the cyclic process and impeding further deterioration. The results indicate that, after 10 minutes, the length of the polyene in both compounds falls within a similar range, whereas after 90 minutes, a significant disparity arises. Specifically, the length of the polyene ranges from 20-21 for CS-R2 and 12-13 for MC-9OA, respectively. Furthermore, based on the FTIR peaks (**Figure A.7** and **Figure A.8** in Appendix A) the polyene index (PI) is determined utilizing Equation

5.3 [188]:

$$PI = \frac{I_{1579}}{I_{2956}} = \frac{I_{1600}}{I_{2956}} \tag{5.3}$$

The intensities of the FTIR peaks measured at 1579 cm^{-1} and 1600 cm^{-1} in PVC are denoted by I_{1579} and I_{1600}, respectively. These peaks correspond to the C=C bond vibrations in PVC. Meanwhile, the intensity of the peak observed at 2956 cm^{-1} in the PVC spectrum is represented by I_{2956} and signifies the presence of C−H bonds. The polyene index, a measure of the degree of C=C conjugated bonds in PVC, demonstrates a positive correlation with the intensities of the 1579 cm^{-1} and 1600 cm^{-1} FTIR peaks. Specifically, an increase in the intensities of the peaks at 1600 cm^{-1} and 1579 cm^{-1} corresponds to a higher polyene index, indicating a greater abundance of C=C conjugated bonds and degradation of PVC. In this context, the peak at 2956 cm^{-1} serves as a reference point for calculating the polyene index. The results reveal that the rate of increase in PI matches the increasing length of polyenes, thereby confirming that temperature exerts a greater influence on CS-R2 compared to MC-9OA.

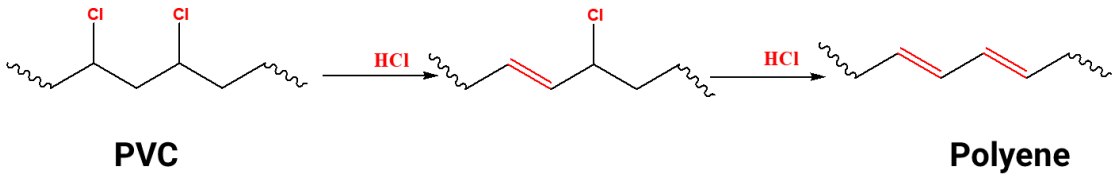

Figure 5.11: Mechanism of Polyene formation during the thermal degradation of PVC.

5.3.2 Activation energy

To assess the impact of LDH surface modification on the activation energy in PVC degradation we used non-isothermal technique. Non-isothermal methods typically involve the

Table 5.4: Raman and FTIR analysis for different samples and thermal aging durations.

Sample*	Raman			FTIR	
	Peak	Area	n	PI_{1579}	PI_{1600}
C-R2	-	-	-	0.0613	0.08348
MC-9OA	-	-	-	0.06567	0.08112
C-R2-10	1516	28.821	12.95	0.11935	0.12074
MC-9OA-10	1522	25.32	11.62	0.11606	0.12018
C-R2-90	1491	32.092	20.71	0.24328	0.24627
MC-9OA-90	1517	29.325	12.72	0.21769	0.22177
C-R2-180	1478	63.25	27.98	0.3	0.29225
MC-9OA-180	1485	48.680	23.57	0.23881	0.24328

*Compound name- 10, 90, 180 indicate the duration of thermal aging in minutes.

measurement of reaction kinetics through the determination of conversion [189]:

$$\alpha = \frac{m_0 - m_i}{m_0 - m_t} \tag{5.4}$$

which represents the reaction rate. In conversion, mo represents the original mass of the sample, m_i denotes the instantaneous mass at any time, and m_t signifies the final mass of the sample. The kinetic rate equation is expressed by the temperature-dependent rate constant, $k(T)$, and the temperature-independent reaction model, $f(X)$:

$$\frac{d\alpha}{dt} = K(T)f(X) \tag{5.5}$$

Arrhenius's equation describes the temperature dependence of reaction rates. It is commonly used for kinetic studies, where temperature plays a central role in reactions [190].

Equation 5.6 presents the Arrhenius formula [191]:

$$K(T) = Aexp(\frac{E_a}{RT}) \tag{5.6}$$

By substituting equation 5.5 in 5.6 and assuming that $T = T_0 + \beta t$:

$$\frac{d\alpha}{dt} = ln[\frac{AR}{\beta E_a}](1 - \frac{2RT}{E_a}) - \frac{E_a}{RT} \tag{5.7}$$

Equation 5.7 presented the Coats–Redfern method is a non-isothermal model-fitting approach used to determine the kinetic parameters of solid-state materials [192] wherein the reaction temperature increases at a constant rate [193]. Assuming that the $\frac{2RT}{E_a}$ term is much less than 1, we can neglect the factor in parentheses, resulting in the modified equation [192]:

$$\frac{d\alpha}{dt} = ln[\frac{AR}{\beta E_a}] - \frac{E_a}{RT} \tag{5.8}$$

The parameter (β) denotes the heating rate (°C/min), while (K) and (A) represent the frequency factors (min^{-1}). The gas constant, (R), has a value of 8.3143 $J/mol.K$.

By plotting $ln[\frac{(g(\alpha))}{(T^2(K))}]$ against $\frac{1}{T}$, we determined both the activation energyE_a and the frequency factor A. The slope of the straight line corresponds to $(\frac{-E_a}{R})$, and the intercept represents the product of the frequency factor and the gas constant $ln[\frac{AR}{(\beta E_a)}]$ [194]. The function $g(\alpha)$ varies depending on the kinetics model and is calculated for the solid-state degradation mechanism that in this research we considered $g(x) = -ln(1-\alpha)$ as the first-order reaction in the PVC degradation process. The analysis was performed during two identified TGA mass-loss stages, as discussed in previous sections, and at the temperature corresponding to the maximum rate of mass loss T_{Max} for each stage.

The influence of LDHs on the stability and thermal degradation behavior of the sam-

ples is depicted in **Figure A.9** in Appendix A using a conversion versus temperature plot based on the TGA results in **Figure.5.9-a**. The conversion curve exhibits a sigmoidal shape for all samples. However, in the case of the MC-9OA sample, the conversion rate initiates at a lower temperature. This can be attributed to the physical absorption of small molecules and unreacted OA on the surface of LDHs. As the temperature increases, the CS compound displays a higher conversion rate compared to C-R2 and MC-9OA. Upon reaching a conversion level of 30%, the MC-9OA exhibits a shift towards higher temperatures, indicating a slower degradation rate for these compounds. At 50% conversion, the temperatures are 288°C, 299°C, and 311°C for CS, C-R2, and MC-9OA compounds, respectively.

The plots of the differential conversion rate ($\frac{d\alpha}{dT}$) versus temperature offer additional insights into the degradation rates of the compounds (**Figure.5.12-a,b,c**). For CS compounds, a sharp peak at 554 K with an FWHM of 36.8 indicates a rapid thermal degradation phase, suggesting a swift conversion [195]. On the other hand, the C-R2 compound exhibits a higher conversion rate at a higher temperature of 565 K, although the FWHM is 28.6. MC-9OA, on the other hand, displays a broader peak with an FWHM of 59.8 at higher temperatures (583 K), suggesting a more gradual degradation process. This is consistent with its higher activation energy at higher conversions. The broader peak for MC-9OA may be attributed to the presence of OA, which potentially acts as a barrier to the migration of the destructive polar factors to the system and expands the PVC degradation, slowing down the degradation process and resulting in a more controlled release of thermal energy.

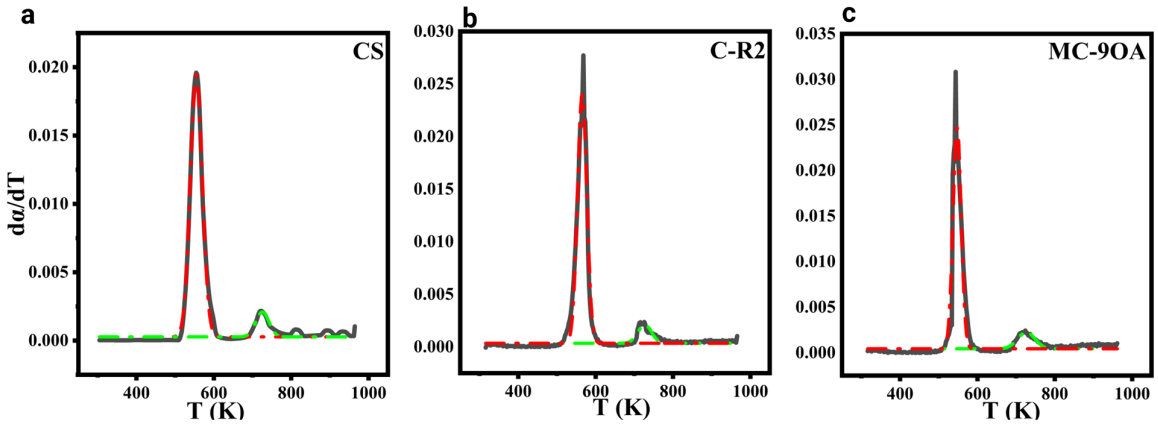

Figure 5.12: Thermogravimetric curves: a, b, and c) derivative conversion curves for Cs, C-R2, and MC-9OA compounds, respectively

The activation energy was measured for two stages, CS and CR-2, as well as MC-9OA. When LDH was incorporated into PVC compounds, the activation energy in stage I increased from 145 to 152.8kJ/mol for CS and CR-2, respectively. This indicates that the degradation of PVC requires more energy in the presence of LDH. Moreover, the organo-modified LDH had a contributing effect on the activation energy, leading to an increase to 158.56kJ/mol. This suggests that OA enhances the thermal stability efficiency of LDH, reduces the presence of HCl, and eliminates its catalytic effect. In stage II, the activation energy increased by 77%(257.76kJ/mol), 74%(267kJ/mol), and 63% (264.8kJ/mol) for CS, CR-2, and MC-9OA, respectively. This behavior signifies the emergence of reactions that culminate in the creation of more enduring structures, including stable residues and polyene compounds [196, 197]. These structures are generated after the dehydrochlorination process, wherein decomposition transpires and robust structures such as aromatic and graphitic structures come into existence [198]. Overall, the average activation energy calculated in this study for pure PVC dehydrochlorination (145 kJ/mol) completely matches the value reported by Zhou et al. [192](145.33 kJ/mol) using the CR model. This confirms the validity of the procedure used to calculate the kinetic data.

Chapter 6

Conclusions and Future Work

6.1 Conclusions

High-performance surface-engineered LDH synthesis treated by OA as a sustainable surfactant from renewable sources. The finest thermal stabilization in PVC compounds was achieved with MgAlZn-LDH, with a molar ratio of Mg/Zn = 2. Increasing the Mg content reduced the incorporation of Zn, an element with higher electronegativity and atom radius, resulting in reduced $ZnCl_2$ compounds as a catalytic agent in PVC degradation. LDHs with different compositions had an impact on the color stability and long-term thermal stability of the PVC compounds. The C-R0.5 compound showed better color stability in the early stage of degradation, while the C-R2 compound exhibited higher long-term thermal stability and maintained a more stable LDH structure during PVC degradation. The finest surface-treated LDH, with an OA/LDH ratio of 9 mmol, displayed larger crystal structures with lower defects. XPS results indicated a lower surface energy, suggesting that OA improved the chemical stability of LDHs. Organo-modified LDHs enhanced the thermal stability of PVC compounds compared to reference and unmodified compounds. The MC-9OA compound showed a more than two-fold increase in static thermal stabil-

ity compared to CS compounds, and the initial thermal degradation occurred at higher temperatures. Moreover, the modified compound exhibited considerably improved color stability, indicating the effect of OA on the efficiency of LDHs in improving the thermal stability of PVC compounds. EDS results demonstrated that OA not only improved the thermal stability of PVC compounds but also facilitated the uniform distribution and high dispersity of LDHs in PVC, reducing additive agglomerations. Raman spectroscopy provided significant insights into the absorption of HCl by LDHs and the formation of metal chloride structures during PVC degradation. OA acted as a surfactant and played a crucial role in enhancing the yield of LDHs. Furthermore, Raman spectroscopy revealed the number of polyenes in the PVC backbone after 10, 90, and 180 minutes at 180°C. The results showed that after 180 minutes, the length of polyenes for MC-9OA was in the range of 23-24, while for C-R2 compounds, it was in the range of 27-28. These results were confirmed by the polyene index (PI) measured by FTIR.

6.2 Challenges and future works

A few challenges and future pathways are introduced as follows:

1. Changing synthesis method

   In this project, we synthesized the LDHs using the PH constant co-precipitation method. However, various other methods can be used, such as Urea hydrolysis, Hydrothermal, Sol-gel, and Template method. We aimed to study the effect of different synthesis methods on the absorption of HCl during PVC degradation.

2. Changing modification method

   In this study, we carried out surface modification of LDHs in two stages. We propose the in-situ surface modification of LDHs using OA. Additionally, we investigated

the impact of the modification method on particle size distribution, crystal parameters, LDH dispersity in PVC, and the thermal stabilization mechanisms during PVC degradation.

3. Using OA as the anion interlayer

   We determined that the critical molar ratio of OA/LDH was 12 mmol, which allowed for the incorporation of OA molecules between the LDH layers. We suggest using OA as an anion in the interlayer and increasing its amount in the system to study the absorption capacity of LDHs in the HCl absorption process.

4. Quantification of HCl absorption

   It is crucial to quantify the amount of HCl absorbed by LDHs during degradation. Therefore, we propose quantifying the amount of HCl absorbed by LDH at each stage of PVC degradation.

5. Optimizing the required amount of LDH in the compound To investigate the effect of surface modification of LDHs on the thermal stability of PVC compounds, we used a constant OA-LDH ratio in the compounds. However, it is essential to determine the amount of organo-modified LDH required to improve the thermal stability of PVC compounds compared to commercial LDHs.

6. Cost analysis for scaled-up production

   The use of organo-modified LDHs allowed us to achieve strong dispersity of LDHs with a uniform distribution, which directly contributed to the improvement of thermal stability in PVC. A comprehensive analysis of the cost of materials and methodologies provides an overview of the feasibility of large-scale production.

References

[1] J. Purmova, K. F. D. Pauwels, W. van Zoelen, E. J. Vorenkamp, A. J. Schouten, and M. L. Coote, "New insight into the formation of structural defects in poly(vinyl chloride)," *Macromolecules*, vol. 38, no. 15, pp. 6352–6366, 2005.

[2] W. Starnes, "Overview and assessment of recent research on the structural defects in poly(vinyl chloride)," *Polymer Degradation and Stability*, vol. 97, no. 9, pp. 1815–1821, 2012.

[3] O. Biotidara, I. Eromosele, C. Eromosele, and O. Folarin, "Thermal degradation of poly (vinyl chloride)/polystyrene blends in the presence of derivatives of hura crepitans seed oil.," *Journal of Chemical Society of Nigeria*, vol. 48, no. 6, 2023.

[4] W. Han, M. Zhang, Y. Kong, D. Li, L. Liu, S. Tang, J. Ding, and S. Liu, "Pentaerythritol stearate ester-based tin (ii) metal alkoxides: A tri-functional organotin as poly (vinyl chloride) thermal stabilizers," *Polymer Degradation and Stability*, vol. 175, p. 109129, 2020.

[5] D. Li and P. Liu, "Trends and prospects for thermal stabilizers in polyvinyl chloride," *Journal of Vinyl and Additive Technology*, vol. 28, no. 4, pp. 669–688, 2022.

[6] M. Wang, J. Xia, J. Jiang, S. Li, and M. Li, "Mixed calcium and zinc salts of n-(3-amino-benzoic acid) terpene-maleamic acid: preparation and its application as

novel thermal stabilizer for poly (vinyl chloride)," *RSC advances*, vol. 6, no. 99, pp. 97036–97047, 2016.

[7] M. Wang, X. Song, J. Jiang, J. Xia, and M. Li, "Binary amide-containing tung-oil-based ca/zn stabilizers: effects on thermal stability and plasticization performance of poly (vinyl chloride) and mechanism of thermal stabilization," *Polymer Degradation and Stability*, vol. 143, pp. 106–117, 2017.

[8] H. A. Shnawa, "Synthesis and evaluation of calcium and zinc humates for stabilization of poly (vinyl chloride) and study their self-synergistic effect," *Journal of Polymer Research*, vol. 30, no. 6, p. 201, 2023.

[9] M. Wang, X. Song, J. Jiang, J. Xia, S. Li, and M. Li, "Excellent hydroxyl and nitrogen rich groups-containing tung-oil-based ca/zn and polyol stabilizers for enhanced thermal stability of pvc," *Thermochimica Acta*, vol. 658, pp. 84–92, 2017.

[10] M. Zhang, W. Han, X. Hu, D. Li, X. Ma, H. Liu, L. Liu, W. Lu, and S. Liu, "Pentaerythritol p-hydroxybenzoate ester-based zinc metal alkoxides as multifunctional antimicrobial thermal stabilizer for pvc," *Polymer Degradation and Stability*, vol. 181, p. 109340, 2020.

[11] G. Fan, F. Li, D. G. Evans, and X. Duan, "Catalytic applications of layered double hydroxides: recent advances and perspectives," *Chemical Society Reviews*, vol. 43, no. 20, pp. 7040–7066, 2014.

[12] S. Naseem, B. Gevers, R. Boldt, F. Labuschagné, and A. Leuteritz, "Comparison of transition metal (fe, co, ni, cu, and zn) containing tri-metal layered double hydroxides (ldhs) prepared by urea hydrolysis, rsc adv. 9 (2019) 3030–3040."

[13] Z. Rao, K. Li, P. Liu, Y. Lin, and X. Lyu, "Study on the thermal stabilizing process of layered double hydroxides in pvc resin," *Molecules*, vol. 28, no. 23, p. 7792, 2023.

[14] Y.-J. Lin, D.-Q. Li, D. G. Evans, and X. Duan, "Modulating effect of mg–al–co3 layered double hydroxides on the thermal stability of pvc resin," *Polymer Degradation and Stability*, vol. 88, no. 2, pp. 286–293, 2005.

[15] J. Labuschagné, D. Molefe, W. W. Focke, and O. Ofosu, "Layered double hydroxide derivatives as flame retardants for flexible pvc," in *Macromolecular Symposia*, vol. 384, p. 1800148, Wiley Online Library, 2019.

[16] F. J. Labuschagne, D. M. Molefe, W. W. Focke, I. Van der Westhuizen, H. C. Wright, and M. D. Royeppen, "Heat stabilising flexible pvc with layered double hydroxide derivatives," *Polymer Degradation and Stability*, vol. 113, pp. 46–54, 2015.

[17] C. Cui, Y. Zhang, M. A. Wladyka, T. Wang, W. Song, and K. Niu, "Ultrasound-assisted adsorption of perchlorate using calcined hydrotalcites and the thermal stabilization effect of recycled adsorbents on poly (vinyl chloride)," *ACS omega*, vol. 8, no. 20, pp. 17689–17698, 2023.

[18] S.-T. Liu, P.-P. Zhang, K.-K. Yan, Y.-H. Zhang, Y. Ye, and X.-G. Chen, "Sb-intercalated layered double hydroxides–poly (vinyl chloride) nanocomposites: Preparation, characterization, and thermal stability," *Journal of Applied Polymer Science*, vol. 132, no. 39, 2015.

[19] J. Yan and Z. Yang, "Intercalated hydrotalcite-like materials and their application as thermal stabilizers in poly (vinyl chloride)," *Journal of Applied Polymer Science*, vol. 134, no. 22, 2017.

[20] S. Aisawa, C. Nakada, H. Hirahara, N. Takahashi, and E. Narita, "Preparation of dipentaerythritol-combined layered double hydroxide particle and its thermostabilizing effect for polyvinyl chloride," *Applied Clay Science*, vol. 180, p. 105205, 2019.

[21] D. Tong, Y. Zhu, K. Li, K. Du, W. Liu, and Y. Lin, "Surface control of layered double hydroxides by in-situ initiating & terminating polymerization," *Nano Research*, vol. 15, no. 2, pp. 1538–1546, 2022.

[22] H. Yang and Z. Yang, "The effect of sodium stearate-modified hydrocalumite on the thermal stability of poly (vinyl chloride)," *Journal of Applied Polymer Science*, vol. 135, no. 4, p. 45758, 2018.

[23] J. Liu, G. Chen, and J. Yang, "Preparation and characterization of poly (vinyl chloride)/layered double hydroxide nanocomposites with enhanced thermal stability," *Polymer*, vol. 49, no. 18, pp. 3923–3927, 2008.

[24] D. Jin, S. Khanal, and S. Xu, "Effects of znal layered double hydroxide and benzimidazole derivative on the dechlorination of poly (vinyl chloride)," *Applied Clay Science*, vol. 208, p. 106114, 2021.

[25] Z. Gao, L. Lu, C. Shi, and X. Qian, "The effect of ocoal-ldh and ocofe-ldh on the combustion behaviors of polyvinyl chloride," *Polymers for Advanced Technologies*, vol. 31, no. 4, pp. 675–685, 2020.

[26] T. L. K. Dao, K. A. Tieu, and B. H. Tran, "Tribochemical synergy between phosphate-intercalated layered double hydroxide additives and super high oleic safflower oil on sliding contacts," *Physical Chemistry Chemical Physics*, vol. 24, no. 34, pp. 20282–20293, 2022.

[27] K. Lewandowski and K. Skórczewska, "A brief review of poly(vinyl chloride) (pvc) recycling," *Polymers*, vol. 14, no. 15, 2022.

[28] J. W. Summers, "A review of vinyl technology," *Journal of Vinyl and Additive Technology*, vol. 3, no. 2, pp. 130–139, 1997.

[29] S. M. D. Prestes, S. D. Mancini, J. Antonio Rodolfo, and R. C. Keiroglo, "Construction and demolition waste as a source of pvc for recycling," *Waste Management & Research*, vol. 30, no. 2, pp. 115–121, 2012. PMID: 21967989.

[30] M. Karstadt, "Pvc: health implications and production trends.," *Environmental Health Perspectives*, vol. 17, pp. 107–115, 1976.

[31] M. Day, J. Cooney, C. Touchette-Barrette, and S. Sheehan, "Pyrolysis of mixed plastics used in the electronics industry," *Journal of Analytical and Applied Pyrolysis*, vol. 52, no. 2, pp. 199–224, 1999.

[32] J. Guo, H. Zhu, Y. Ma, L. Du, and J. Gao, "Application performance of bio-based plasticizer for pvc automotive interior material," *Materials Testing*, vol. 65, no. 7, pp. 1097–1104, 2023.

[33] S. Kim, "Pyrolysis kinetics of waste pvc pipe," *Waste Management*, vol. 21, no. 7, pp. 609–616, 2001.

[34] K. Anandakumaran, S. Barreca, N. Seidl, and P. Castaldo, "Nuclear qualification of pvc insulated cables," *IEEE Transactions on Dielectrics and Electrical Insulation*, vol. 8, no. 5, pp. 818–825, 2001.

[35] R. Lomax, "Recent developments in coated apparel," *Journal of Coated Fabrics*, vol. 14, no. 2, pp. 91–99, 1984.

[36] R. Pearson, "Pvc as a food packaging material," *Food Chemistry*, vol. 8, no. 2, pp. 85–96, 1982.

[37] J. Yu, L. Sun, C. Ma, Y. Qiao, and H. Yao, "Thermal degradation of pvc: A review," *Waste Management*, vol. 48, pp. 300–314, 2016.

[38] Y. Furukawa, *Staudinger, carothers, and the emergence of macromolecular chemistry*. The University of Oklahoma, 1983.

[39] M. Kaufman, *The History of PVC: The Chemical and Industrial Production of Polyvinyl Chloride*. Maclaren, 1969.

[40] K. Mulder and M. Knot, "Pvc plastic: a history of systems development and entrenchment," *Technology in Society*, vol. 23, no. 2, pp. 265–286, 2001.

[41] W. L. Semon and G. A. Stahl, "History of vinyl chloride polymers," *Journal of Macromolecular Science—Chemistry*, vol. 15, no. 6, pp. 1263–1278, 1981.

[42] J. K. Sears and J. R. Darby, "The technology of plasticizers," *(No Title)*, 1982.

[43] J. Sears and J. Darby, "Solvation and plasticization," *Marcel Dekker, Inc., Encyclopedia of PVC.*, vol. 1, pp. 435–554, 1986.

[44] H. Stichnothe and A. Azapagic, "Life cycle assessment of recycling pvc window frames," *Resources, Conservation and Recycling*, vol. 71, pp. 40–47, 2013.

[45] J. Uddin *et al.*, "Effects of scrap addition on the physico-chemical properties of rigid polyvinyl chloride products," 2014.

[46] R. Amanna, Z. Mahal, E. C. S. Vieira, M. Samavi, and S. K. Rakshit, "Plastics: Toward a circular bioeconomy," *Biomass, Biofuels, Biochemicals*, pp. 781–811, 2021.

[47] A. D. Godwin, "Plasticizers," in *Applied plastics engineering handbook*, pp. 595–618, Elsevier, 2024.

[48] R. M. Williams, L. E. Ray, J. H. Lever, and A. M. Burzynski, "Crevasse detection in ice sheets using ground penetrating radar and machine learning," *IEEE Journal of Selected Topics in Applied Earth Observations and Remote Sensing*, vol. 7, no. 12, pp. 4836–4848, 2014.

[49] pvc4pipes, "Pvc pipe categories."

[50] J. López-Cervantes and P. Paseiro-Losada, "Determination of bisphenol a in, and its migration from, pvc stretch film used for food packaging," *Food Additives & Contaminants*, vol. 20, no. 6, pp. 596–606, 2003. PMID: 12881134.

[51] E. Grosu, *Applications of Polyvinylchloride (PVC)/Thermoplastic Nano-, Micro- and Macroblends*, pp. 75–89. Cham: Springer International Publishing, 2022.

[52] S. Bidoki and R. Wittlinger, "Environmental and economical acceptance of polyvinyl chloride (pvc) coating agents," *Journal of Cleaner Production*, vol. 18, no. 3, pp. 219–225, 2010.

[53] T. A. Taha, "Optical properties of pvc/al2o3 nanocomposite films," *Polymer Bulletin*, vol. 76, pp. 903–918, February 2019.

[54] A. Konstantinov and A. Verkhovsky, "Assessment of the wind and temperature loads influence on the pvc windows deformation," *IOP Conference Series: Materials Science and Engineering*, vol. 753, p. 032022, feb 2020.

[55] J. Czogała, E. Pankalla, and R. Turczyn, "Recent attempts in the design of efficient pvc plasticizers with reduced migration," *Materials*, vol. 14, no. 4, 2021.

[56] C. Amaral, N. Gama, F. Mohseni, J. Amaral, V. Amaral, P. Marques, A. Barros-Timmons, and R. Vicente, "Development of structural layers pvc incorporating phase change materials for thermal energy storage," *Applied Thermal Engineering*, vol. 179, p. 115707, 2020.

[57] C. Koester, A. M. Ibrahim, M. Cancel, and M. R. Labedi, "The ubiquitous premature ventricular complex," *Cureus*, vol. 12, p. e6585, January 2020.

[58] S. Ramesh, C.-W. Liew, E. Morris, and R. Durairaj, "Effect of pvc on ionic conductivity, crystallographic structural, morphological and thermal characterizations in

pmma–pvc blend-based polymer electrolytes," *Thermochimica Acta*, vol. 511, no. 1-2, pp. 140–146, 2010.

[59] N. Kumar, A. Dixit, N. Kumar, and A. Dixit, "Nanomaterials-enabled lightweight military platforms," *Nanotechnology for defence applications*, pp. 205–254, 2019.

[60] A. A. Ţurcanu, *Factors Affecting the Properties of Polyvinylchloride (PVC) Nano-, Micro- and Macro-Blends*, pp. 91–110. Cham: Springer International Publishing, 2022.

[61] A. N. Ede and A. Ogundiran, "Thermal behaviour and admissible compressive strength of expanded polystyrene wall panels of varying thickness,"," *Current Trends in Technology and Science*, vol. 3, no. 2, pp. 110–117, 2014.

[62] A. S. Mohammed, "Properties of wood-plastic composites made from alien invasive tree waste and recycled low-density polyethylene for interior use in social housing," 2022.

[63] A. Akelah and A. Akelah, "Polymers in food packaging and protection," *Functionalized polymeric materials in agriculture and the food industry*, pp. 293–347, 2013.

[64] grandviewresearch, "North america pvc films market size, share trends analysis report by technology (calendering, extrusion), by product (rigid pvc films, monomeric flexible pvc films), by end-use, by region, and segment forecasts, 2023 - 2030."

[65] H. Saleh, M. AL-KAHLIDI, H. Abulridha, S. Banoon, and M. Abdelzaher, "Current situation and future prospects for plastic waste in maysan governorate: Effects and treatment during the covid-19 pandemic," *Egyptian Journal of Chemistry*, vol. 64, no. 8, pp. 4449–4460, 2021.

[66] Y. Wu, J. He, and L. Xiong, "Price discovery in chinese pvc futures and spot markets: Impacts of covid-19 and benchmark analysis," *Heliyon*, 2024.

[67] Y.-N. Chen, A. Rani, C.-Y. Chiang, H. Kim, and S.-Y. Pan, "Monitoring, control and assessment of microplastics in bioenvironmental systems," *Environmental Technology Innovation*, vol. 32, p. 103250, 2023.

[68] Y. Liu, C. Zhou, F. Li, H. Liu, and J. Yang, "Stocks and flows of polyvinyl chloride (pvc) in china: 1980-2050," *Resources, Conservation and Recycling*, vol. 154, p. 104584, 2020.

[69] Y. Zhou, N. Yang, and S. Hu, "Industrial metabolism of pvc in china: A dynamic material flow analysis," *Resources, Conservation and Recycling*, vol. 73, pp. 33–40, 2013.

[70] W. Starnes, "Structural defects in poly(vinyl chloride) and the mechanism of vinyl chloride polymerization: Comments on recent studies," *Procedia Chemistry*, vol. 4, pp. 1–10, 2012. The International Conference on Innovation in Polymer Science and Technology.

[71] Z. Wang, G. Liang, S. Jiang, F. Wang, H. Li, B. Li, H. Zhu, A. Lu, and W. Gong, "Understanding the environmental impact and risks of organic additives in plastics: A call for sustained research and sustainable solutions," *Emerging Contaminants*, vol. 10, no. 4, p. 100388, 2024.

[72] Y. Wang and H. Qian, "Phthalates and their impacts on human health," *Healthcare*, vol. 9, no. 5, 2021.

[73] A. A. Sokan-Adeaga, M. A. Sokan-Adeaga, E. D. Sokan-Adeaga, A. N. Oparaji, H. Edris, E. O. Tella, F. A. Balogun, M. Aledeh, and O. E. Amubieya, "Environmental toxicants and health adversities: A review on interventions of phytochemicals," *Journal of Public Health Research*, vol. 12, no. 2, p. 22799036231181226, 2023.

[74] P. B. Tchounwou, C. G. Yedjou, A. K. Patlolla, and D. J. Sutton, *Heavy Metal Toxicity and the Environment*, pp. 133–164. Basel: Springer Basel, 2012.

[75] T. Sanders, Y. Liu, V. Buchner, and P. B. Tchounwou, "Neurotoxic effects and biomarkers of lead exposure: A review," *Reviews on Environmental Health*, vol. 24, no. 1, pp. 15–46, 2009.

[76] C. Chaine, A. S. Hursthouse, B. McLean, I. McLellan, B. McMahon, J. McNulty, J. Miller, and E. Viza, "Recycling plastics from weee: A review of the environmental and human health challenges associated with brominated flame retardants," *International Journal of Environmental Research and Public Health*, vol. 19, no. 2, 2022.

[77] W. Starnes Jr, "Structural and mechanistic aspects of the thermal degradation of poly (vinyl chloride)," *Progress in polymer science*, vol. 27, no. 10, pp. 2133–2170, 2002.

[78] W. H. Starnes Jr, "Structural defects in poly (vinyl chloride)," *Journal of Polymer Science Part A: Polymer Chemistry*, vol. 43, no. 12, pp. 2451–2467, 2005.

[79] W. Starnes, "Structural and mechanistic aspects of the thermal degradation of poly(vinyl chloride)," *Progress in Polymer Science*, vol. 27, no. 10, pp. 2133–2170, 2002.

[80] W. Starnes Jr and B. Wojciechowski, "Mechanism and microstructure in the free-radical polymerization of vinyl chloride: Head-to-head addition revisited," in *Makromolekulare Chemie. Macromolecular Symposia*, vol. 70, pp. 1–11, Wiley Online Library, 1993.

[81] W. Starnes Jr, H. Chung, B. Wojciechowski, D. Skillicorn, and G. Benedikt, "Auxiliary mechanism for transfer to monomer during vinyl chloride polymerization: Implications for thermal stability of poly (vinyl chloride)," ACS Publications, 1996.

[82] W. Starnes, V. Zaikov, H. Chung, B. Wojciechowski, H. Tran, K. Saylor, and G. Benedikt, "Intramolecular hydrogen transfers in vinyl chloride polymerization: routes to doubly branched structures and internal double bonds," *Macromolecules*, vol. 31, no. 5, pp. 1508–1517, 1998.

[83] W. H. Starnes Jr., "Structural defects in poly(vinyl chloride)," *Journal of Polymer Science Part A: Polymer Chemistry*, vol. 43, no. 12, pp. 2451–2467, 2005.

[84] N. Gonzalez, A. Mugica, and M. J. Fernandez-Berridi, "Application of high resolution thermogravimetry to the study of thermal stability of poly (vinyl chloride) resins," *Polymer degradation and stability*, vol. 91, no. 4, pp. 629–633, 2006.

[85] A. Marcilla and M. Beltrán, "Thermogravimetric kinetic study of poly (vinyl chloride) pyrolysis," *Polymer degradation and stability*, vol. 48, no. 2, pp. 219–229, 1995.

[86] K. J. Jordan, S. Suib, and J. Koberstein, "Determination of the degradation mechanism from the kinetic parameters of dehydrochlorinated poly (vinyl chloride) decomposition," *The journal of physical chemistry B*, vol. 105, no. 16, pp. 3174–3181, 2001.

[87] C.-H. Wu, C.-Y. Chang, J.-L. Hor, S.-M. Shih, L.-W. Chen, and F.-W. Chang, "Two-stage pyrolysis model of pvc," *The Canadian Journal of Chemical Engineering*, vol. 72, no. 4, pp. 644–650, 1994.

[88] C.-H. Wu, C.-Y. Chang, J.-L. Hor, S.-M. Shih, and L.-W. Chen, "Pyrolysis kinetics of waste pvc at high conversion," *The Chemical Engineering Journal and the Biochemical Engineering Journal*, vol. 55, no. 1-2, pp. 87–92, 1994.

[89] M. H. Fisch and R. Bacaloglu, "Degradation and stabilization of poly (vinyl chloride). 6: Model studies on dehydrochlorination of 6 (4)-chloro-4 (5)-tetradecenes in the

presence of alkyl phosphites and zinc di (dialkyl phosphites)," *Journal of Vinyl and Additive Technology*, vol. 5, no. 4, pp. 205–217, 1999.

[90] P. Bredereck, "Pvc stabilization mechanisms in the light of practical results," *Journal of Vinyl Technology*, vol. 1, no. 4, pp. 218–220, 1979.

[91] E. Michell, "True stabilization: A mechanism for the behavior of lead compounds and other primary stabilizers against pvc thermal dehydrochlorination," *Journal of Vinyl Technology*, vol. 8, no. 2, pp. 55–65, 1986.

[92] A. Ara, J. A. Usmani, *et al.*, "Lead toxicity: a review," *Interdisciplinary toxicology*, vol. 8, no. 2, pp. 55–64, 2015.

[93] D. R. Ortega, D. F. G. Esquivel, T. B. Ayala, B. Pineda, S. G. Manzo, J. M. Quino, P. C. Mora, and V. P. de la Cruz, "Cognitive impairment induced by lead exposure during lifespan: mechanisms of lead neurotoxicity," *Toxics*, vol. 9, no. 2, 2021.

[94] W. T. Piver, "Organotin compounds: industrial applications and biological investigation.," *Environmental health perspectives*, vol. 4, pp. 61–79, 1973.

[95] E. Arkış and D. Balköse, "Thermal stabilisation of poly (vinyl chloride) by organotin compounds," *Polymer Degradation and Stability*, vol. 88, no. 1, pp. 46–51, 2005.

[96] G. Wypych, *PVC degradation and stabilization*. Elsevier, 2020.

[97] R. Kalouskova, M. Novotna, and Z. Vymazal, "Investigation of thermal stabilization of poly (vinyl chloride) by lead stearate and its combination with synthetic hydrotalcite," *Polymer degradation and stability*, vol. 85, no. 2, pp. 903–909, 2004.

[98] W. Manzoor, S. Yousaf, and Z. Ahmad, "Degradation of pvc: effect of zinc chloride on the concentration of polyenes," *Polymer degradation and stability*, vol. 51, no. 3, pp. 295–299, 1996.

[99] B. Wu, Y. Wang, S. Chen, M. Wang, M. Ma, Y. Shi, and X. Wang, "Stability, mechanism and unique "zinc burning" inhibition synergistic effect of zinc dehydroacetate as thermal stabilizer for poly (vinyl chloride)," *Polymer Degradation and Stability*, vol. 152, pp. 228–234, 2018.

[100] Z. Fu, Z. Yang, L. Deng, Y. Rong, and J. Wu, "Tris (hydroxymethyl) aminomethane and its derivative as organic thermal stabilizers for flexible poly (vinyl chloride)," *Journal of Vinyl and Additive Technology*, vol. 28, no. 4, pp. 696–705, 2022.

[101] Y. Guo, F. Leroux, W. Tian, D. Li, P. Tang, and Y. Feng, "Layered double hydroxides as thermal stabilizers for poly (vinyl chloride): A review," *Applied Clay Science*, vol. 211, p. 106198, 2021.

[102] Q. Wang and D. O'Hare, "Recent advances in the synthesis and application of layered double hydroxide (ldh) nanosheets," *Chemical reviews*, vol. 112, no. 7, pp. 4124–4155, 2012.

[103] P. Wang, X. Zhang, B. Zhou, F. Meng, Y. Wang, and G. Wen, "Recent advance of layered double hydroxides materials: Structure, properties, synthesis, modification and applications of wastewater treatment," *Journal of Environmental Chemical Engineering*, p. 111191, 2023.

[104] D. G. Evans and X. Duan, "Preparation of layered double hydroxides and their applications as additives in polymers, as precursors to magnetic materials and in biology and medicine," *Chemical Communications*, no. 5, pp. 485–496, 2006.

[105] A. Farhan, A. Khalid, N. Maqsood, S. Iftekhar, H. M. A. Sharif, F. Qi, M. Sillanpää, and M. B. Asif, "Progress in layered double hydroxides (ldhs): Synthesis and application in adsorption, catalysis and photoreduction," *Science of the Total Environment*, p. 169160, 2023.

[106] Y. Tokudome, M. Fukui, N. Tarutani, S. Nishimura, V. Prevot, C. Forano, G. Poologasundarampillai, P. D. Lee, and M. Takahashi, "High-density protein loading on hierarchically porous layered double hydroxide composites with a rational mesostructure," *Langmuir*, vol. 32, no. 35, pp. 8826–8833, 2016.

[107] Q. Sun, X. Hu, H. Wang, Y. Lin, J. Zhang, X. Dong, J. Sheng, *et al.*, "Interfacial engineering and vacancy design of quasi-2d nicoal-ldh/kaolin hybrid for activating peroxymonosulfate to boost degradation of antibiotics," *Separation and Purification Technology*, p. 128674, 2024.

[108] L. Xu, P. Guo, J. Xu, B. Shen, and S.-Q. Guo, "Promoting the generation of hydroxyl radicals to improve the photocatalytic toluene oxidation: A combined strategy of morphology regulation and layered double hydroxide assistance," *Separation and Purification Technology*, p. 128662, 2024.

[109] S. Cometa, F. Busto, A. C. Scalia, A. Castellaneta, P. Gentile, A. Cochis, M. Manfredi, V. Borrini, L. Rimondini, and E. De Giglio, "Effectiveness of gellan gum scaffolds loaded with boswellia serrata extract for in-situ modulation of pro-inflammatory pathways affecting cartilage healing," *International Journal of Biological Macromolecules*, p. 134079, 2024.

[110] Y. Dong, L. Chen, J. Hou, Y. Sun, Z. Han, J. Zhang, Y. Liang, Y. Feng, J. Ren, Q. Li, *et al.*, "Dna programmed mg-al layered double hydroxide-based bi-adjuvant nanovaccines," *Nano Today*, vol. 57, p. 102352, 2024.

[111] X. Geng, Y. Tang, B. Yuan, Y. Dai, H.-P. Yu, Z.-C. Xiong, Y.-J. Zhu, and X. Chen, "Biomimetically ordered ultralong hydroxyapatite nanowires-based hierarchical hydrogel scaffold with osteoimmunomodulatory and osteogenesis abilities for augmenting bone regeneration," *Chemical Engineering Journal*, vol. 488, p. 151136, 2024.

[112] S. Mallakpour and M. Naghdi, "A green strategy toward the preparation of poly (vinyl chloride) nanocomposites reinforced with mno 2@ layered double hydroxide nanohybrids as efficient uv shielding materials," *New Journal of Chemistry*, vol. 44, no. 27, pp. 11566–11576, 2020.

[113] S. Daniel, S. Joseph, P. S. Alapat, N. Kalarikkal, and S. Thomas, "Silver-sandwiched natural rubber/st-ldh/mwcnt hybrid bio-nano-composite system as a high-performing multimedia laminated electromagnetic interference shield through a tripling mechanism," *ACS Sustainable Chemistry & Engineering*, vol. 10, no. 45, pp. 14897–14913, 2022.

[114] C. Cui, Y. Zhang, W. Song, and K. Niu, "Biomass carboxylic acid modified hydrotalcites for improving the mechanical strength and recyclability of 100% biobased carbon content epoxy soybean oil based vitrimers," *Progress in Organic Coatings*, vol. 190, p. 108410, 2024.

[115] H. Zhang, Y. Di, Q. Yang, and X. Zhou, "Composites of layered double hydroxide nanosheets, hydroxy-functionalized carbon nanotubes, and hydroxyapatite nanoparticles as flame retardants for epoxy resins," *ACS Applied Nano Materials*, vol. 4, no. 11, pp. 11753–11762, 2021.

[116] B. E. Al-Jumaili, "Microstructural, dielectric, and microwave absorption properties of polyvinyl chloride/mg/al-layered double hydroxide composites," *Journal of Materials Science: Materials in Electronics*, vol. 34, no. 11, p. 968, 2023.

[117] X. Wen, Z. Yang, J. Yan, and X. Xie, "Green preparation and characterization of a novel heat stabilizer for poly (vinyl chloride)–hydrocalumites," *RSC Advances*, vol. 5, no. 40, pp. 32020–32026, 2015.

[118] Y. Guo, Q. Zhang, Q. Hu, W. Tian, F. Leroux, P. Tang, D. Li, and Y. Feng, "Size-dependent effect of mgal-layered double hydroxides derived from mg (oh) 2 on ther-

mal stability of poly (vinyl chloride)," *Materials Today Communications*, vol. 29, p. 102851, 2021.

[119] G. Wang, M. Yang, Z. Li, K. Lin, Q. Jin, C. Xing, Z. Hu, and D. Wang, "Synthesis and characterization of zn-doped mgal-layered double hydroxide nanoparticles as pvc heat stabilizer," *Journal of nanoparticle research*, vol. 15, pp. 1–8, 2013.

[120] P. Jia, J. Duan, Z. Liu, Y. Li, G. Du, Y. Hu, and J. Wu, "Preparation of rare-earth ldhs stabilizers and their effects on the thermal stability of poly (vinyl chloride)," *Iranian Polymer Journal*, pp. 1–11, 2024.

[121] W. Runjuan, Y. Zhanhong, C. Hongyan, H. Youwang, and D. Ji'an, "Zn-al-la hydrotalcite-like compounds as heating stabilizer in pvc resin," *Journal of Rare Earths*, vol. 30, no. 9, pp. 895–902, 2012.

[122] S. Yi, Z.-H. Yang, S.-W. Wang, D.-R. Liu, S.-Q. Wang, Q.-Y. Liu, and W.-W. Chi, "Effects of mgalce-co3 layered double hydroxides on the thermal stability of pvc resin," *Journal of Applied Polymer Science*, vol. 119, no. 5, pp. 2620–2626, 2011.

[123] S. Mallakpour, M. Dinari, and M. Hatami, "Novel nanocomposites of poly (vinyl alcohol) and mg–al layered double hydroxide intercalated with diacid n-tetrabromophthaloyl-aspartic: Optical, thermal and mechanical properties," *Journal of Thermal Analysis and Calorimetry*, vol. 120, pp. 1293–1302, 2015.

[124] X. Zhang, T. Zhao, H. Pi, and S. Guo, "Preparation of intercalated mg-al layered double hydroxides and its application in pvc thermal stability," *Journal of applied polymer science*, vol. 124, no. 6, pp. 5180–5186, 2012.

[125] J. Liu, G. Chen, J. Yang, and L. Ding, "Improved thermal stability of poly (vinyl chloride) by nanoscale layered double hydroxide particles grafted with toluene-2,

4-di-isocyanate," *Materials Chemistry and Physics*, vol. 118, no. 2-3, pp. 405–409, 2009.

[126] M. Alexandre and P. Dubois, "Polymer-layered silicate nanocomposites: preparation, properties and uses of a new class of materials," *Materials science and engineering: R: Reports*, vol. 28, no. 1-2, pp. 1–63, 2000.

[127] Y.-Z. Bao, Z.-M. Huang, and Z.-X. Weng, "Preparation and characterization of poly (vinyl chloride)/layered double hydroxides nanocomposite via in situ suspension polymerization," *Journal of applied polymer science*, vol. 102, no. 2, pp. 1471–1477, 2006.

[128] X. Wang and Q. Zhang, "Effect of hydrotalcite on the thermal stability, mechanical properties, rheology and flame retardance of poly (vinyl chloride)," *Polymer International*, vol. 53, no. 6, pp. 698–707, 2004.

[129] H. Obata, "Preparation of oleate/layered double hydroxides (ldhs) composites from ldhs with different porous properties and its acid-resistant properties," *Abstracts of 50th Clay Science Society of Japan, 2006*, pp. 186–187, 2006.

[130] D. G. Evans and R. C. Slade, "Structural aspects of layered double hydroxides," *Layered double hydroxides*, pp. 1–87, 2006.

[131] L. Zhonghui and S. Guida, "Factors affecting acidity and basal spacing of cross-linked smectites," in *Studies in Surface Science and Catalysis*, vol. 24, pp. 493–500, Elsevier, 1985.

[132] B. R. Gevers, S. Naseem, A. Leuteritz, and F. J. Labuschagné, "Comparison of nano-structured transition metal modified tri-metal mgmal–ldhs (m= fe, zn, cu, ni, co) prepared using co-precipitation," *RSC advances*, vol. 9, no. 48, pp. 28262–28275, 2019.

[133] S. Bhattacharjee, "Synthesis and application of layered double hydroxide-hosted 2-aminoterephthalate for the knoevenagel condensation reaction," *Inorganic and Nano-Metal Chemistry*, vol. 48, no. 7, pp. 340–346, 2018.

[134] K. Nejati, A. R. Akbari, S. Davari, K. Asadpour-Zeynali, and Z. Rezvani, "Zn–fe-layered double hydroxide intercalated with vanadate and molybdate anions for electrocatalytic water oxidation," *New Journal of Chemistry*, vol. 42, no. 4, pp. 2889–2895, 2018.

[135] S. Riahi, B. Roux, and C. N. Rowley, "Qm/mm molecular dynamics simulations of the hydration of mg (ii) and zn (ii) ions," *Canadian Journal of Chemistry*, vol. 91, no. 7, pp. 552–558, 2013.

[136] X. Zhang, L. Zhou, H. Pi, S. Guo, and J. Fu, "Performance of layered double hydroxides intercalated by a uv stabilizer in accelerated weathering and thermal stabilization of pvc," *Polymer degradation and stability*, vol. 102, pp. 204–211, 2014.

[137] A.-E. Sakr, T. Zaki, O. Elgabry, M. Ebiad, S. El-Sabagh, and M. Emara, "Mg-zn-al ldh: Influence of intercalated anions on co2 removal from natural gas," *Applied Clay Science*, vol. 160, pp. 263–269, 2018.

[138] L. Valeikiene, R. Paitian, I. Grigoraviciute-Puroniene, K. Ishikawa, and A. Kareiva, "Transition metal substitution effects in sol-gel derived mg3-xmx/al1 (m= mn, co, ni, cu, zn) layered double hydroxides," *Materials Chemistry and Physics*, vol. 237, p. 121863, 2019.

[139] N. A. G. Gomez and F. Wypych, "Nanocomposites of polyethylene and ternary (mg+ zn/al) layered double hydroxide modified with an organic uv absorber," *Journal of Polymer Research*, vol. 26, pp. 1–10, 2019.

[140] Z. Karami, M. Jouyandeh, J. A. Ali, M. R. Ganjali, M. Aghazadeh, M. Maadani, M. Rallini, F. Luzi, L. Torre, D. Puglia, *et al.*, "Development of mg-zn-al-co3 ternary ldh and its curability in epoxy/amine system," *Progress in Organic Coatings*, vol. 136, p. 105264, 2019.

[141] S. Naseem, B. Gevers, R. Boldt, F. J. J. Labuschagné, and A. Leuteritz, "Comparison of transition metal (fe, co, ni, cu, and zn) containing tri-metal layered double hydroxides (ldhs) prepared by urea hydrolysis," *RSC Adv.*, vol. 9, pp. 3030–3040, 2019.

[142] N. Rahman and A. Raheem, "Graphene oxide/mg-zn-al layered double hydroxide for efficient removal of doxycycline from water: Taguchi approach for optimization," *Journal of Molecular Liquids*, vol. 354, p. 118899, 2022.

[143] X. Zhou, H. Chen, Q. Chen, and Q. Ling, "Synthesis and characterization of two-component acidic ion intercalated layered double hydroxide and its use as a nanoflame-retardant in ethylene vinyl acetate copolymer (eva)," *RSC advances*, vol. 7, no. 84, pp. 53064–53075, 2017.

[144] S. Klempová, M. Oravec, and K. Vizárová, "Analysis of thermally and uv–vis aged plasticized pvc using uv–vis, atr-ftir and raman spectroscopy," *Spectrochimica Acta Part A: Molecular and Biomolecular Spectroscopy*, vol. 294, p. 122541, 2023.

[145] A. A. Yaseen, E. Yousif, E. T. Al-Tikrity, G. A. El-Hiti, B. M. Kariuki, D. S. Ahmed, and M. Bufaroosha, "Ftir, weight, and surface morphology of poly (vinyl chloride) doped with tin complexes containing aromatic and heterocyclic moieties," *Polymers*, vol. 13, no. 19, p. 3264, 2021.

[146] M. Pandey, G. M. Joshi, A. Mukherjee, and P. Thomas, "Electrical properties and thermal degradation of poly (vinyl chloride)/polyvinylidene fluoride/zno polymer nanocomposites," *Polymer International*, vol. 65, no. 9, pp. 1098–1106, 2016.

[147] A. Ul-Hamid, K. Y. Soufi, L. M. Al-Hadhrami, and A. M. Shemsi, "Failure investigation of an underground low voltage xlpe insulated cable," *Anti-Corrosion Methods and Materials*, vol. 62, no. 5, pp. 281–287, 2015.

[148] H.-m. Zhang, S.-h. Zhang, P. Stewart, C.-h. Zhu, W.-j. Liu, A. Hexemer, E. Schaible, and C. Wang, "Thermal stability and thermal aging of poly (vinyl chloride)/mgal layered double hydroxides composites," *Chinese Journal of Polymer Science*, vol. 34, pp. 542–551, 2016.

[149] J. Yu, L. Sun, C. Ma, Y. Qiao, and H. Yao, "Thermal degradation of pvc: A review," *Waste management*, vol. 48, pp. 300–314, 2016.

[150] G. Wypych, *Handbook of material weathering*. Elsevier, 2018.

[151] H. Wang, C. Li, T. Geng, N. Du, and W. Hou, "Oleic acid-modified layered double hydroxide for pickering emulsion:(ii) emulsification behavior," *Colloids and Surfaces A: Physicochemical and Engineering Aspects*, vol. 687, p. 133568, 2024.

[152] R. K. Donato, L. Luza, R. F. da Silva, C. C. Moro, R. Guzatto, D. Samios, L. Matějka, B. Dimzoski, S. C. Amico, and H. S. Schrekker, "The role of oleate-functionalized layered double hydroxide in the melt compounding of polypropylene nanocomposites," *Materials Science and Engineering: C*, vol. 32, no. 8, pp. 2396–2403, 2012.

[153] R. Haarindraprasad, U. Hashim, S. C. Gopinath, M. Kashif, P. Veeradasan, S. Balakrishnan, K. Foo, and P. Poopalan, "Low temperature annealed zinc oxide nanostructured thin film-based transducers: characterization for sensing applications," *PLoS One*, vol. 10, no. 7, p. e0132755, 2015.

[154] P. Zhang, T. He, P. Li, X. Zeng, and Y. Huang, "New insight into the hierarchical microsphere evolution of organic three-dimensional layer double hydroxide: the key role of the surfactant template," *Langmuir*, vol. 35, no. 42, pp. 13562–13569, 2019.

[155] Q. Zhang, G. Zhang, Y. Huang, S. He, Y. Li, L. Jin, and J. Han, "Surface-modified ldh nanosheets with high dispersibility in oil for friction and wear reduction," *ACS Applied Materials & Interfaces*, vol. 16, no. 4, pp. 5316–5325, 2024.

[156] Y. Kameshima, H. SASAKI, T. ISOBE, A. NAKAJIMA, and K. OKADA, "Intercalation behavior of various fatty acids into mg-al-layered double hydroxide," *Clay Science*, vol. 14, no. 2, pp. 87–94, 2009.

[157] D. Lee, R. Condrate, and W. Lacourse, "Ftir spectral characterization of thin film coatings of oleic acid on glasses part ii coatings on glass from different media such as water, alcohol, benzene and air," *Journal of materials science*, vol. 35, pp. 4961–4970, 2000.

[158] J. Ibarra, J. Melendres, M. Almada, M. G. Burboa, P. Taboada, J. Juárez, and M. A. Valdez, "Synthesis and characterization of magnetite/plga/chitosan nanoparticles," *Materials Research Express*, vol. 2, no. 9, p. 095010, 2015.

[159] N. Shukla, C. Liu, P. M. Jones, and D. Weller, "Ftir study of surfactant bonding to fept nanoparticles," *Journal of Magnetism and Magnetic materials*, vol. 266, no. 1-2, pp. 178–184, 2003.

[160] R. Shorey and T. H. Mekonnen, "Oleic acid decorated kraft lignin as a hydrophobic and functional filler of cellulose acetate films," *International Journal of Biological Macromolecules*, vol. 268, p. 131672, 2024.

[161] X. Lei, W. Lu, Q. Peng, H. Li, T. Chen, S. Xu, and F. Zhang, "Activated mgal-layered double hydroxide as solid base catalysts for the conversion of fatty acid methyl esters

to monoethanolamides," *Applied Catalysis A: General*, vol. 399, no. 1-2, pp. 87–92, 2011.

[162] C. N. Dibenedetto, T. Sibillano, R. Brescia, M. Prato, L. Triggiani, C. Giannini, A. Panniello, M. Corricelli, R. Comparelli, C. Ingrosso, *et al.*, "Pbs quantum dots decorating tio2 nanocrystals: synthesis, topology, and optical properties of the colloidal hybrid architecture," *Molecules*, vol. 25, no. 12, p. 2939, 2020.

[163] K. Fa, T. Jiang, J. Nalaskowski, and J. D. Miller, "Optical and spectroscopic characteristics of oleate adsorption as revealed by ftir analysis," *Langmuir*, vol. 20, no. 13, pp. 5311–5321, 2004.

[164] P. Roonasi and A. Holmgren, "A fourier transform infrared (ftir) and thermogravimetric analysis (tga) study of oleate adsorbed on magnetite nano-particle surface," *Applied Surface Science*, vol. 255, no. 11, pp. 5891–5895, 2009.

[165] Z.-H. Tang, H.-Y. Zeng, K. Zhang, H.-L. Yue, L.-Q. Tang, S.-B. Lv, and H.-B. Wang, "Engineering core–shell nic2o4@ c/n-direct-doped nicozn-ldh for supercapacitors," *Chemical Engineering Science*, vol. 289, p. 119865, 2024.

[166] G. Zeng, G. Li, Y. Wu, C. Tang, W. Yuan, H. Zhong, N. Deng, Q. Liu, J. Liu, K. Ouyang, *et al.*, "Preparation of high specific surface area zn/al/zr ldh@ htcc for enrichment and recovery of phosphorus from water," *Surfaces and Interfaces*, vol. 42, p. 103330, 2023.

[167] Y. Wu, X. Liu, X. Bai, and W. Wu, "Ultrasonic-assisted preparation of ultrafine pd nanocatalysts loaded on cl–intercalated mgal layered double hydroxides for the catalytic dehydrogenation of dodecahydro-n-ethylcarbazole," *Ultrasonics Sonochemistry*, vol. 88, p. 106097, 2022.

[168] J. Cai, Y. Zhang, Y. Qian, C. Shan, and B. Pan, "Enhanced defluoridation using novel millisphere nanocomposite of la-doped li-al layered double hydroxides supported by polymeric anion exchanger," *Scientific Reports*, vol. 8, no. 1, p. 11741, 2018.

[169] Y. Chen, L. Wu, W. Yao, J. Wu, Z. Xie, Y. Yuan, B. Jiang, and F. Pan, "In situ growth of mg-zn-al ldhs by zif-8 carrying zn source and micro-arc oxidation integrated coating for corrosion and protection of magnesium alloys," *Surface and Coatings Technology*, vol. 451, p. 129032, 2022.

[170] S.-J. Huang, S. Balu, N. R. Barveen, and K. S. Bayikadi, "Construction of fe-substituted cozn layered double hydroxide as an efficient electrocatalyst for the oxygen evolution reaction," *Journal of the Taiwan Institute of Chemical Engineers*, vol. 152, p. 105157, 2023.

[171] J. Zhao, Y. Lu, D. Wu, Y. Qin, Y. Xie, Y. Guo, W. Raza, G. Luo, M. A. Mushtaq, Y. Wu, *et al.*, "Regulating divalent metal species in aluminum-based layered double hydroxides to selectively promote photocatalytic co production from co2," *Separation and Purification Technology*, vol. 305, p. 122508, 2023.

[172] K. Liu, Y. Xu, Z. Yao, H. N. Miras, and Y.-F. Song, "Polyoxometalate-intercalated layered double hydroxides as efficient and recyclable bifunctional catalysts for cascade reactions," *ChemCatChem*, vol. 8, no. 5, pp. 929–937, 2016.

[173] M. Kotal and S. K. Srivastava, "Synergistic effect of organomodification and isocyanate grafting of layered double hydroxide in reinforcing properties of polyurethane nanocomposites," *Journal of Materials Chemistry*, vol. 21, no. 46, pp. 18540–18551, 2011.

[174] Z. P. Xu, P. S. Braterman, K. Yu, H. Xu, Y. Wang, and C. J. Brinker, "Unusual hydrocarbon chain packing mode and modification of crystallite growth habit in the

self-assembled nanocomposites zinc- aluminum-hydroxide oleate and elaidate (cis- and trans-[zn2al (oh) 6 (ch3 (ch2) 7ch ch (ch2) 7coo-)] and magnesium analogues," *Chemistry of materials*, vol. 16, no. 14, pp. 2750–2756, 2004.

[175] Z. Xu and H. Zeng, "Decomposition processes of organic-anion-pillared clays co a mg b al (oh) c (ta) d n h2o," *The Journal of Physical Chemistry B*, vol. 104, no. 44, pp. 10206–10214, 2000.

[176] M. Tsuji, G. Mao, T. Yoshida, and Y. Tamaura, "Hydrotalcites with an extended al3+-substitution: Synthesis, simultaneous tg-dta-ms study, and their co2 adsorption behaviors," *Journal of materials research*, vol. 8, no. 5, pp. 1137–1142, 1993.

[177] M. Li, J. Zhang, K. Huang, S. Li, J. Jiang, and J. Xia, "Mixed calcium and zinc salts of dicarboxylic acids derived from rosin and dipentene: preparation and thermal stabilization for pvc," *RSC advances*, vol. 4, no. 108, pp. 63576–63585, 2014.

[178] M. Li, J. Zhang, J. Xin, K. Huang, S. Li, M. Wang, and J. Xia, "Design of green zinc-based thermal stabilizers derived from tung oil fatty acid and study of thermal stabilization for pvc," *Journal of Applied Polymer Science*, vol. 134, no. 14, 2017.

[179] Y. Li, D. Li, W. Han, M. Zhang, B. Ai, L. Zhang, H. Sun, and Z. Cui, "Facile synthesis of di-mannitol adipate ester-based zinc metal alkoxide as a bi-functional additive for poly (vinyl chloride)," *Polymers*, vol. 11, no. 5, p. 813, 2019.

[180] O. Babushkina and S. Volkov, "Raman spectroscopy of the heteronuclear complexes in the zncl2 cdcl2 li, k/cl and alcl3 mgcl2 li, k/cl melts," *Journal of molecular liquids*, vol. 83, no. 1-3, pp. 131–140, 1999.

[181] A. Q. Alsayoud, M. Venkateswara Rao, A. N. Edwards, P. A. Deymier, K. Muralidharan, B. G. J. Potter, K. Runge, and P. Lucas, "Structure of zncl2 melt. part i:

Raman spectroscopy analysis driven by ab initio methods," *The Journal of Physical Chemistry B*, vol. 120, no. 17, pp. 4174–4181, 2016. PMID: 27070739.

[182] X. Zhang, S. Li, J. Yuan, and Z. Shi, "Influence of magnesium chloride on the electrodeposition of zinc from the 1,3-dimethyl-2-imidazolidinone/zncl2 system," *Journal of Electroanalytical Chemistry*, vol. 957, p. 118131, 2024.

[183] H. Sano, H. Miyaoka, T. Kuze, H. Mori, G. Mizutani, N. Otsuka, and M. Terano, "Raman spectra of magnesium chloride thin films," *Surface Science*, vol. 502-503, pp. 70–74, 2002.

[184] G. Begun, J. Brynestad, K. Fung, and G. Mamantov, "Raman spectra of the molten alcl3zncl2 system and molten cs2zncl4," *Inorganic and Nuclear Chemistry Letters*, vol. 8, no. 1, pp. 79–88, 1972.

[185] Y. Guo, F. Leroux, W. Tian, D. Li, P. Tang, and Y. Feng, "Layered double hydroxides as thermal stabilizers for poly(vinyl chloride): A review," *Applied Clay Science*, vol. 211, p. 106198, 2021.

[186] S. M. Kuznetsov, E. A. Sagitova, K. A. Prokhorov, G. Y. Nikolaeva, D. I. Mendeleev, P. Donfack, and A. Materny, "Raman spectroscopic detection of polyene-length distribution for high-sensitivity monitoring of photo- and thermal degradation of polyvinylchloride," *Spectrochimica Acta Part A: Molecular and Biomolecular Spectroscopy*, vol. 252, p. 119494, 2021.

[187] M. Gilbert, K. C. Ho, D. J. Hitt, and D. Vrsaljko, "Assessment of pvc stabilisation using hydrotalcites – raman spectroscopy and other techniques," *Polymer Degradation and Stability*, vol. 98, no. 8, pp. 1537–1547, 2013.

[188] S. Mojtaba, G. Ismaeil, and K. Mohammad, "Thermal degradation of poly(vinyl chloride): Effect of nanoclay and low density polyethylene content," *Journal of Polymer Degradation and Stability*, vol. 96, no. 6, pp. 1005–1012, 2011.

[189] P. Sánchez-Jiménez, L. Pérez-Maqueda, A. Perejón, and J. Criado, "Combined kinetic analysis of thermal degradation of polymeric materials under any thermal pathway," *Polymer Degradation and Stability*, vol. 94, no. 11, pp. 2079–2085, 2009.

[190] Z. Wang, T. Xie, X. Ning, Y. Liu, and J. Wang, "Thermal degradation kinetics study of polyvinyl chloride (pvc) sheath for new and aged cables," *Waste Management*, vol. 99, pp. 146–153, 2019.

[191] N. Hamidi, "Upcycling poly(vinyl chloride) waste tubes: Studies of thermal stability and kinetics of films made of waste polyvinylchloride tube at the initial steps of degradation," *Journal of Applied Polymer Science*, vol. 140, no. 13, p. e53663, 2023.

[192] R. Zhou, B. Huang, Y. Ding, W. Li, and J. Mu, "Thermal decomposition mechanism and kinetics study of plastic waste chlorinated polyvinyl chloride," *Polymers*, vol. 11, no. 12, 2019.

[193] M. Raza, B. Abu-Jdayil, A. H. Al-Marzouqi, and A. Inayat, "Kinetic and thermodynamic analyses of date palm surface fibers pyrolysis using coats-redfern method," *Renewable Energy*, vol. 183, pp. 67–77, 2022.

[194] J. Rami, C. Patel, C. Patel, and M. Patel, "Thermogravimetric analysis (tga) of some synthesized metal oxide nanoparticles," *Materials Today: Proceedings*, vol. 43, pp. 655–659, 2021. 1st International Conference on Energy, Material Sciences and Mechanical Engineering.

[195] P. E. Sánchez-Jiménez, A. Perejón, J. M. Criado, M. J. Diánez, and L. A. Pérez-Maqueda, "Kinetic model for thermal dehydrochlorination of poly(vinyl chloride)," *Polymer*, vol. 51, no. 17, pp. 3998–4007, 2010.

[196] H. Gao and J. Li, "Thermogravimetric analysis of the co-combustion of coal and polyvinyl chloride," *PLOS ONE*, vol. 14, p. e0224401, Oct 28 2019.

[197] S. Altarawneh, M. Al-Harahsheh, A. Buttress, C. Dodds, and S. Kingman, "A thermo-kinetic investigation on the thermal degradation of polyvinyl chloride in the presence of magnetite and hematite," *Thermochimica Acta*, vol. 718, p. 179390, 2022.

[198] K. J. Jordan, S. L. Suib, and J. T. Koberstein, "Determination of the degradation mechanism from the kinetic parameters of dehydrochlorinated poly(vinyl chloride) decomposition," *The Journal of Physical Chemistry B*, vol. 105, no. 16, pp. 3174–3181, 2001.

APPENDICES

Appendix A

supplementary information

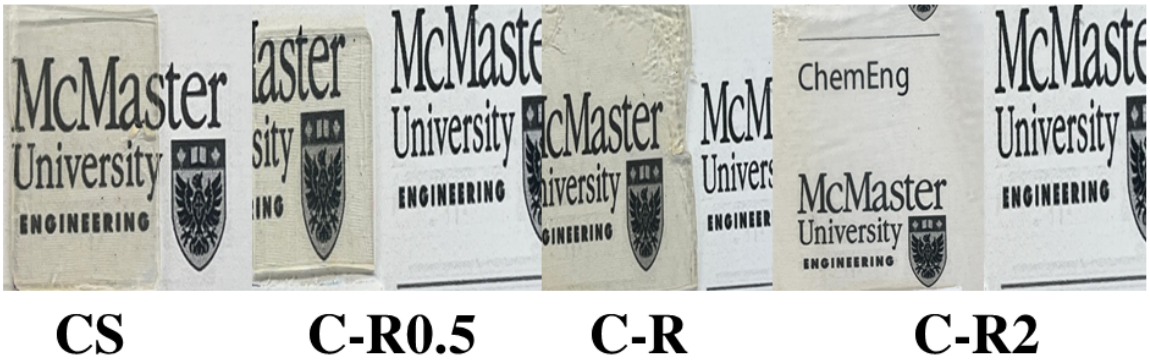

Figure A.1: Effect of LDHs on the transparency of plasticized PVC compounds.

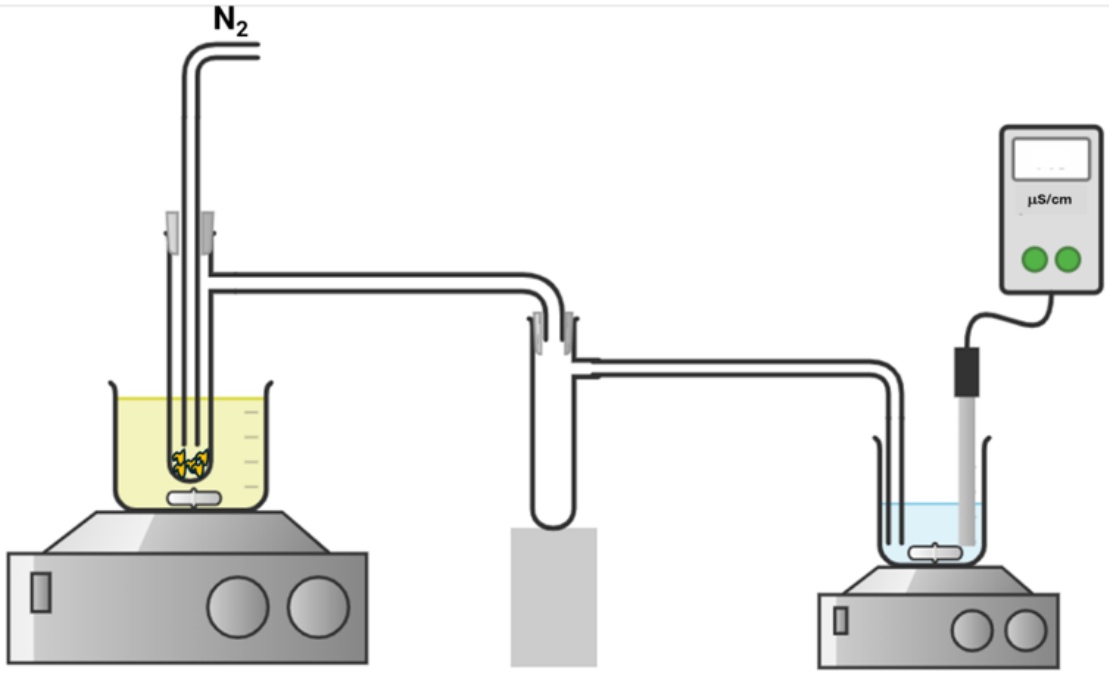

Figure A.2: Schematic of dehydrochlorination test.

Detailed TGA data in **TableA.1** provide the assigned temperature for a 5% weight loss ($T_{5\%}$), which occurs after the Tonset, indicating that the CS sample has a higher or equivalent assigned temperature in comparison to the samples with LDHs. This can be attributed to the absorption nature of LDHs, which causes the physisorption of small molecules and moisture. The $T_{25\%}$, representing the temperature at which the samples lose $T_{25\%}$ of their total weight, is 276°C for the CS sample, whereas it increases to 287°C for the C-R2 samples. This observation indicates the activation of LDHs' stabilization mechanism as a thermal stabilizer. Furthermore, the incorporation of LDHs with a higher Mg content leads to an increase in T1Max from 282°C for the CS sample to 292°C for the C-R2 sample.

Table A.1: TGA results of unmodified PVC compounds.

Sample	$T_{5\%}$ (°C)	$T_{25\%}$ (°C)	$T_{50\%}$ (°C)	$T_{80\%}$ (°C)	T_{1Max} (°C)	T_{2Max} (°C)	WR (%)
CS	260	276	291	457	282	446	6.47
C-R0.5	253	274	289	468	284	446	7.7
C-R	258	279	293	475	287	450	8.50
C-R2	261	287	299	480	292	452	8.65

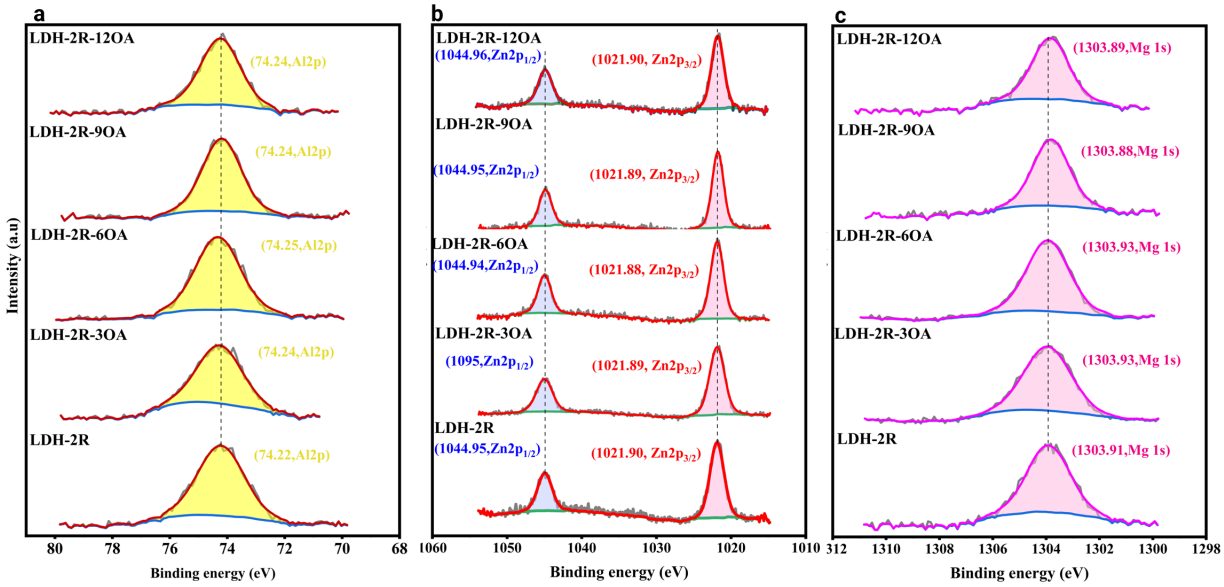

Figure A.3: XPS spectra for a) Al 2s, b) Zn 2p, and c) Mg 1s of surface-modified LDHs.

Table A.2: Formulation of Modified Compounds.

Sample	PVC	Plasticizer	Thermal Stabilizer	LDH	LDH Code	Sample ID
Compound 5	100	45	2.5	2.5	LDH-2R-3OA	MC-3OA
Compound 6	100	45	2.5	2.5	LDH-2R-6OA	MC-6OA
Compound 7	100	45	2.5	2.5	LDH-2R-9OA	MC-9OA
Compound 8	100	45	2.5	2.5	LDH-2R-12OA	MC-12OA

*The unit for all components is phr (per hundred resin).

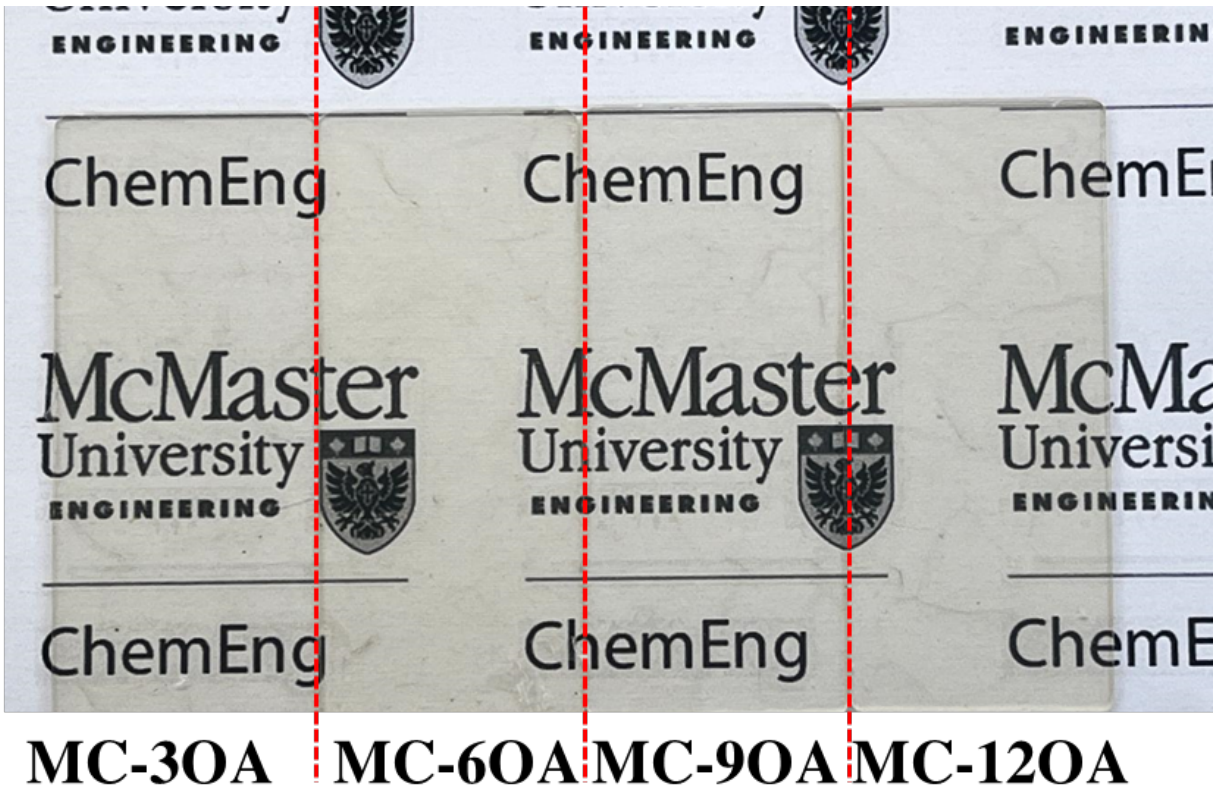

Figure A.4: Effect of surface modification of LDHs on the transparency of PVC compounds.

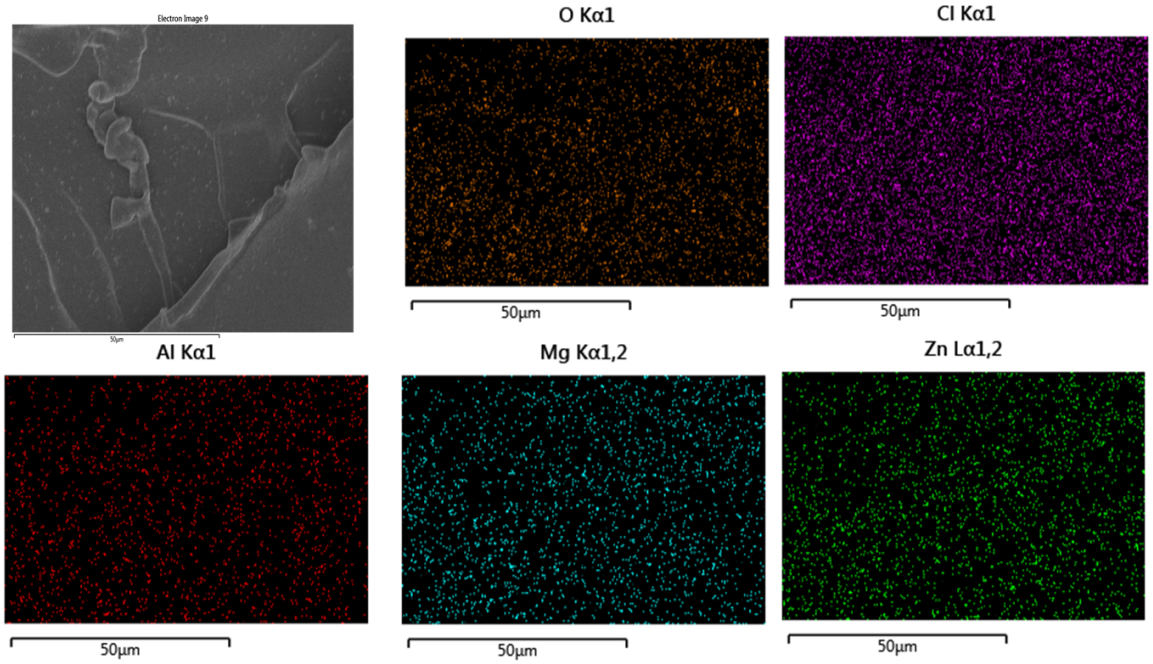

Figure A.5: EDS maps of modified compounds.

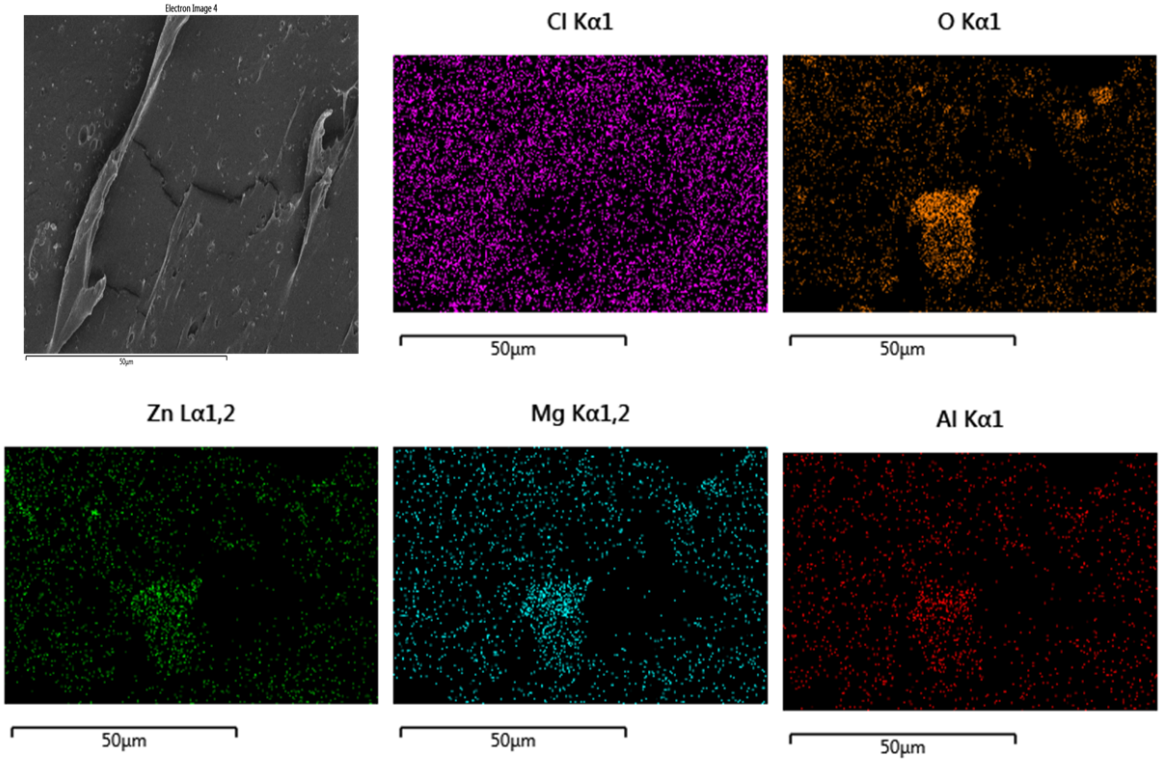

Figure A.6: EDS maps of unmodified compounds.

Table A.3: Detailed results of Raman spectroscopy.

Structure	**Sample**	**Peak**	**FWHM**	**Intensity**	**Area**
$MgCl_2$	C-R2-180	160.328	4.32939	497.6818	2293.564
	MC-9OA-180	160.4856	10.83196	723.5057	8342.203
$AlCl_3$	C-R2-180	184.0257	3.17184	444.7461	1501.605
	MC-9OA-180	184.0365	9.76073	862.2645	8958.904
$ZnCl_2$	C-R2-10	217.6198	14.37785	432.1895	6614.551
	MC-9OA-10	221.3789	21.10085	1034.063	23226.26
	C-R2-90	221.0533	20.73849	972.2457	21462.75
	MC-9OA-90	220.8527	11.23545	1687.794	20185.61
	C-R2-180	220.2401	9.3928	874.1846	8740.381
	MC-9OA-180	223.667	6.37407	2757.809	18711.7
$ZnCl_2$	C-R2-10	253.9056	13.6845	552.9025	8053.967
	MC-9OA-10	259.3401	18.39258	1333.131	26100.42
	C-R2-90	249.5645	13.77787	928.5721	13618.52
	MC-9OA-90	247.3532	12.22744	2546.192	33140.5
	C-R2-180	249.9054	5.56459	940.1387	5568.747
	MC-9OA-180	251.3082	9.75286	4011.334	41644.05
$MgCl_2$	C-R2-90	265.1281	12.89119	906.3298	12436.88
	MC-9OA-90	267.3153	11.20149	1186.126	14142.91
	C-R2-180	261.96	9.3362	1152.617	11454.8
	MC-9OA-180	264.3535	7.1692	4015.924	30647.03

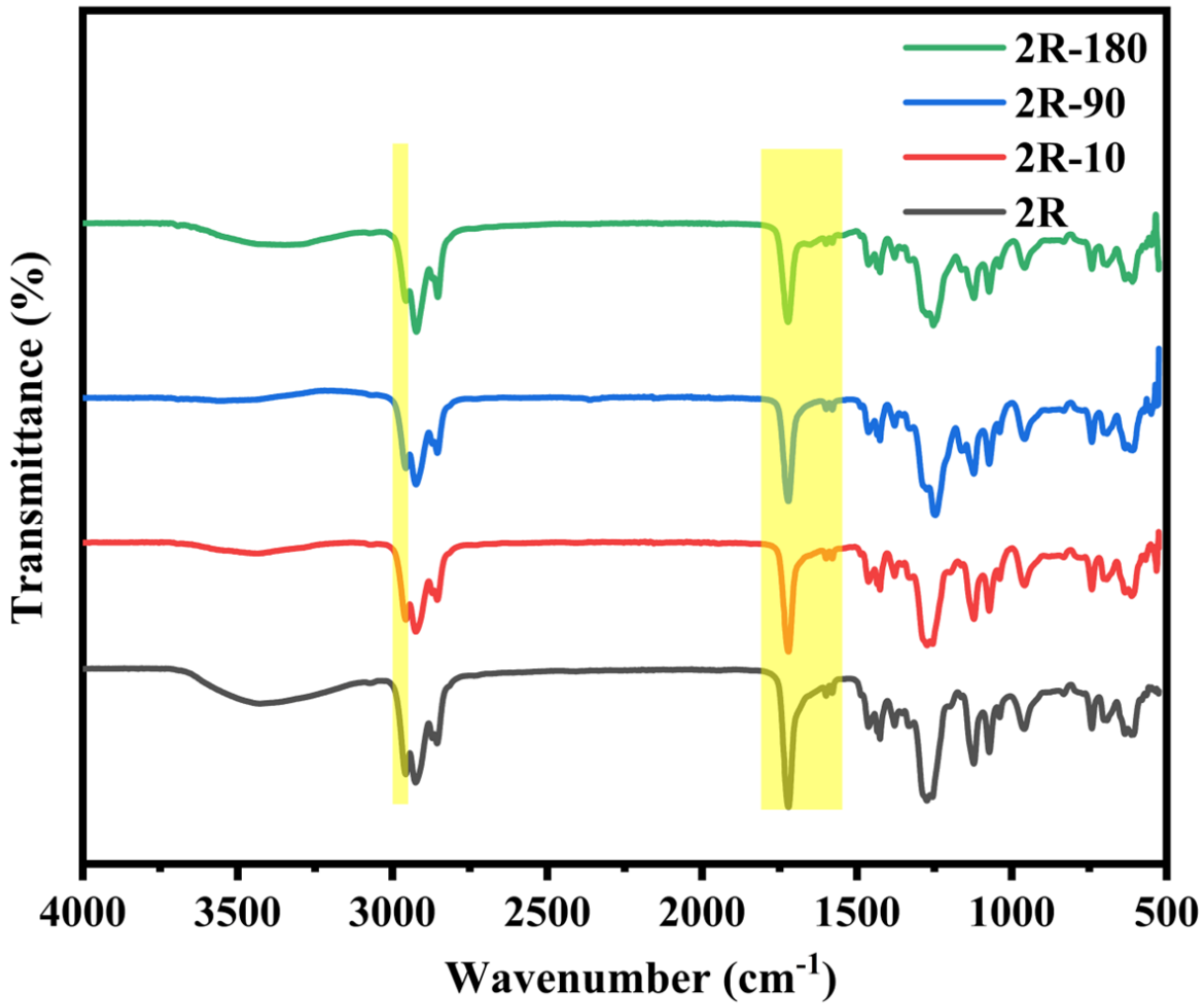

Figure A.7: FT-IR spectra of C-R2 compounds after 10,90 and 180 min at 180 °C.

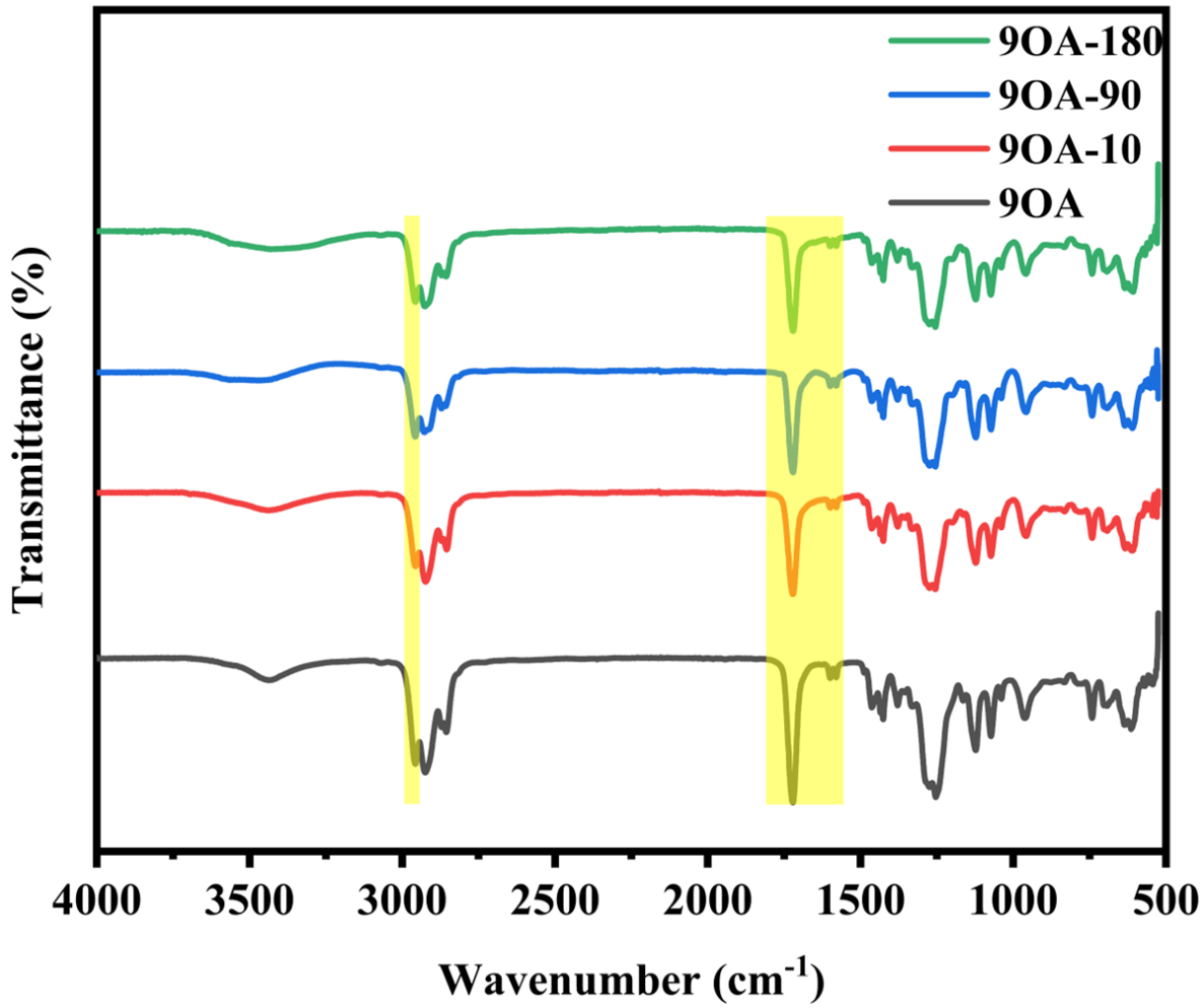

Figure A.8: FTIR spectra of MC-9OA PVC compounds after 10,90 and 180 min at 180 °C.

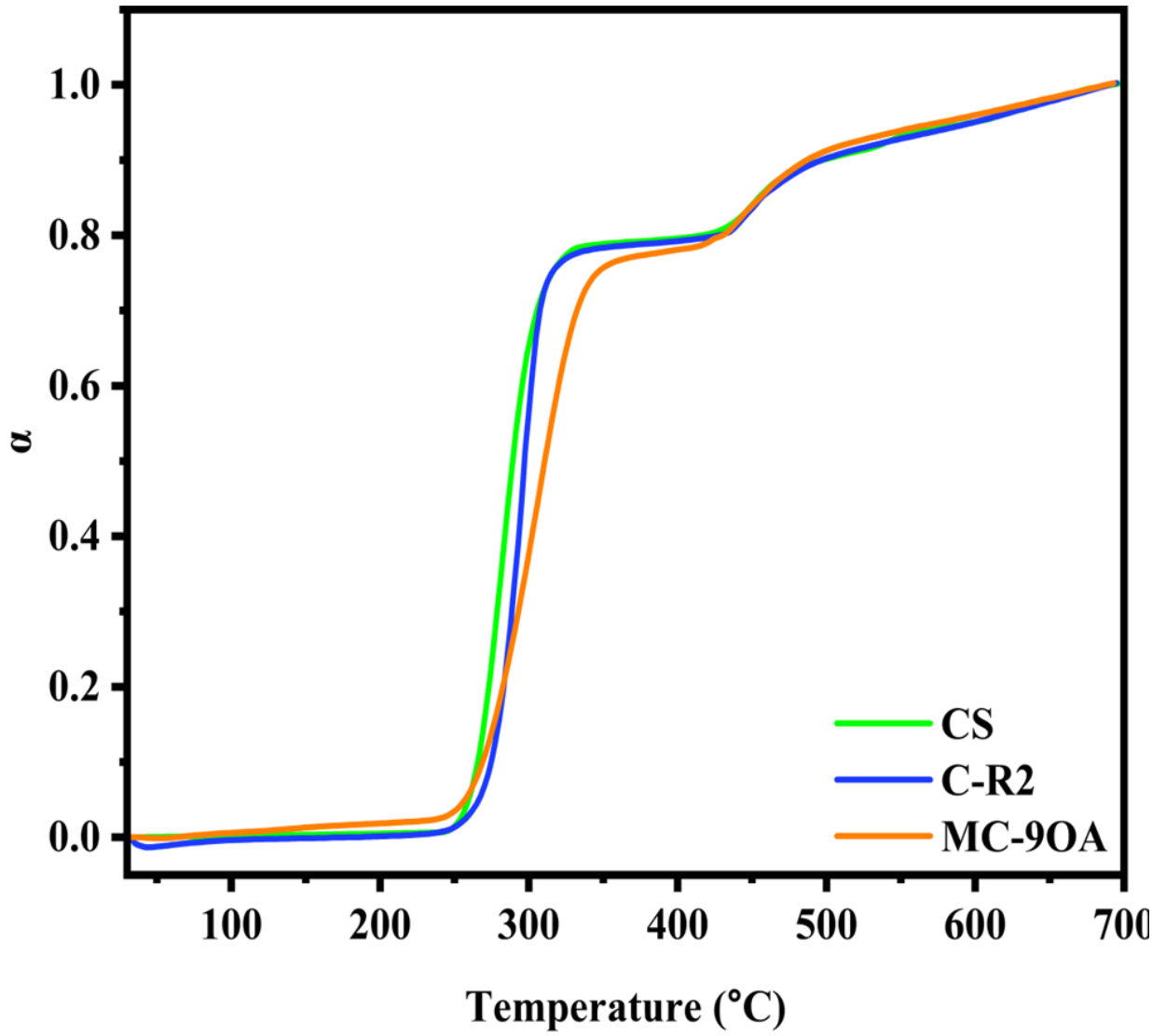

Figure A.9: Conversion (α) vs. Temperature (°C).